People's Democratic Republic of Algeria
Ministry of Higher Education and Scientific Research
Ahmed Draïa Adrar University
Faculty of Materials Sciences, Mathematics and Computer Science

Thesis

Presented to obtain the 3rd cycle Doctorate degree in

Materials sciences

Option: Radiation physics

By:

ABBANE SARA

Contribution to the study of materials for shielding against Gamma nuclear radiation in Adrar desert environment

Discuss publicly: 20 / 01 / 2026. In front of the jury:

Mr. BEN ATAILLAH Ali	**President**	**Professeur**	**U. Adrar**
Mr. BOUSSAID Mohammed	**Supervisor**	**Professeur**	**U. Adrar**
Mr. BELADEL Brahim	**Examiner**	**Professeur**	**U. Djelfa**
Mr. TIGRINE Rachid	**Examiner**	**Professeur**	**U. Adrar**
Mme. BOUDAOUD Lahouaria	**Examiner**	**Professeur**	**U. Adrar**

College year: 2025/2026

République Algérienne Démocratique et Populaire
Ministère de l'Enseignement Supérieur et de la Recherche Scientifique
Université Ahmed Draïa Adrar
Faculté des Sciences des Matériaux, Mathématiques et Informatique

Thèse

Présentée en vue de l'obtention du diplôme de Doctorat 3eme cycle en

Sciences des Matériaux

Option : Physique des rayonnements

Par :

ABBANE SARA

Contribution à l'étude des matériaux de protection contre le rayonnement nucléaire gamma dans l'environnement désertique d'Adrar

Soutenue publiquement le : 20 / 01 / 2026 Devant le jury :

Mr. BEN ATAILLAH Ali	**Président**	**Professeur**	**U. Adrar**
Mr. BOUSSAID Mohammed	**Rapporteur**	**Professeur**	**U. Adrar**
Mr. BELADEL Brahim	**Examinateur**	**Professeur**	**U. Djelfa**
Mr. TIGRINE Rachid	**Examinateur**	**Professeur**	**U. Adrar**
Mme. BOUDAOUD Lahouaria	**Examinateur**	**Professeur**	**U. Adrar**

Année Universitaire : 2025/2026

Acknowledgment

I wish to convey my profound appreciation to Allah for bestowing upon me the capability and success to finalize my doctoral dissertation. This accomplishment in my academic career would not have been attainable without His grace. I am appreciative of this blessing and express my gratitude for it.

I express my profound gratitude to Pr. Boussaid Mohamed and Professor Dr. Dib Anis Sami Amin for their willingness to supervise my dissertation, providing invaluable time, substantial information, and considerable expertise that significantly enriched my research.

I convey my sincere gratitude to all the outstanding committee members for consenting to evaluate my dissertation.

I would additionally like to express my gratitude to:

Pr.Kaddi Mohammed

Lagouch Akila

Rafai Hajira

Regragui Sarah

Slimani Zahia

Benyba Abdelkader

Your assistance in my research has been invaluable.

I would want to express my gratitude to my university colleagues, as well as to the laboratories LEESI and LDDI, and to all those who fostered optimism and offered support, resources, ideas, and information, possibly without recognizing their contributions. I express my gratitude to all of you.

ABBANE SARA

إهداء

إلى أمي الحبيبة، نبع الحنان والدعاء، وسرّ القوة في ضعفي،

إلى أبي رحمه الله ، سندي الأول، ومصدر حكمتي وثباتي،

أتممت الوعــد يا أبي

إلى زوجي الغالي، رفيق دربي، وداعمي في كل خطوة،

إلــى أميري الصغير عبد الصمد

إلى إخوتي وأخواتي، من شاركوني الحلم، ورفعوا معنوياتي في كل لحظة،

وإلى كل أساتذتي الأفاضل، من غرسوا في قلبي حبّ العلم، وأناروا لي درب المعرفة...

أهدي ثمرة هذا الجهد، عرفانًا وامتنانًا.

ملخص

تبحث هذه الدراسة في إمكانات مواد الطين الطبيعية من جنوب الجزائر كبدائل فعّالة ومستدامة لمواد الحماية الإشعاعية التقليدية. ونظرًا للاعتماد المتزايد على الإشعاع المؤين في المجالات الطبية والصناعية والزراعية، أصبح ضمان الحماية الكافية من آثاره الضارة ضرورةً ملحة. وقد استُخدمت مواد مثل الرصاص والخرسانة تقليديًا للحماية نظرًا لقدراتها العالية على التوهين. إلا أن لهذه المواد عيوبًا كبيرة: فالرصاص سام وضار بالبيئة، بينما قد تكون الخرسانة ضخمة وغير مرنة ومكلفة في التطبيقات المتخصصة. وقد دفعت هذه القيود إلى البحث عن مواد بديلة غير سامة وفعالة من حيث التكلفة ومتوفرة بسهولة.في هذا السياق، برز الطين الطبيعي ومركباته كمرشحين واعدين، نظرًا لوفرته ورخص ثمنه واستقراره الحراري وقدرته على التوهين الإشعاعي. وتهدف هذه الدراسة إلى تقييم كفاءة الحماية لعينات الطين التي جُمعت من منطقة أدرار في الجزائر من خلال حساب معاملات التوهين الخطي والكتلي. تم استخدام : WinXcom، التي تقدم تقديرات نظرية بناءً على التركيب العنصري، وGeant4، وهي مجموعة أدوات محاكاة مبنية على نموذج مونت كارلو تُنمذج تفاعلاتالجسيمات مع المادة بدقة عالية.

أظهرت النتائج أن فعالية حجب عينات الطين تختلف باختلاف مستويات طاقة أشعة غاما. عند طاقات الفوتونات المنخفضة، يهيمن الامتصاص الكهروضوئي، وتُظهر المواد المختبرة أداءً جيدًا، مما يُشير إلى ملاءمتها للحماية من الإشعاع منخفض الطاقة. مع زيادة طاقة الفوتون، يزداد تشتت كومبتون، بينما عند الطاقات العالية، يبدأ إنتاج الأزواج في التأثير على سلوك التوهين، مما يستلزم استخدام مواد ذات أعداد ذرية أعلى.

لُوحظ بين العينات المختبرة تسلسل هرمي واضح في أداء الحجب، حيث برز S2 باعتباره الأكثر كفاءة، يليه S4، وS1، وS3. لا تؤكد هذه النتائج جدوى استخدام الطين الجزائري في تطبيقات حجب الإشعاع فحسب، بل تُبرز أيضًا إمكانية تحسين المواد من خلال التحسين التركيبي أو الهيكلي.

علاوة على ذلك، يُوفر استخدام محاكاة Geant4 بديلاً عمليًا للاختبارات التجريبية، خاصةً عند عدم توفر البنية التحتية التجريبية. فهو يُمكّن من التخطيط الشامل، وتقليل الأخطاء، والتنبؤ الدقيق بسلوك المواد في ظل ظروف إشعاعية متنوعة.

وفي نهاية المطاف، تُسهم هذه الدراسة في السعي العالمي لإيجاد حلول سهلة المنال وفعالة وصديقة للبيئة للحماية من الإشعاع، من خلال الاستفادة من الموارد المتاحة محليًا باستخدام أدوات المحاكاة الحديثة.

الكلمات المفتاحية: الطين؛ معامل التوهين؛ برنامج WinXCom؛ Genat4.

Abstract

This study examines the feasibility of natural clay materials from southern Algeria as effective and ecological substitutes for traditional radiation shielding materials. Due to the growing dependence on ionising radiation in medical, industrial, and agricultural sectors, ensuring sufficient protection from its detrimental effects has become essential. Historically, materials like lead and concrete have been employed for shielding because of their superior attenuation properties. Nonetheless, these materials had considerable disadvantages: lead is toxic and environmentally detrimental, whilst concrete may be cumbersome, rigid, and expensive in specialised contexts. These constraints have necessitated the exploration of alternate materials that are non-toxic, economical, and easily accessible.

In this context, natural clays and their composites have emerged as viable alternatives due to their abundance, cost-effectiveness, thermal stability, and capacity for radiation attenuation. This study aims to assess the shielding efficacy of clay samples obtained from the Adrar region in Algeria by determining their linear and mass attenuation coefficients. Two computational tools were utilised: WinXcom, which provides theoretical estimates based on elemental composition, and Geant4, a Monte Carlo simulation toolbox that accurately represents particle interactions with matter.

The findings indicate that the shielding efficacy of the clay samples fluctuates based on gamma-ray energy levels. At low photon energies, photoelectric absorption prevails, and the evaluated materials exhibit commendable performance, signifying their appropriateness for low-energy radiation shielding. As photon energy escalates, Compton scattering becomes increasingly significant, whilst at elevated energies, pair formation starts to affect attenuation characteristics, requiring materials with greater atomic numbers.

A distinct hierarchy in shielding efficacy was noted across the evaluated samples, with S2 demonstrating the highest efficiency, succeeded by S4, S1, and S3. These findings indicate the viability of utilising Algerian clays for radiation shielding applications and underscore the potential for material optimisation via compositional or structural modification.

Furthermore, Geant4 simulations provide a viable substitute for experimental testing, particularly in the absence of experimental infrastructure. It facilitates thorough planning, minimises errors, and ensures precise forecasting of material performance under diverse radiation situations.

This study ultimately advances the global quest for affordable, effective, and environmentally sustainable radiation shielding solutions by utilising locally sourced materials with contemporary simulation tools.

Keywords:clay; attenuation coefficient ; WinXCom program; Genat4 .

Résume

Cette recherche explore la capacité des matériaux argileux naturels du sud de l'Algérie à servir d'alternatives durables et efficaces aux matériaux classiques utilisés pour la protection contre les rayonnements. Étant donné l'augmentation de la dépendance aux rayonnements ionisants dans les secteurs médical, industriel et agricole, il est impératif de garantir une protection adéquate contre leurs effets néfastes. Historiquement, le plomb et le béton ont été des choix privilégiés pour le blindage en raison de leur capacité élevée d'atténuation. Toutefois, ces matériaux comportent des inconvénients significatifs : le plomb est considéré comme toxique et néfaste pour l'écosystème, tandis que le béton peut se révéler encombrant, rigide et onéreux dans des contextes spécifiques. Ces contraintes ont motivé la recherche de matériaux de substitution qui soient non toxiques, abordables et facilement accessibles. Dans ce cadre, les argiles naturelles et leurs composites ont montré un fort potentiel, en raison de leur disponibilité, de leur coût abordable, de leur stabilité thermique et de leur capacité à atténuer les rayonnements. Cette étude vise à évaluer l'efficacité du blindage des échantillons d'argile provenant de la région d'Adrar en Algérie en déterminant leurs coefficients d'atténuation linéaire et massique. Deux logiciels de calcul ont été employés dans cette étude : WinXcom, qui propose des estimations théoriques en se basant sur la composition élémentaire, et Geant4, un outil de simulation utilisant la méthode Monte-Carlo pour représenter de manière précise les interactions des particules avec la matière. Les résultats indiquent que l'efficacité de la protection des échantillons d'argile contre les rayonnements gamma varie en fonction des niveaux d'énergie de ces derniers. À des niveaux d'énergie photonique bas, la prédominance de l'absorption photoélectrique et les performances satisfaisantes des matériaux évalués suggèrent leur pertinence pour la protection contre les radiations à faible énergie. Lorsque l'énergie des photons augmente, on observe une augmentation significative de la diffusion Compton, tandis qu'à des niveaux d'énergie plus élevés, l'impact de la production de paires sur le phénomène d'atténuation devient prépondérant, ce qui implique l'utilisation de matériaux ayant des numéros atomiques plus élevés.

Une hiérarchie claire des performances de blindage a été identifiée parmi les échantillons testés, avec S2 se démarquant comme le plus efficace, suivi de S4, S1 et S3. Ces résultats non seulement confirment la possibilité d'utiliser les argiles algériennes pour des applications de protection contre les rayonnements, mais mettent également en évidence le potentiel d'amélioration des matériaux par des ajustements compositionnels ou structuraux. Par ailleurs, recourir aux simulations Geant4 constitue une solution pratique en remplacement des expérimentations, particulièrement en l'absence d'une infrastructure expérimentale. Elle facilite une planification exhaustive, une diminution des erreurs et une prédiction précise du comportement des matériaux sous différentes conditions de rayonnement.

En conclusion, cette recherche apporte sa contribution à l'effort mondial visant à trouver des solutions de protection contre les rayonnements qui soient à la fois accessibles, efficaces et respectueuses de l'environnement, en utilisant les ressources locales disponibles et en s'appuyant sur des outils de simulation de pointe.

Mots clés : argile; coefficient d'atténuation; programme Win X Com ; Geant4.

Table of contents

Contents

List of Figures and Tables

General introduction

Ionising radiation has become an essential instrument across various domains, including energy generation, industrial uses, contemporary healthcare, and agricultural advancements. Nuclear medicine facilitates sophisticated diagnostic imaging and oncological therapies; in manufacturing, it aids in non-destructive evaluation and material examination; and in agriculture, it enhances food preservation and pest management. The extensive use of radiation, however advantageous, presents considerable hazards to human health and the environment if inadequately regulated. Consequently, radiation protection has become a vital field of research and practical importance.

The fundamental principle of radiation protection is shielding, which involves employing physical barriers to diminish or eradicate exposure to detrimental radiation. The efficacy of any shielding material is chiefly defined by its attenuation coefficient, a metric that measures the material's capacity to absorb or deflect incoming radiation. This coefficient arises from the amalgamation of three primary photon interaction mechanisms: photoelectric absorption, Compton scattering, and pair creation. The likelihood and characteristics of these interactions are significantly affected by the energy of the photon, together with the atomic number and density of the absorbing substance.

Historically, materials like lead, iron, and concrete have been the preferred options for radiation shielding because of their superior attenuation efficiency. Lead is preferred due to its elevated atomic number and density, rendering it particularly efficient at attenuating gamma rays and X-rays. Concrete, despite its lower density, is frequently utilised in substantial quantities in construction owing to its cost-effectiveness and structural characteristics. Nonetheless, both materials exhibit significant problems. Lead is hazardous and presents significant environmental and health risks, particularly with extensive or prolonged exposure. Concrete, although non-toxic, is cumbersome, expensive for specialised formulations, and exhibits restricted flexibility in certain applications.

The aforementioned limitations have stimulated an increasing volume of research aimed at identifying alternative shielding materials that are economically viable, locally sourced, non-toxic, and environmentally sustainable. Natural clays and composite materials have demonstrated significant potential among these options. Their extensive availability, affordability, and simplicity of processing render them appealing options. Moreover, certain clays demonstrate thermal stability, radiation resistance, and adequate attenuation

characteristics, particularly when augmented or combined with additions such as sand, heavy metal oxides, or polymer binders.

A multitude of experimental and computational investigations have been undertaken to assess the radiation shielding capabilities of clays from various places. A study on Egyptian clay samples demonstrated attenuation properties akin to those of standard concrete, indicating its potential for use in structural radiation shielding [17]. Nigerian clay samples were evaluated at photon energies between 100 keV and 2 MeV, exhibiting enhanced performance compared to concrete at lower energy and similar performance at elevated photon energies [16].

Researchers frequently utilise simulation tools such as WinXcom to evaluate the shielding efficacy of materials, as it is a theoretical database that computes mass attenuation coefficients based on elemental composition and photon energy. Geant4 is a powerful Monte Carlo simulation toolbox that accurately mimics the interaction of particles with matter. Comparative investigations indicate that WinXcom provides highly dependable theoretical estimates, but Geant4 results frequently correspond closely with actual data, rendering them optimal complements in radiation shielding research [18], [19].

This work aims to further the burgeoning research field by examining the attenuation characteristics and shielding efficacy of clay materials from southern Algeria, an area abundant in varied geological formations. This study intends to utilise both WinXcom and Geant4 tools to:

Determine the linear and mass attenuation coefficients of chosen clay samples. Evaluate their efficacy in relation to conventional shielding materials like lead and concrete. Compare the results with prior research conducted in Egypt and Nigeria. Assess the appropriateness of these local materials for radiation shielding in medical, industrial, or research applications.

This research aims to facilitate the creation of cost-effective, sustainable, and locally derived shielding alternatives, especially in poor nations where access to traditional shielding materials may be restricted.

Thesis outline

This thesis is structured in a coherent manner to elaborate on all previously examined concepts. Subsequent to the introduction, our study's methodology is delineated across four chapters, detailed as follows:

Chapter 1: This chapter introduces atomic and nuclear energy levels and offers a comprehensive examination of several radioactive decay processes, including electron capture, beta decay, positron emission, and alpha decay. It additionally addresses the concept of half-life and examines the interaction processes between various forms of radiation (alpha, beta, gamma, and X-rays) and matter. These foundational ideas underpin the comprehension of radiation behaviour and its impacts in various contexts..

Chapter 2: This section examines the essential principles of radiation protection, emphasising the reduction of exposure via time management, distance, and shielding. It underscores the significance of protective materials and elucidates the mechanisms of photon attenuation and absorption. This section examines how various materials diminish radiation intensity and the parameters affecting their efficacy.

Chapter 3: This section delineates the methodology employed to analyse the clay samples and assess their radiation shielding efficacy. The process encompasses sample preparation and characterisation, together with the utilised computational methodology. The attenuation coefficients were computed using WinXcom for theoretical data and Geant4 for simulation-based modelling.

Chapter 4: This section gives the results derived from simulation models concerning the attenuation characteristics of the analysed clay samples. The study assesses the shielding efficacy of several clay types, emphasising their ability to mitigate ionising radiation at varying photon energy levels. The findings indicate that certain clay samples have favourable attenuation properties, underscoring its potential as efficient and eco-friendly radiation shielding materials..

References

[1] S. F. Olukotun et al., “Investigation of gamma radiation shielding capability of two clay materials,” Nuclear Engineering and Technology, vol. 50, no. 6, pp. 957–962, Aug. 2018, doi: 10.1016/j.net.2018.05.003.

[2] M. Elsafi, Y. Koraim, M. Almurayshid, F. I. Almasoud, M. I. Sayyed, and I. H. Saleh, “Investigation of photon radiation attenuation capability of different clay materials,” Materials, vol. 14, no. 21, Nov. 2021, doi: 10.3390/ma14216702.

[3] L. Gerward, N. Guilbert, K. B. Jensen, and H. Levring, “WinXCom - A program for calculating X-ray attenuation coefficients,” in Radiation Physics and Chemistry, Oct. 2004, pp. 653–654. doi: 10.1016/j.radphyschem.2004.04.040.

[4] M. E. Medhat and V. P. Singh, “Mass attenuation coefficients of composite materials by Geant4, XCOM and experimental data: Comparative study,” Radiation Effects and Defects in Solids, vol. 169, no. 9, pp. 800–807, Sep. 2014, doi: 10.1080/10420150.2014.950264.

Chapter I: Fundamentals of Atomic and Nuclear Physics

I.1 Introduction

Everyone who lives on this planet or objects belonging to it is exposed to permanent radiation from several sources, especially cosmic rays, and this happens every second, except for a, this radiation is simple and organized and does not expose humans to any dangers. But man's use of atoms to achieve his greed and aspirations is what exposes living organisms to environmental pollution and extreme danger[1].

Before starting to know the permissible limits of radiation and the methods of prevention from it, it is necessary to know the rationale and preliminary concepts about radiation science, its activity, and how it interacts with matter. This is what we will find within the papers of the first chapter.

I.2The Atom

Now we know that all matter is made up of atoms, which are frequently grouped together to create molecules. Each atom is made up of a nucleus in the center surrounded by an electron cloud in orbit. as shown in Figure 1.1.

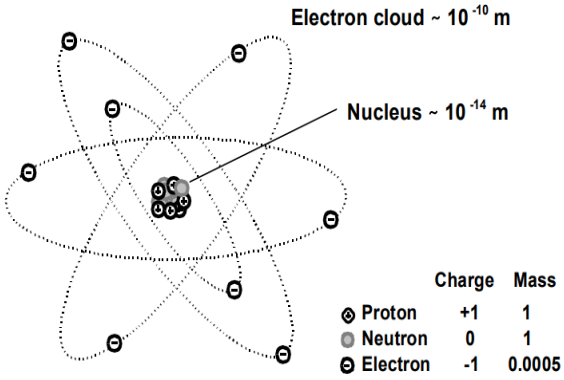

Figure 1. 1: Atom structure ***[2]***

When the atom is in its normal state, electrostatic interaction between the positively charged nucleus and the negatively charged electrons holds exactly Z electrons in orbit around the nucleus. The atom's total charge is then zero. Because atoms join to form molecules through the interaction of their electrons, the chemistry of the atom is determined by the arrangement of the atomic electrons. Because they function chemically the same, all atoms with the same Z belong to the same element.

The protons and neutrons in the nucleus are referred to collectively as nucleons. Because each nucleon is 2000 times heavier than an electron, the nucleus retains nearly all of the atom's mass

despite its modest size. As a consequence, the total mass of the atom is determined by the sum of the number of protons, Z, and neutrons, N, it contains. Thus, the atom's mass number,A, is given byA= Z + N[2].

I.2.1 Atomic EnergyLevels

The electrons in an atom can only reside in well-defined orbits, or shells, each with a distinct energy level, as Rutherford and Bohr discovered. As more electrons are introduced, they must reside in higher energy levels as the lower shells fill up since each shell can only house a finite amount of electrons. This explains why there is a periodicity in the elements table since it is the outer electrons that chemically interact with other atoms. has repeating comparable chemical characteristics as each energy shell is filled[3].

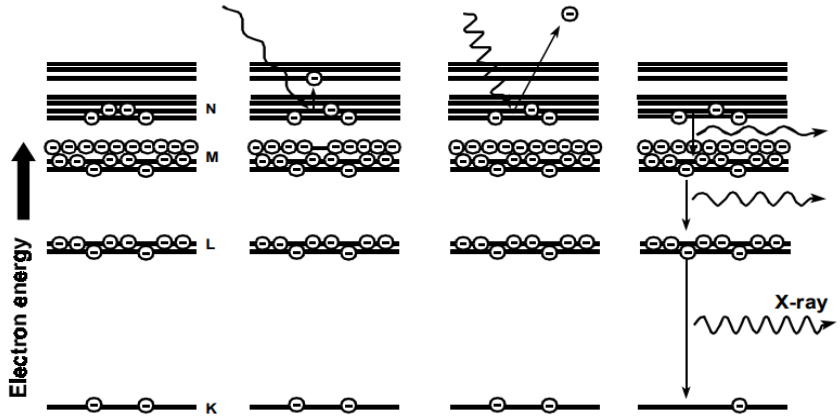

Figure 1. 2: Atomic energy levels [3]

Figure 1.2 shows some atomic energy levels at progressively greater energies corresponding to the so-called K, L, M, and N shells. A maximum of two electrons can fit in the K shell and eight in the L shell. The valency electrons, which determine the chemistry of the atom, are located in the outer, partially filled shell. The atom's ground state, in which the electrons occupy the lowest conceivable levels, is seen in Figure 1.2.a. Excitation happens when one of the electrons is boosted to a higher energy level by absorbing some incoming energy, as seen in Figure 1.2.b. When the absorbed energy is enough to completely evict an electron from the atom, this is known as ionization Figure 1.2.c. In this situation, the atom will still have a net positive charge. Figure 1.2.d illustrates the results of removing an electron from an inner shell. Other electrons from higher shells cascade down to fill the gap left behind, immediately filling it. They lose energy in the process equal to the energy difference between the shells, which is typically equal to a few keV. One or more typical X-rays, so named because of their energies, which are distinctive of the element in question, release this energy. When an atom fails to emit the expected X-rays, it releases its energy by ejecting another electron from the atom. Figure 3

depicts the auger emission process, which results in the formation of low energy electrons known as auger electrons.

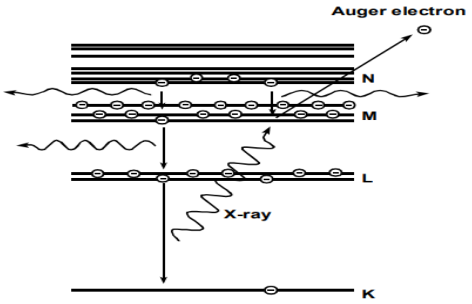

Figure 1. 3: Auger emission process [3]

I.2.2 Nuclear Energy Levels

In the same way that atomic electrons can only exist in well defined energy shells, the nucleons in an atomic nucleus also exist in specific energy levels. The situation in the nucleus is however complicated by the fact that there are two types of nucleon, protons and neutrons, to accommodate. Whereas the electrons are held in their shells by electrostatic attraction to the nucleus, the nucleons are held together by the much stronger nuclear force. This is a short range attractive force which exists between protons and neutrons and is strong enough to overcome the electrostatic repulsion which exists between the charged protons.

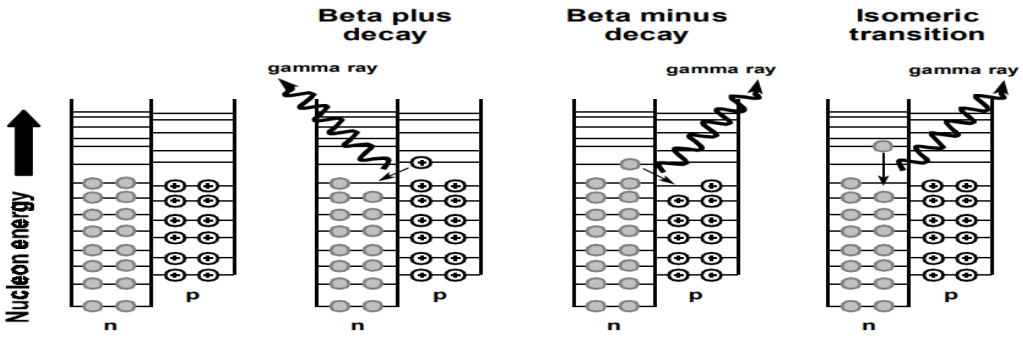

Figure 1. 4: Nuclear energy levels [3]

Figure 1.4 illustrates some schematic nuclear energy levels, with one set for protons and one for neutrons. Because charged protons repel each other in an electrical manner that uncharged neutrons do not, proton levels appear at somewhat greater energies than neutron levels. The energies involved are on the order of MeV, which is substantially greater than the energies of atomic electron levels. Each nuclear level, like atomic electrons, can only hold a specific amount of protons or neutrons, in this instance only two protons or two neutrons in each level. Figure 1.4.a depicts a nucleus with all of its lowest energy levels occupied. Because this nucleus

is stable, it is not radioactive. Because of the higher energy levels of the proton levels, stable nuclei will have slightly more neutrons than protons. Figure 1.4.b depicts a nucleus with much too many protons to be stable. It has a single proton with a high energy level and a vacancy for a neutron with a lower energy level. If it can convert a proton to a neutron, it can decay to a lower energy configuration, as depicted, and emit its excess energy as a gamma ray. This is known as beta plus decay. Figure 1.4.c depicts the inverse situation that occurs when a nucleus has too many neutrons for stability. In this situation, the nucleus can decay to a lower energy by converting a neutron into a proton, which is known as beta minus decay. Figure 1.4.d depicts a distinct example in which the nucleon configuration is energized and can decay by isomeric transition without changing the number of protons or neutrons.

Internal conversion is an event that can occur after gamma emission and is equivalent to auger emission in X-rays. Internal conversion occurs when a gamma ray released from a decaying nucleus gives up its energy to eject an atomic electron. An internal conversion electron is thus emitted instead of a gamma ray. Because this creates a vacancy in one of the electron shells, it will certainly result in the emission of distinctive X-rays.

It is important to note that X-rays and gamma rays are both high intensity electromagnetic radiation.

The only distinction between X-rays and gamma rays is their source. X-rays are produced by electron transitions between atomic energy levels, whereas gamma rays are produced by nucleon transitions between energy levels in the nucleus. Gamma rays contain more energy than X-rays, however this isn't always the case. When electrons are violently stopped, as in an X-ray tube, X-rays are created, however, this creates a range of energies rather than a single value[4].

I.3 Radioactive Processes

Figure 1.5 illustrates a simple nuclide chart created by showing the number of neutrons N on the horizontal axis and the number of protons Z on the vertical axis. As a result, each square represents a different nuclide. The black squares represent all of the non-radioactive nuclides that are stable along a diagonal line. Near the bottom of the chart, stable nuclei have almost equal amounts of protons and neutrons, but as you move up the chart, stable nuclei require more neutrons than protons. A careful examination also reveals that nuclei with an even number of protons and neutrons are more likely to be stable than those with an odd number. This behavior is exactly what the nuclear energy level model predicts Figure 1.5. Stable nuclides have an optimal number of protons and neutrons in their nuclei which reduces the nucleus' energy. The

other squares represent radioactive nuclides, also known as radionuclides. These nuclides are unstable because they lack the ideal ratio of protons and neutrons. They will decay by a variety of processes, transforming into various nuclides until they approach the line of stability.

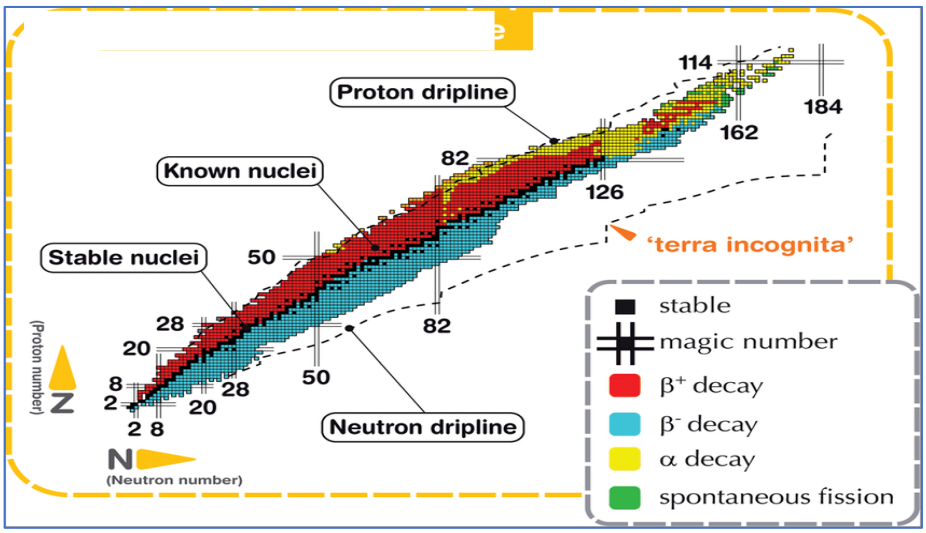

Figure 1. 5: A chart of nuclides [5]

Nuclides with too many protons as shown in Figure 1.4.b decay through positron emission also known as beta plus decay or by electron capture. Nuclides below and to the right of the stability line have too many neutrons as shown in Figure 1.4.c and decay by electron emission also known as beta minus decay. They are too heavy to be stable and either fission or alpha decay is used to decay them. The nuclide chart can be compared to a contour map of a valley with steep sides, illustrating the path that rocks will take to descend the slope, losing energy along the way until they reach the valley floor.

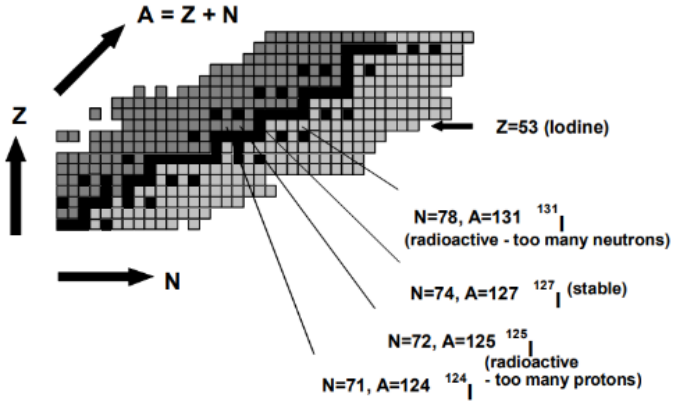

Figure 1. 6:Stability Chart for Iodine Isotopes (Z = 53)[6]

An enlarged version of the nuclides chart is shown in Figure 1.6 All of the iodine isotopes are present in the row that corresponds to Z=53 This row has only one stable isotope 127 I which corresponds to N=74. Because they have more protons than is ideal.

the nuclides 124 I and 125 I both reside above the line of stability and are radioactive. However, because it has an excessive number of neutrons, 131I, which is on the other side of the line of stability, is radioactive[5], [6], [7].

I.3.1 Electron Capture

By converting a proton into a neutron, a nuclide with too many protons can strengthen the stability of its nucleus. This can be accomplished, for example, if a circling electron of the nucleus is taken in by the nucleus. Figure 1.7 illustrates this procedure. A neutral neutron and a neutral neutrino are created when a negatively charged atomic electron from an inner orbit meets with a positively charged proton in the nucleus. The following can be written:

$$\boldsymbol{P + e^{-} = n + \nu} \qquad \text{(I.1)}$$

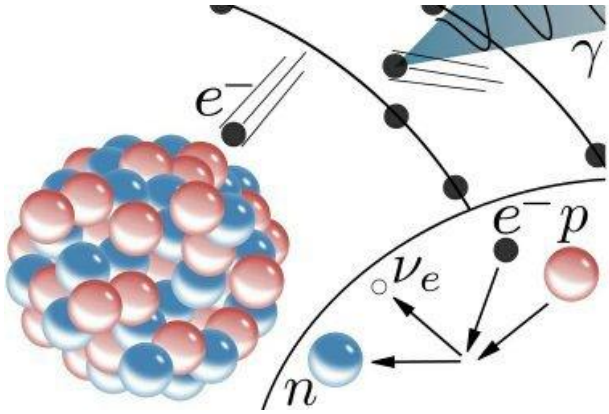

Figure 1. 7: Electron capture [8]

The atom's overall outcome is to increase N by 1 and decrease Z by 1 to maintain the same value of A, which is the product of Z and N. But the atom has transmuted from one element into another since Z has altered. Since the emitted neutrino has no charge very little mass, and is very unlikely to interact with anything else, it may typically be ignored in the decay. the process is known as electron capture decay or occasionally K capture since the caught electron originates from the K shell, the outermost circling electron shell. One electron will be absent from the K shell as a result of this, and additional electrons will come down right away to fill the void while generating distinctive X-rays. The exchange of a proton for a neutron in the

nucleus results in a change in the nucleons' configuration and the emission of gamma rays from the surplus energy of the nucleus.

An example of a nuclide that decays by electron capture is Iodine-125. We can write:

$$^{125}_{53}\mathbf{I} \rightarrow {}^{125}_{52}\mathbf{Te} + \mathbf{neutrino} + \mathbf{gamma\ ray} + \mathbf{X\ ray} \qquad \text{(I.2)}$$

This demonstrates how an iodine atom with 53 electrons, 53 protons, and 72 neutrons decomposed into a tellurium atom with 52 electrons, 52 protons, and 73 neutrons. It has done this by liberating energy from the atomic electrons and the nucleus in the form of gamma rays and X-rays, respectively.

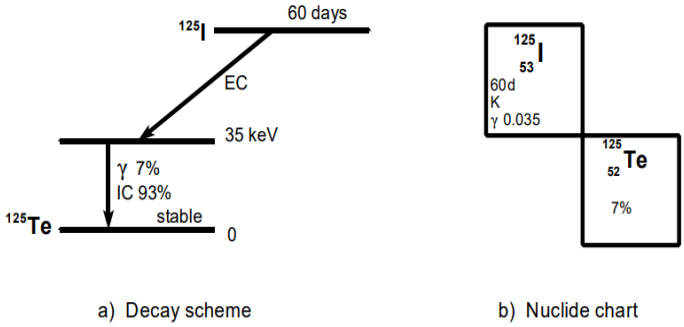

Figure 1. 8: Decay of Iodine-125 [8]

This decay scheme is depicted in Figure 1.8.a in a layout that is frequently found in reference materials. Increasing atomic numbers are indicated by moving to the right of the figure while increasing nuclear energy levels are represented by moving up the diagram. The half-life of the state that represents 125I at the top of the diagram is 60 days. Because the atomic number has dropped by one, it decays via electron capture to 125Te, which is at a lower energy level and is located further to the left on the diagram. 35 keV more energy than the lowest possible energy level is present in the 125Te nucleus' final state. In 93% of decays, an internal conversion electron is released in place of the 35 keV gamma ray that would have been released. The result is a stable ground state or the nucleus in its lowest energy state.

The data shown in Figure 1.8.b corresponds to what would be shown on a detailed chart of the nuclides. The box for 125I displays that it has a half-life of 60 days (shown as 60d), decays by electron capture (represented by K for K capture), and releases a 35 keV gamma ray (represented as 0.035 MeV). The resulting nuclide will always be the box one down and one to the right on the chart of the nuclides because electron capture decay always results in a reduction in Z by one and an increase in N by one. This is discovered to be 125Te, which is stable and

lacks any evidence of degradation. The 7% displayed in this box is the natural percentage[8], [9].

I.3.2 Electron Emission (Beta minus decay)

By changing a neutron into a proton, a nuclide with too many neutrons can approach stability. It must also emit an electron to balance charge and a neutrino to balance energy. This electron emission process is the exact opposite of the electron capture decay process[10]. One way to write it is as:

$$n \rightarrow P + e^{-} + \bar{\nu} \qquad \text{(I.3)}$$

where is another type of neutrino that can be disregarded, as before. Again, there is no change in A as the net effect for the atom is an increase in Z of 1 and a decrease in N of 1. The atom has transformed into the element with the next higher atomic number as indicated by the change in Z. Because the decayed electron is what is seen as a beta particle, this process is also known as beta minus decay (or just beta decay for short). Similar to electron capture decay, the resultant nucleus may release one or more gamma rays as a result of the surplus energy. It should be noted that, unlike electron capture decay, this decay does not involve atomic electrons, and as a result, no X-rays are usually released (although there could be some if an internal conversion process occurs later)[8].

One nuclide that decays by beta minus decay is iodine-131. We are able to write :

$$^{131}_{53}\mathrm{I} \rightarrow {}^{131}_{54}\mathrm{Xe} + \textbf{neutrino} + \textbf{beta particle} + \textbf{gamma ray} \qquad \text{(I.4)}$$

A xenon atom has replaced an iodine atom due to an increase in atomic number of one. It did this by emitting a beta particle, an undetected neutrino, and some gamma ray energy from the nucleus.

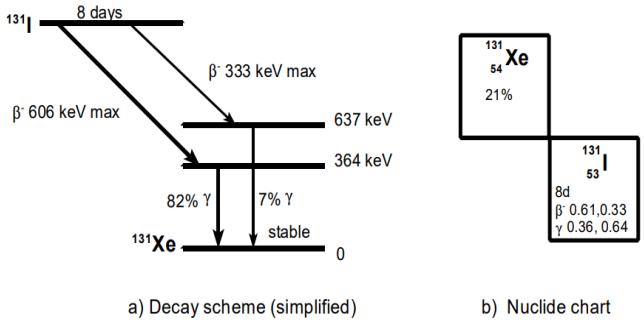

Figure 1. 9: Decay of Iodine-131 [10]

This decay method can be seen in a simplified form in Figure 9a. The state of 131I decays by beta disintegrating to one of two forms of 131Xe and has a half-life of 8 days. Because the atomic number has increased by one, these are located further to the right on the diagram. The decay may either generate a beta particle with a maximum energy of 606 keV, which would excite the 131Xe nucleus to a state that is 364 keV above the ground state, or a beta particle with a maximum energy of 333 keV, which would excite the nucleus to a state that is 637 keV above the ground state. These are beta particle energies at their highest. The beta particles' energy can actually range from zero to this maximum, with a usual average of one-third of the maximum. Pauli hypothesized that neutrinos must exist even though they have not been discovered since they are responsible for removing the residual energy. The excited states of 131Xe instantly decay to the ground state, with gamma rays emitting energy of 364 keV in 82% of cases and 637 keV in 7%. For the sake of clarity, this condensed version of the decay scheme has not included the additional outcomes associated with the other 11% of decays.

The data shown in Figure 9b is identical to what would be shown on a detailed chart of the nuclides. The box for 131I displays its 8-day half-life and beta minus decay, which produces beta particles with maximal energies of 0.61 and 0.33 MeV (in decreasing order of likelihood). Additionally, 0.36 MeV and 0.64 MeV gamma rays are released. The resulting nuclide will always be the box one up and one to the left on the nuclide chart since beta minus decay always results in a rise of Z by one and a drop of N by one. This is 131Xe, which has a steady composition and a 21% natural abundance.[10], [11], [12]

I.3.3Positron Emission (Beta plus decay)

One type of decay that could happen when a nucleus contains too many protons was already discussed : electron capture. Positron emission is a different process that also occurs in these kinds of nuclei. A proton transforms into a neutron, positron, and neutrino throughout this process:

$$\boldsymbol{P \rightarrow n + e^{+} + \nu} \qquad \text{(I.5)}$$

It is sometimes referred to as beta plus decay because it is very similar to regular beta decay but with the proton and neutron roles reversed and the emitted particle being positively charged rather than negatively. As with electron capture decay, the net effect of positron emission is to decrease the Z of the atom by 1 and increase N by 1 so that there is no change in A.

Usually, the positron that is released only travels a short distance before stopping in the substance. Since it is an antiparticle of a regular electron, it will then instantly annihilate with an electron from the material it is surrounded by. The positron and the electron are both destroyed during the annihilation, but their energy, which is equal to 511 keV , is not lost. Two 511 keV each gamma rays are created from the energy, and they both shoot off in the opposite direction. The annihilation radiation is what is causing this[13].

Iodine-124 is a case study of a radionuclide that can decay via positron emission, albeit this only occurs in about 25% of decays; the other 75% occur through electron capture. The positron emission decay mode can be expressed as:

$$^{124}_{53}\mathrm{I} \rightarrow {}^{124}_{52}\mathrm{Te} + \textbf{positron} + \textbf{neutrino} + \textbf{gamma ray} \qquad \text{(I.6)}$$

then, after the annihilation of the positron :

$$\textbf{positron} + \textbf{elecrton} \rightarrow \textbf{two 511 gamma ray}$$

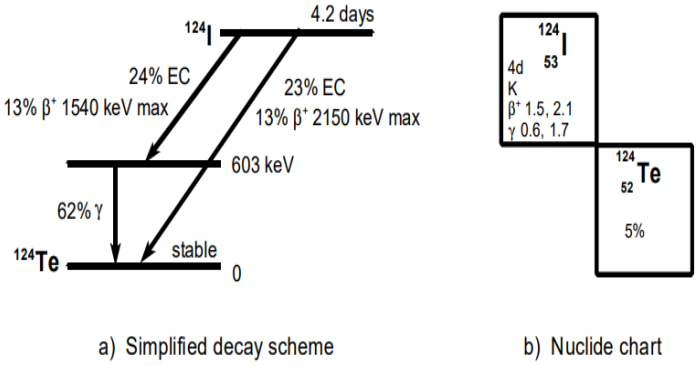

Figure 1. 10: Decay of Iodine-124 [10]

has a half-life of 4.2 days, can either decay to the ground state or an excited state of 124Te, which will emit a 603 keV gamma ray. 24% of decays involve an electron capture to a level of 603 keV, and 23% involve an electron capture that occurs directly to the ground state. With a maximum beta plus energy of 1540 keV and another 13% with a maximum beta plus energy of 2150 keV, positron emission accounts for 13% of decays.

However, the majority of them eventually decay down to the 603 keV level. The remaining 27% of decays are by electron capture to higher energy levels not depicted on this simplified picture. As a result, 62% of all decays result in the emission of a 603 keV gamma ray, and additional, less frequent gamma ray emissions from the upper levels are also present but are not depicted. In all, 26% of decays involve positron emission, which produces two annihilation gamma rays for each decay[14].

I.3.4Parents and Daughter

One nuclide has changed into another of a different element in each of the aforementioned cases of radioactive decay. The first nuclide is referred to as the parent, and the one it degrades into is the daughter. The daughter nuclide in the examples currently has been stable, preventing further decay even though the parent nuclide has been radioactive. However, The daughter nuclide may occasionally be radioactive as well, though this is not always the case. This can result in chains of multiple generations of radioactive nuclides until a stable one is obtained, as Rutherford and Soddy discovered in their investigations of radioactivity. This isn't always true because the daughter's nuclide could occasionally also be radioactive. Rutherford and Soddy discovered in their studies of radioactivity that this can lead to chains of several generations of radioactive nuclides before a stable one is reached. Once a daughter's nuclide has reached stability, further decay cannot occur[4].

Strontium-90, which decays with a half-life of 28 years by electron emission (beta minus decay) into yttrium-90, is a straightforward example of a parent with a radioactive daughter. This in turn degrades via electron emission into zirconium 90, which is stable, and has a half-life of 64 hours[15]. This can be written as:

$$^{90}_{38}Sr \rightarrow {}^{90}_{39}Y + beta\ particle \qquad (I.7)$$

Daughter

$$^{90}_{40}Zr + beta\ particle$$

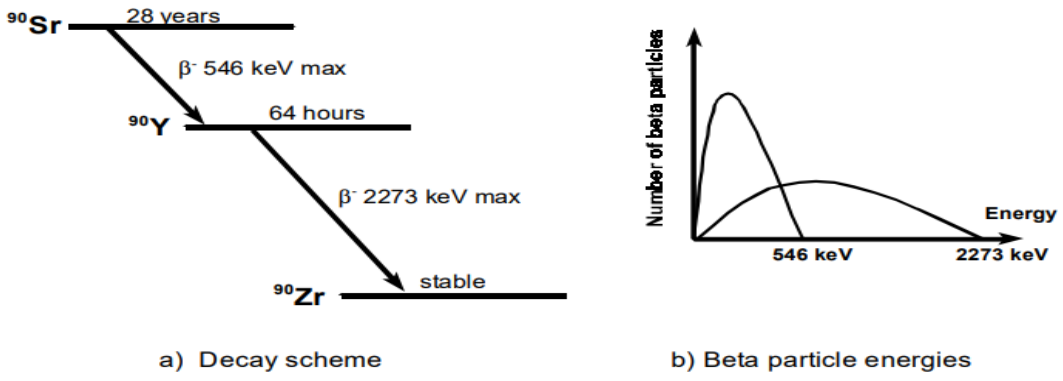

Figure 1. 11: Decay of Strontium-90 [10]

This decay pattern is shown in Figure 1.11.a, where 90Sr is the parent and 90Y is the daughter. Even though the daughter has a lower half-life than the parent, it is never able to totally decompose since the parent's decay constantly produces new daughter atoms. In fact, an equilibrium is attained whereby the decay of the parenthesis results in the gain of a new atom for each daughter atom that is lost by decay. As a result, at equilibrium, the daughter's and the parent's disintegrations per second are equal in number. In other words, the daughter's activity is equal to the parent's activity. As a result, every source that contains 90Sr will also include an equivalent amount of 90Y[16].

The parent 90Sr decays to beta particles with a maximum energy of 546 keV, as depicted in Figure 1.11.a. Beta particles with a maximum energy of 2,273 keV are created during the daughter 90Y's decay. Figure 1.11.b illustrates how the quantity of beta particles released varies with their energy and reveals that the beta particles actually have a range of energies from zero to the maximum. Since the beta particles from a source like this have a well-defined range in tissue, only tissues adjacent to the source will be irradiated, making it useful for external therapy in medicine. The number of beta particles at each energy will decide how far away from the source the dose is distributed, with the higher energy particles traveling further[17].

I.3.5 Isomeric transition and Metastable States

There has been a change in both Z and N in every decay example that has been investigated thus far. An isomeric transition is a decay in which Z or N remains unchanged. According to Figure 1.4.d, it corresponds to the decay from an excited nuclear energy level. This excited nuclear state can be visualized on the nuclide chart Figure 1.5 as being represented in a third dimension perpendicular to the N and Z plane. The nuclide is kept in the same square on the chart throughout an isomeric transition by a change in the paper's plane. A gamma ray will be released as a result of an isomeric transition, but without any additional particles emissions [18].

Other decay mechanisms depend heavily on nuclear transitions from an excited state. Nuclear energy levels at 364 keV and 637 keV, for instance, rapidly decay to the ground state in the 131I decay scheme depicted in Figure 1.9.a Because these transitions take place concurrently with the beta emission, they are regarded as a component of the same decay.

However, on sometimes, an excited nuclear energy level may last for several seconds or even hours. When this occurs, the excited state is referred to as being metastable and can be regarded as a distinct nuclide in and of itself. This is accomplished by following its mass number with the letter "m" (for metastable).

Figure 1.12.a's depiction of the decay of 99Mo provides an example of a metastable state in action. 99Mo decays to 99Tc by electron emission over a period of 67 hours. Some decays result in the ground state of 99Tc extremely quickly, which has a half-life of 200,000 years and is hence nearly stable enough on a human scale for its activity to be disregarded. With an energy 142 keV above the ground state, one of the excited states of the 99Tc nucleus is metastable and has a half-life of 6 hours. It is known as 99mTc and is the metastable state in which about 85% of 99Mo decays leave the nucleus[19].

We can display the decay scheme of 99mTc separately as shown in Figure 1.12.b since it has a half-life long enough to exist on its own. This is an excellent illustration of isomeric transition. The 142 keV energy level decays directly to the ground state of 99Tc in roughly 2% of decays, however this transition is always internally converted , therefore no gamma rays are produced and only one internal conversion electron is released. In 98% of decays, the nucleus first transitions to a level of energy at 140 keV, which happens once again by internal conversion. This energy level decays to the ground state and undergoes internal conversion in 10% of decays, resulting in the emission of a 140 keV gamma ray in 88% of decays. A single energy (monoenergetic) gamma ray is produced by this decay, with the exception of a tiny number of low energy internal conversion electrons. As a result, 99mTc is a very helpful radionuclide for nuclear medicine diagnostic imaging. Furthermore, despite having a 6-hour half-life, 99mTc is constantly present due to the degradation of its parent 99Mo. The 99mTc activity of a generator holding 99Mo will shortly reach parity. The fact that Tc is soluble in saline solution whereas Mo is not can be used to chemically separate the daughter Tc from the parent Mo because they are distinct elements[19], [20].

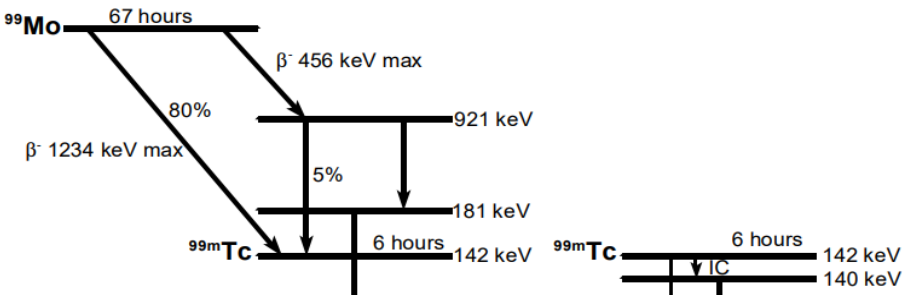

Figure 1. 12: Decay of Molybdenum-99 [10]

I.3.6Alpha decay and fission

The extreme top right nuclides on the nuclide chart are unstable because they are simply too heavy. The short-range nuclear force that binds the nucleus together. Too many nucleons cause the nuclear force to be ineffective at holding the individual nucleons together, and the repelling electrostatic force between the protons takes precedence instead. There are two possible outcomes in this case[18].

A group of two protons and two neutrons are emitted from the nucleus during alpha decay. These particles form a very stable group known as an alpha particle that is held together by the nuclear force. Alpha particles are actually doubly ionized (two electrons removed) helium atoms since this group of two protons and two neutrons also serves as the nucleus of a helium atom. Z and N are both reduced by two as a result of alpha decay, which causes a nuclide to move left and right by two positions in the nuclide chart. Although many of the naturally occurring radionuclides Rutherford and Soddy studied showed alpha decay, alpha-emitting nuclides have little practical use in medicine[8], [21].

For heavy nuclides, nuclear fission is an alternate decay process in which the nucleus breaks into two roughly equal fragments. Nuclear energy is produced by this process, however radionuclides that fission have no immediate medical applications. However, the plentiful fission products from the fission of 235U include the radionuclides 131I and 99Mo, two useful radionuclides that we have already highlighted. Just separate them from the rest of the radioactive fission pieces in the nuclear waste[18].

I.4 Half-life

Early studies by Becquerel and the Curies, as well as Rutherford and Soddy, had demonstrated that a radioactive source's activity decreased over a time period that varied for each chemical. The half-life of the source is the length of time it takes for an activity to lose half of its initial value. It is not true that the activity will have completely decreased after two half-lives because the activity does not decrease at a constant rate. Instead, the activity declines at a steadily decreasing pace, halving in every half-life[22].

A graph of a source's activity over time is shown in Figure 13. If the activity starts off at a value of A0, it will have decreased to half of A0 after one half-life. The activity will have decreased to one eighth of A0 after three half-lives and to one quarter of A0 after two half-lives. It is evident that the activity is declining more slowly and will, in theory, never ever hit zero.

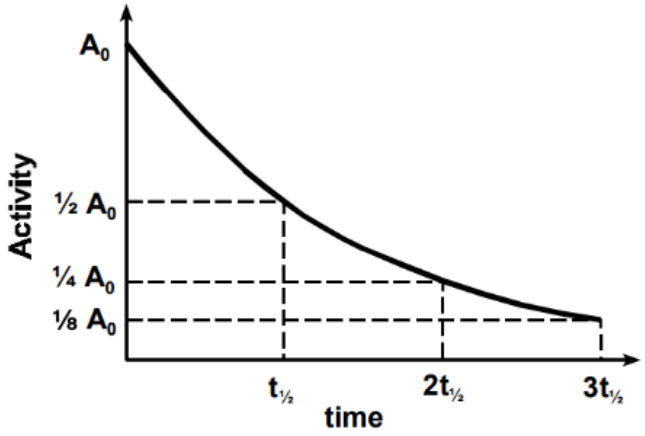

Figure 1. 13: Decay of Activity[22]

the activity will have decreased to a negligible level after a suitably extended period of time. This type of curve is described as having an exponential form, and hence, radioactivity is considered to experience exponential decay. The formula can be used to describe it mathematically[23].

$$A_t = A_0 e^{-0.693\frac{t}{t_{1/2}}} \qquad \text{(I.8)}$$

where the half-life is $t_{1/2}$.$A_0$is the activity at time zero, while A_t denotes the activity at time t. The function ex is pre-programmed into the majority of scientific calculators. The sign "e" stands for a number that is the base of natural logarithms. Despite not being a straight line when displayed regularly, as in Figure 1.13, the exponential curve has the unique virtue of appearing

as one when plotted on a logarithmic vertical axis, as in Figure 1.14. This makes it simple to check off the action whenever you want[22].

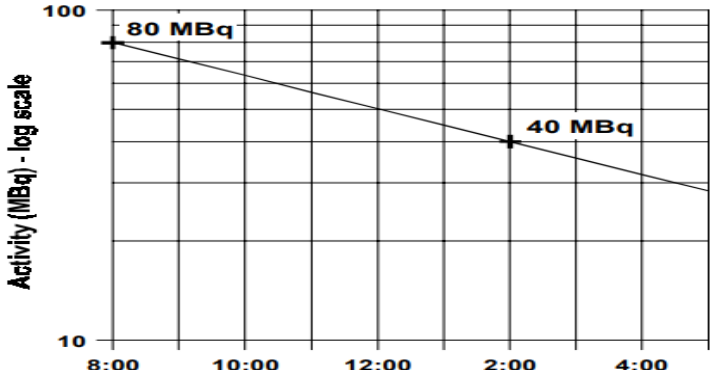

Figure 1. 14: Decay on a logarithmic scale [18]

Figure 1.14 gives an illustration of the decay of a source having a six-hour half-life. Using specialized log-linear graph paper, the vertical axis was plotted on a logarithmic scale and displayed an initial activity of 80 MBq at 8:00 a.m. This must have decreased to 40 MBq after one half-life (2:00 pm) so that these two points (on the logarithmic graph scale) can be plotted and connected by a straight line. The activity can then simply be read off the graph at any time; for instance, at noon, the source's activity would be 50 MBq.

By using a calculator and the aforementioned exponential equation, an identical result can be achieved without the need for a graph. The exponent of the exponential, which is represented by the superscript -0.693 t / t12, is the first item we must determine. We first calculate t divided by t12, which is the ratio of the half-life (6 hours in this case) to the time since the activity was measured (4 hours in this case). We next enter this result on the calculator by entering 4, dividing by 6. After that, we multiply the result by 0.693 and use the calculator's +/- button to make the result negative. The result will be -0.46, which is the required exponent. Then, multiply the result by A0 (in this case, 80) using the calculator's ex function, which should yield a value of 0.63, to obtain the answer of 50.4[18].

I.5Interaction of radiation with matter

I.5.1The nature of the interaction of radiation with matter

Radiation, whether in the form of particles such as neutrons, protons, alpha and beta particles, or in the form of electromagnetic radiation such as gamma rays and In general, all interactions that occur with radiation with matter, whether they lead to complete or partial absorption or

dispersion of radiation energy, work to ionize the atoms of the matter by causing them to lose a number of electrons orbiting the atom, leaving them in a state of ionization as a result of the loss of these electrons. The atom in this case is positively charged as a result of this loss. Or through excitation by raising the electrons to higher orbits to leave the atom in an excited state, or by transforming radiation from one form to another, such as photons resulting from the process of annihilation of the electron and positron. But in general, charged particles lose most of their energy through the ionization process, while neutrons and photons do not lose their energy through the scattering and absorption process[24].

The nature of the interaction of radiation with matter:

There are several ways to express the interaction of radiation with matter, which describes the loss of energy by particles as it passes through matter. One of these methods is the stopping power, which is symbolized by the symbol Sand which is defined as the amount of the particle losing its energy dE along its path dx in the material, which can be written as follows mathematically:

$$S = -\frac{dE}{dx} \qquad (I.9)$$

The negative sign in the equation means that there is a decrease in the energy of the particle as it crosses a distance dx in the material. The linear rate at which particles lose energy in matter along their path, or the ability of the medium to stop these particles. Using relative quantum mechanics, the scientist Bethe was able to derive a mathematical formula for the ability of matter to stop charged particle heavy is as follows and known as the Bethe formula for stopping power[25]:

$$\frac{\partial E}{\partial x} = \frac{4\pi z^2 e^4 n}{mc^2\beta^2}\left[\ln\frac{2mc^2\beta^2}{I(1-\beta^2)} - \beta^2\right] \qquad (I.10)$$

Where z the atomic number of the particle, e the charge of the electron, n the number of electrons per unit volume in the substance, m its mass of the electron at rest, $\beta = v/c$ the speed of the electron over the speed of light, and I the average excitation energy of the atoms of the substance. Therefore, it becomes clear to us that the stopping power depends on the charge, the number of protons of the particle, and the speed of the particle, all of which are properties of the charged particle. As for matter, it depends on the number of electrons in the matter and on its average excitation energy[26].

The nature of the reaction can also be expressed by a linear transfer of energy to the material LET $= -(dE / dL)$. This expression is similar to the expression for stopping power, as the linear transfer of energy to the material is equal to the stopping ability, with the difference that the first expresses the process of the particle losing its energy within a certain size. The last one expresses the process of giving energy to the absorbing medium or where exactly the particle's energy was absorbed. Also, the second expresses the rate of energy that was transferred locally to the material medium within a specific energy dE and a specific distance dL, and locally it expresses the place where the collision and transfer process occurred. The energy from the particle to the matter or the place very close to it, noting that the expression transferred locally may refer to the maximum of the path or to the maximum energy determined for the energy of the particle lost in the matter[27].

In addition to these two expressions, there is also the specific ionization SI, which is the number of ionic pairs formed per unit distance, meaning $(SI = dN/ dx)$, where N is the number of ion pairs formed along the path dx. The average energy required to form one pair of ions in air is 33.97 MeV, which is It is usually approximated to the number (34e/ip).

The term kerma is used to express interaction, and kerma is an abbreviation for the kinetic energy released in matter. It is one of the units of expression for radiation as well. It expresses the amount of exposure to radiation in rad units, which is the amount of energy given per unit of exposed mass. Radiation through secondary particles resulting from non-particle radiation such as gamma rays and Radiation.

I.5.2Interaction of alpha particles and charged particles with matter:

Alpha particles and charged nuclei have a large electrical charge because they do not have any orbital electrons when they emerge from the nuclear reaction. They interact with matter through ionization processes with the atoms of the material medium as a result of the forces of electrical attraction between them and the electrons of matter, as they transfer part of their energy to these electrons so that they become It is capable of escaping from its orbit and leaving the atom in a state of ionization. In this case, an ion pair is formed, which is the escaping electron and the ionized atom, in addition to the energy of the escaping electron, which may be sufficient to interact with another electron and remove it from its orbit as well. Because of the high charge that these particles carry, their path is characterized by a high density of ionized atoms, and the energy transfer is very large per millimeter, so they are characterized by a small range of their

path, which is within The micrometer inside the substance is able to determine the density of the ionization of the atoms of the substance.

When alpha particles penetrate the substance, they begin to lose their energy by ionizing the atoms of the substance, and this leads to a decrease in their speed, and thus it gives them more time to spend near the atoms of the substance, which increases the possibility of interaction occurring between them and the atoms of the substance until they lose all their energy and stop, after which they carry electrons from the atoms. The substance becomes an electrically neutral helium atom. An alpha particle with energy MeV (5-7) can form ion pairs of up to 50-80 thousand ion pairs per cm at the end of its path. This property is known as the peak of the Bragg curve, which is characterized by the appearance of a peak at the end of the curve as a result of the increase in ionization concentration at the end of the path when the relationship is represented graphically[28]. Show the number of ions per unit distance m The distance and the Bragg peak are shown in Figure 1.15.

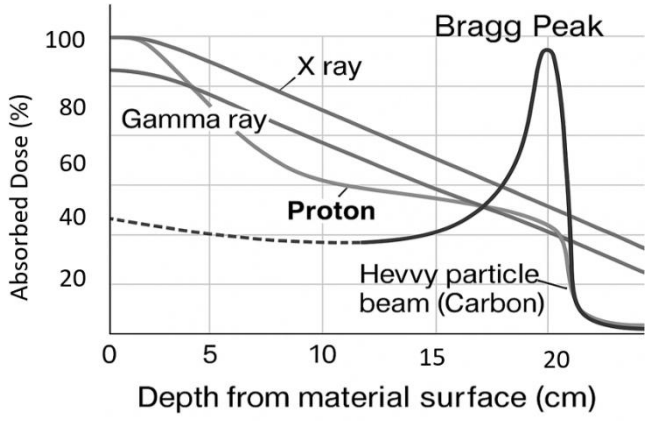

Figure 1. 15.the Bragg peak [28]

This property has found its way into medical applications, where it is currently used to treat cancerous tumors with protons, but on a limited scale, as this peak is focused on the area to eliminate cancer cells. Protons are used instead of alpha particles because their range in living tissue is greater than the range of alpha particles. Thus, protons can reach cells located at greater depths, which are difficult for alpha particles to reach, which have limited range, as they can be stopped by the outer skin layer (the non-living layer). And do not reach Deep tissue.

I.5.2.1The range of alpha particles and heavy charged particles

Alpha particles are considered mono-energetic, meaning that when they are emitted, all particles emitted from the nuclei of the same material are equal in energy, so they must have the same range in the air or in the material. For example, if we place a source of radioactive alpha particles, and place a very thin barrier in front of it, as shown in Figure 1.16, and at the other end we place a radiation detector to measure the number of these particles, we will find that almost all alpha particles have the same range, and the word "approximate" here means that there is an average range for these particles, and it may increase or decrease by a very small amount as a result of the irregular spread of these particles (dispersion), and this difference falls statistically within the normal distribution of measuring these particles, as shown in Figure1.17. The range of alpha particles is usually measured in centimeters in the air, as there is a mathematical relationship between the energy of the alpha particle and its spread in the air, and this relationship is as shown below:

$$\mathrm{R(Range)} = 0.325E^{3/2} \qquad \text{(I.11)}$$

Where R is measured in centimeters of air and E is measured in million electron volts.

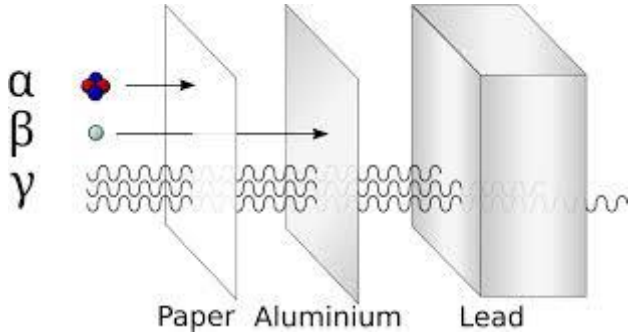

Figure 1. 16.matter penetration [29]

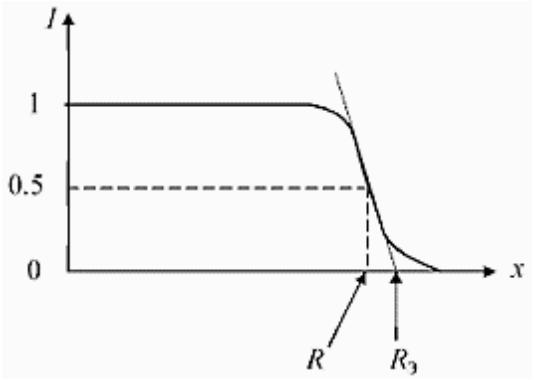

Figure 1. 17.Distribution curve of alpha particles subsequent to material penetration[28]

The range of alpha particles in air can also be used to determine their presence in other materials using the Bragg-Clement rule, which is as follows:

$$R_m = \left(\frac{\rho_{Al}}{\rho_{air}}\right) \times R_a \times \sqrt{\frac{M}{M_a}} = 3.2 \times 10^{-4} \times \sqrt{\frac{M}{\rho_m}} R_a \qquad \text{(I.12)}$$

For the purposes of radiation protection, and in the case of living tissue, the mass stopping power is mostly the same value In air, because there are similarities in the components, the alpha range in tissues is equal to the alpha range in air, multiplied by a ratio The density of air into the fabric is as shown below:

$$R_{tissue} = \frac{\rho_{Al}}{\rho_{tissue}} R_a \qquad \text{(I.13)}$$

It is also possible to calculate the range of any charged particle in relation to the range of the proton in the material if this range is defined as coupling With the speed of the particle, which can be known from its kinetic energy through the following relationship:

$$R(\beta) = \frac{M}{Z^2} \times R_P(\beta) \qquad \text{(I.14)}$$

Where$\beta = \text{v} / \text{c}$ the speed of the particle over the speed of light and this value can be found from the kinetic energy and M the mass of the particle and $R_P(\beta)$the range of protons in matter at the energy equivalent to the particle's velocity is as follows:

$$T = Mc^2 \left(\frac{1}{\sqrt{1-\beta^2}} - 1\right) \qquad \text{(I.15)}$$

I.5.3Interaction of beta particles with matter

The beta particle is an electron emitted from inside the nucleus and its mass is very small compared to other particles, reaching 3.1×10^{-28} in a state of rest, and the small mass of the particle gives it super speed when its energy is about a million an electron volt and its speed may be close to the speed of light. The beta particle interacts with matter in several ways, including direct ionization Delta rays, which result from ionized electrons, the emission of scavenging rays, and Cherenkov radiation[29].

When a beta particle enters matter, its kinetic energy and negative charge affect one of the orbital electrons through electrical repulsion, displacing it from its place, and obtaining kinetic energy gained from the original energy of the entering particle, leaving the atom in a state of ionization. The energy gained by this electron may reach, at most, half the value of the particle's energy inside. Since the mass of the beta particle is equal to the mass of the electron, its

deflection is large, so its path is tortuous, which leads to an increase in its length, and its ionization intensity is less due to its high speed, so its range in matter is greater due to the lower rate of its energy loss. For example, a beta particle with an energy of 3 million electron volts has a range in the air of about 100 cm and works to ionize 50 ion pairs per cm. The collision-stopping ability of a beta particle differs from that of alpha particles for two reasons. The first is that the beta particle can lose most of its energy (half the energy) during a single interaction with one of the orbital electrons. The second reason is that the beta particle is completely identical to the orbital electron, which makes it difficult to distinguish between them. In this case the situation is that the orbital electron receives the least energy, provided that it does not exceed half, unlike the positron, so that its entire energy can be transferred to the orbital electron. Beta particles also lose energy through the interaction Collision with matter electrons or through scattering rays, as the particle's very small mass makes it accelerate more quickly in the electrical mechanism of the positive nucleus, which makes it difficult to ignore the amount of energy lost from During the braking rays , so the Bethe equation to calculate the ability of the material to stop beta particles by A direct collision is as follows[30]:

$$-\frac{\partial \mathrm{E}}{\partial \mathrm{x}} = \frac{4\pi z^2 \mathrm{e}^4 \mathrm{n}}{\mathrm{mc}^2 \beta^2}\left[\ln \frac{\mathrm{mc}^2 \tau\sqrt{\tau+2}}{\sqrt{2}\mathrm{I}} + F^{\mp}(\beta)\right] \qquad \text{(I.16)}$$

Where $\tau = \mathrm{T}/mc^2$ and T is the kinetic energy of the particle and

$$F^{-}(\beta) = \frac{1-\beta^2}{2} + \frac{1}{2(\tau+1)^2}\left[\frac{\tau^2}{8} - (2\tau+1)\ln 2\right] \qquad \text{(I.17)}$$

For the negative electron and the positive positron:

$$F^{+}(\beta) = \ln 2 - \frac{\beta^2}{24}\left[23 + \frac{14}{\tau+2} + \frac{10}{(\tau+2)^2} + \frac{4}{(\tau+2)^3}\right] \qquad \text{(I.18)}$$

The total stopping power is the sum of the collision stopping power and the radiative stopping power resulting from the rays The ratio of collision stopping power to radiation is according to the following equation:

$$\frac{(-dE/dx)_{col}}{(-dE/dx)_{rad}} = \frac{ZE}{800} \qquad \text{(I.19)}$$

From the above equation, it becomes clear to us that there is a critical energy for the particle during its interaction with matter, such that the energy loss through radiation becomes equal to the energy loss through collisions. For example, when beta particles interact with oxygen gas,

which has an atomic number of 8, the radiation energy loss is equal to the collision energy loss. When the energy of the beta particles reaches 100 million electron volts, this matter is important in radiation care and radiation protection when designing radiation shields for beta sources, as it must be taken into account that beta particles, when interacting with the shield material, will produce scavenging rays emerging from the shield material, and the value of these rays depends on the energy Beta particle and on the atomic number of the shield material so it is preferred Use shields with low atomic number beta particles to avoid the occurrence of these rays. The outcome can be estimated These rays are determined by the energy of beta rays and the atomic number of the shield through the following equation:

$$Y = \frac{6\times10^{-4}ZT}{(1+6\times10^{-4})ZT} \qquad \text{(I.20)}$$

Where Z is the atomic number of the substance and T is the energy of the beta particle[31].

I.5.3.1 Range of beta particles

Beta particles in matter are attenuated in several ways, the most important of which is the ionization of the atoms of the material, followed by flaring radiation. The amount of attenuation of beta rays by matter is dealt with by noting the change in the intensity of the radioactive source when we add a different thickness of aluminum each time, for example, which is measured in grams per unit. Square centimetres. Through the results of the experiments, a mathematical formula was developed to determine the distance these particles travel before they are completely stopped after losing their energy. The range is measured in grams per square centimeter. From these experiments it was shown that beta particles, which have an energy of 0.01 up to 2.5 million electron volts, its range in matter is as shown in the following equation[29]:

$$\mathrm{R} = 412\mathrm{E}^{1.265-0.0954\ln\mathrm{E}} \qquad \text{(I.21)}$$

Or in another and more general way, the range of beta particles with energies greater than 0.6 million electron volts can be found from The following equation:

$$\mathrm{R} = 542\mathrm{E} - 133 \qquad \text{(I.22)}$$

For beta particles with energies exceeding 2.5 million electron volts, the range is:

$$\mathrm{R} = 0.53\mathrm{E} - 0.106 \qquad \text{(I.23)}$$

Figure 1.18. shows the range of beta particles in different materials according to their energy.

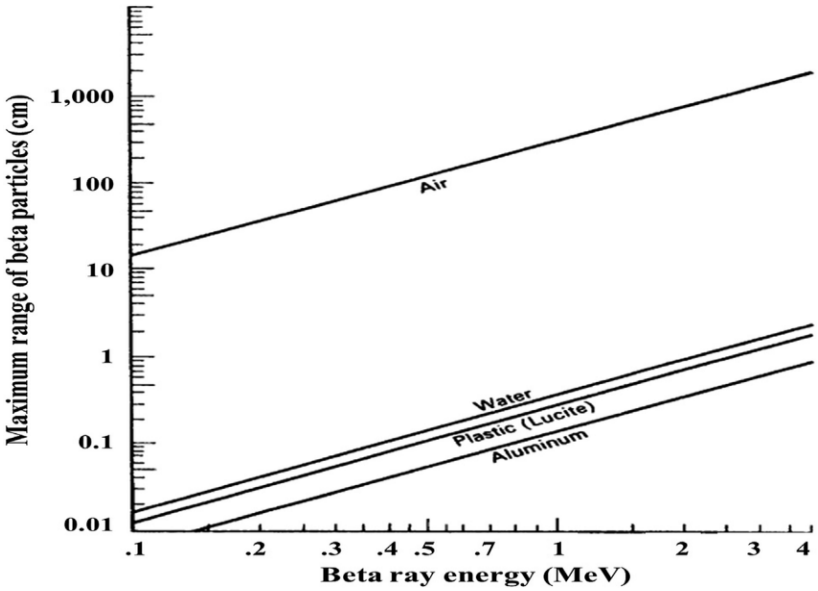

Figure 1. 18. Range of beta particles in different materials[29]

I.5.4 Interaction of Gamma Rays and X-rays with Matter:

The interaction of electromagnetic radiation with matter is more complex than the interaction of other types of radiation with matter because these rays are wave energy and their speed reaches the speed of light. They have no rest mass and do not carry an electrical charge. In general, the interaction of a photon with matter is statistically governed by the probability of its interaction per unit distance it travels in the matter, and this probability depends on the type of matter and the energy of the photon of the rays. When a photon interacts with matter, there is a possibility of it being absorbed and a possibility of it being scattered by changing its path, losing part of its energy, or even passing it without interacting remotely. And despite Its interaction depends on statistical probability, but this probability falls within four main mechanisms for the interaction of photon radiation with matter, and these mechanisms are coherent scattering, the photoelectric effect, Compton scattering, and binary production[30].

I.5.4.1 Coherent dispersion

This scattering is known as conventional scattering, and it occurs when a photon passes next to an orbiting electron, causing it to oscillate with the photon wave, which leads to the radiation of the energy it gained from the original photon. The value of the energy it emits is that this oscillating electron is equal to the energy of the absorbed photon, except that it is in a direction different from the original direction. For the absorbed photon, that is, the energy of the photon is absorbed and then it is radiated again with the same energy that was absorbed, with the difference that it is in a direction different from the original direction at small angles. The probability of this interaction occurring is higher in materials with a large atomic number and

with low-energy photons, and practically, there is no change in energy and a limited change in direction. Consider this type of interaction as having no change in energy and a limited change in direction[27].

I.5.4.2 Photoelectric Effect

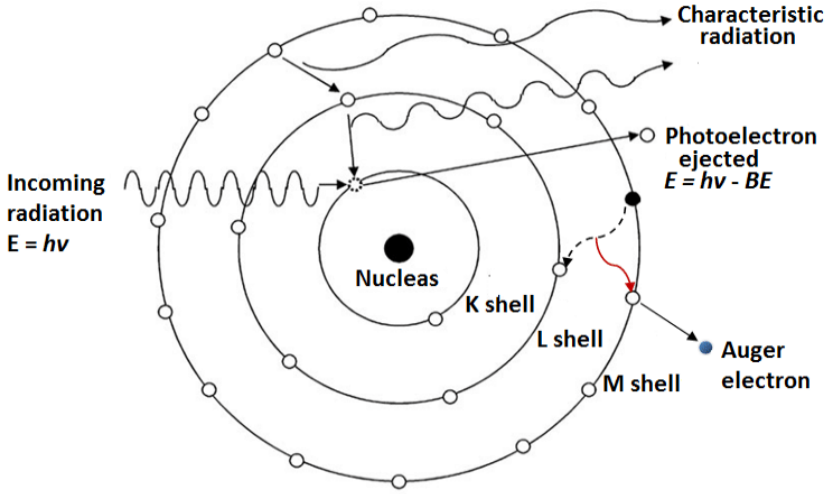

Figure 1. 19.The photoelectric effect [27]

The photoelectric effect is the interaction of a photon with one of the electrons of the material's atoms, which leads to the removal of H from its position. This electron takes the entire energy of the photon in the form of its kinetic energy, except for the energy expended to get rid of the energy of binding an electron in its orbit with the atom. This process can be described mathematically by considering that there is a photon with an energy equal to E $= hv$ interacting with the material, then the energy of the displaced electron will be equal to (E_{etc} $= hv - E$) where E is the energy of binding the electron in the orbit, so for this interaction to occur, the energy of the photon must be greater than the energy of binding. This interaction can happen to any of the electrons in the different orbits K, L, M, N in the atom[25].

The larger the photon and the larger the atomic number, the more likely the energy will be absorbed over a greater distance, which reduces the probability of absorption Energy is generated locally within the boundaries of these orbits and increases the probability of emitting flash radiation.

The probability of the photoelectric effect reaction occurring depends on the energy of the photon and the atomic number of the substance. The occurrence of this reaction is inversely proportional to the cube of the photon energy and directly proportional to 25 (the atomic

number), meaning that the probability of The occurrence of this reaction is expressed mathematically as follows:

$$\tau = K\frac{Z^5}{E^3} \qquad \text{(I.24)}$$

where K is a constant.

From the mathematical relationship above, it is clear that this interaction occurs more when the photon energy is low and the atomic number of the material is high. This interaction is considered the basis for radiological diagnosis, as the energy used for imaging is low, which increases the probability of interaction. In addition, photon absorption depends on the atomic number of the fifth power, which makes it possible to distinguish between the components of the human body, such as distinguishing between bones with a higher atomic number that absorb these photons with greater probability and other tissues with a low atomic number, and thus appear clearly on the radiograph. In the case of homogeneity of living tissue in terms of the closeness of its atomic numbers and it is desired to distinguish between them, the mother is required to give materials with atomic numbers greater or smaller than the atomic number of the tissue, and these materials interact or settle in the tissue to which they are intended. To distinguish it from other tissues, these materials are called contrast materials[27].

This phenomenon can be summarized in several characteristics, namely that this interaction only occurs with one of the orbital electrons associated with the atom of the substance, and the probability of this interaction occurring is greater when the radiation energy is sufficient to overcome the binding energy, and this is in low-energy photons that are equal to or greater than the binding energy in the atomic orbit. In addition, in the case of tissues, the absorption coefficient and the transmission coefficient are almost equal in this Interaction.

I.5.4.3Compton Scattering

Compton scattering is significant in medium-energy gamma-X-rays (0.5- 1 MeV) and materials with low atomic numbers, such as tissues, which are more prevalent than other interactions. Compton scattering is the result of a photon colliding with one of the orbital electrons in the atoms of matter, which leads to this electron being removed from its position and giving it part of the photon's energy. It is called a transformed electron, and a photon that loses part of its energy is scattered in another direction and is called a scattered photon.As shown in Figure 1.20.

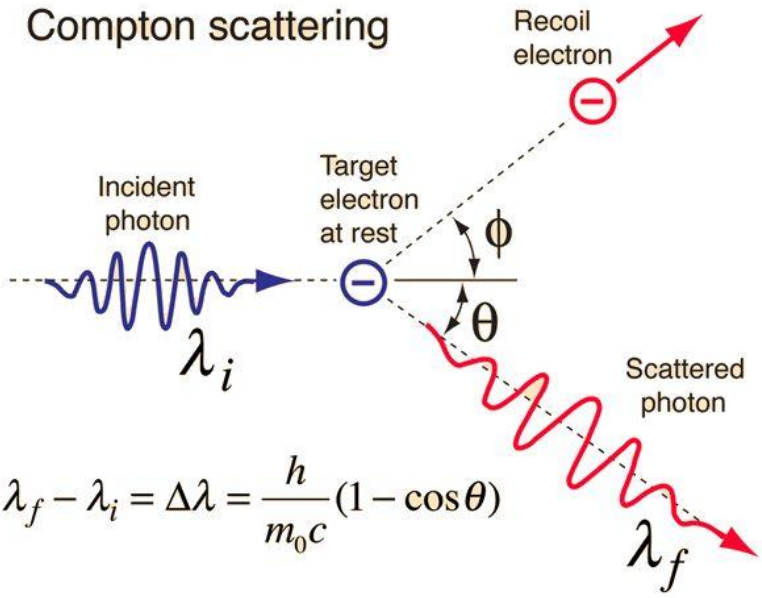

Figure 1. 20.Compton scattering [30]

In the case of Compton scattering, we can consider the orbital electron bound to the atom to be a free electron due to the small value of the binding energy of the electron in the orbit compared to the energy of the photon. In this case, when the photon collides with the electron, it gives it enough energy to move in a direction that makes an angle Øwith the direction of the original photon, and the dispersed photon heads after... The electron lost a value of its energy at an angle θ. By applying the principle of conservation of energy to the x- and y-axes, we conclude that energy of the transformed electron is equal to[24]:

$$E = hv \frac{\alpha(1-cos\theta)}{1+\alpha(1-cos\theta)} \qquad \text{(I.25)}$$

and the energy of the scattered photon :

$$hv' = hv \frac{1}{1+\alpha(1-cos\theta)} \qquad \text{(I.26)}$$

Where E is the energy of the converted electron, hv is the energy of the original photon, and hv' is the energy of the scattered photon. and $\alpha = hv/mc^2$ and the angle at which the electron is launched is:

$$cos\emptyset = (1+\alpha)\tan(\theta/2) \qquad \text{(I.27)}$$

The difference in wavelength of the entering λ_i and scattered photons λ_f can be found as follows:

$$\Delta\lambda = \lambda_f - \lambda_i = \frac{h}{m_0 c}(1 - cos\theta) \qquad \text{(I.28)}$$

There are several important cases in this interaction related to the nature of the interaction between the interacting photon and the electron he mentioned these cases:

Vertical collision on the axis: This occurs when the photon collides directly, vertically, with the electron, which leads to the electron being launched in the same direction along the collision axis at an angle equal to zero, and the photon bounces in the opposite direction at an angle of 180 degrees. In this case, the electron takes the maximum possible energy from the photon, and the scattered photon bounces back with the least backwards energy is called the photon's backscatter, and the maximum energy received by the electron is equal to[24]:

$$E_{max} = hv\frac{2\alpha}{1+2\alpha} \qquad \text{(I.29)}$$

The energy of the scattered photon is as low as possible and equals:

$$hv'_{min} = hv\frac{1}{1+2\alpha} \qquad \text{(I.30)}$$

Scratch collision: occurs in the event that the photon collides with the electron tangentially, which causes the electron to travel in the right direction at an angle of 90 degrees and takes energy equal to zero of the photon’s energy. The scattered photon continues its path in the same original direction at a zero angle and retains all its energy, meaning that the photon touches electron without any change in energies for both.

Scattering of the photon at an angle of 90 degrees. In the case of scattering of the photon at an angle of 90 degrees to the right of the original direction, in this case the angle at which the electron is directed depends on the energy of the photon entering. If the energy is very small, less than the rest energy of the electron, then the electron will take the lower energy and the scattered photon. It takes the most energy. However, if the energy of the photon is very high, the greater energy is taken by the electron and the less energy is taken by the scattered photon. That is, it can be said that in the case of higher energies, the electron is directed at a small angle with the axis of the original photon’s direction, and the scattering ratio increases at a 90-degree angle to the photon.

It is clear from the above that these cases are very important in radiation protection applications when designing radiation shields or determining the safest or most dangerous angle. This means that when the largest proportion of energy is carried by the electron, it is evidence of greater energy absorption within the material medium. When the largest proportion of energy is taken by the scattered photon, this means that this energy will interact and be absorbed elsewhere, which requires other protective measures, especially at angles closest to perpendicularity to the axis of the original photon direction. If we substitute the value of θ The value of 90 degrees in the equation is as follows:

$$hv' = hv\frac{1}{1+\alpha(1-cos\theta)} = \frac{hv}{1+\alpha} \qquad \text{(I.31)}$$

If the photon energy is very high, that is $\alpha \gg 1$ then the above equation can be reduced to:

$$hv' = \frac{hv}{\alpha} \rightarrow or \rightarrow hv' = m_0c^2 \qquad \text{(I.32)}$$

In the same way, if we substitute the angle of 180 degrees for the photon bounced back, the value is equal to$m_0c^2/2$, which is equal to 0.255 MeV. This leads us to generalize in the case of high-energy radiation that the radiation scattered in the right direction is independent of the photon energy and its maximum energy is equal to 0.511 MeV, and the radiation bounced back has a maximum energy equal to 0.255 MeV. The probability of Compton scattering increases with increasing photon energy, and its dependence on the atomic number is small, within the limits of its direct dependence on the number of electrons in one gram of matter, this ratio is almost equal for all materials except hydrogen[24], [25].

I.6. Measurements and units of radiation

I.6.1.Exposure

Exposure is defined as the quantity of ionization produced by gamma rays or X-rays in air. It is quantified in the x-ray unit (R), established as a radiation measurement unit by the General Conference on Radiation in 1928 in Stockholm. The meeting resolved to establish the International Commission on Radiological Protection (ICRP). This definition was first established as the quantity of gamma rays or X-rays necessary to generate an electric charge of one esu (3.336×10^{-10}) due to the ionization of atoms in a mass of air weighing 0.001293g. This weight occupies a volume of one cubic centimeter of air at typical conditions. Exposure was subsequently defined by the International Commission on Radiological Protection as the

quantity of charge produced by the ionization of atoms due to exposure to gamma rays or X-rays per unit mass. This can be articulated numerically as follows:

$$R = \frac{\Delta Q}{\Delta m} \qquad \text{(I.33)}$$

Where Q denotes the amount of charges generated from ionization in a mass m of matter due to the total absorption of photons, thus equating one x-ray to:

$$1R = 2.58 \times 10^{-4}\, C/Kg \qquad \text{(I.34)}$$

I.6.2.Absorbed dose

The definition of radiation exposure is limited to gamma rays and X-rays in the air, thereby excluding a more comprehensive consideration of other radiation types and materials, including biological tissue. Calculations indicate that exposure to a single x-ray results in the absorption of 85 ergs of energy per gram of biological tissue. A unit referred to as rep (radiation equivalent in persons) was utilized for this measurement, denoting the physical equivalent of x-rays. This unit was formerly utilized in radiation protection but is now obsolete. A comprehensive definition has been established that encompasses all forms of radiation, referred to as the absorbed dosage. The absorbed dosage is defined as the energy absorbed in joules per unit mass of a material in kilograms, and is quantified in joules, where:

$$D = \frac{E}{m} = \frac{J}{Kg} = 1Gy \qquad \text{(I.35)}$$

D represents the absorbed dose, E denotes the absorbed energy in the drug, and m signifies the weight of the substance.

The absorbed dose is the fundamental physical metric for quantifying radiation exposure. This unit is inadequate for radiation protection as the harm to biological tissue differs among various radiation types.

I.6.3. Equivalent Dose

Due to the varying interactions of different forms of radiation with matter and the resultant biological effects, even identical absorbed doses might yield varied outcomes. This is attributable to the variance in the ionizing capability of each radiation type, contingent upon the linear energy transfer, and therefore the resultant damage. The biological effects of photon radiation, charged particles, nuclei, and neutrons are distinct from one another. It was essential to establish a correlation between these effects and the absorbed dose to assess them. Consequently, the concept of equal dose was established. The equivalent dose is calculated by multiplying the absorbed dose by the radiation specificity factor (Q), sometimes referred to as

the radiation weighting factor (w_R), as per the International Commission on Radiological Protection Bulletin No. 60 of 1991. Each form of radiation possesses a specificity factor determined by its biological impact, which correlates with the linear energy transfer and the capacity of the radiation to induce ionization in biological tissues. The degree of ionization in matter differs among various types of radiation. Radiation with high linear energy transfer inflicts significantly greater harm to biological matter than radiation with low linear energy transfer.

The equivalent dose is denoted by the symbol H:

$$H = \mathrm{Q} \times \mathrm{D} \qquad \text{(I.36)}$$

Alternatively, based on the updated definition:

$$H = w_R \times D \qquad \text{(I.37)}$$

It is quantified in sieverts, where a sievert represents the energy in joules per unit mass in kilograms, analogous to the unit of running. This moniker was assigned to prevent confusion and to differentiate it from the absorbed dose:

$$1Sv = \frac{J}{Kg} \qquad \text{(I.38)}$$

I.6.4.Effective Equivalent Dose:

The absorbed dose is contingent upon the linear energy transfer, which is intrinsically linked to the site of energy deposition within the body. Consequently, the equivalent dose is influenced by these elements, alongside the sensitivity of the irradiated organ. The probability of getting leukaemia due to radiation exposure is associated with the damage inflicted on bone marrow cells by radiation. Given that these cells are situated deeper within the body and exhibit varying susceptibility to radiation compared to other cells, it is unreasonable to expect the radiation effects to be identical to, or even distinct from, those of a nearby organ after whole-body radiation exposure. Therefore, it was essential to identify a common component to standardise the value of this effect over the entire body. The equivalent effective dose$H_E$is defined as a correlation associated with the organ's radiation exposure site and its susceptibility to radiation. A unique value exists for each organ, determined by these parameters, represented by the weighted tissue factor denoted asW_T. This relationship can be expressed numerically as follows:

$$H_E = \sum \mathrm{W}_T \times \mathrm{Q} \times \mathrm{D} \qquad \text{(I.39)}$$

Conclusion

This chapter examined the essential elements of atomic and nuclear physics, encompassing atomic structure, nuclear characteristics, and radiation emission mechanisms. These notions establish the essential theoretical framework for comprehending radiation interactions and for examining the shielding and protection solutions addressed in the subsequent chapters.

Reference

[1] G. Hazra, “Radioactive Pollution: An Overview The Holistic Approach to Environment,” vol. 8, pp. 48–65, 2018.

[2] Thomson, Joseph John. *The structure of the atom*. Academie Royale de Belgique, 1913.

[3] Cowan, Robert D. *The theory of atomic structure and spectra*. Vol. 3. Univ of California Press, 2023.

[4] Murray, Raymond L., and Keith E. Holbert. "An introduction to the concepts, systems, and applications of nuclear processes." *Nuclear Energy* 6 (2015).

[5] J. Huve, A. Ryzhikov, H. Nouali, V. Lalia, G. Augé, and T. J. Daou, “Porous sorbents for the capture of radioactive iodine compounds: A review,” 2018, *Royal Society of Chemistry*. doi: 10.1039/c8ra04775h.

[6] S. J. Mandel and L. Mandel, “Review Radioactive Iodine and the Salivary Glands,” 2003.

[7] K. Shah and T. Abdeljawad, “Study of radioactive decay process of uranium atoms via fractals-fractional analysis,” *S Afr J Chem Eng*, vol. 48, pp. 63–70, Apr. 2024, doi: 10.1016/j.sajce.2024.01.003.

[8] N. Schunck and D. R. Cea, “Theory of Nuclear Fission,” 2022. [Online]. Available: https://www.elsevier.com/open-access/userlicense/1.0/

[9] Friedlander, G., and W. C. Orr. "The Decay of I 125." *Physical Review* 84.3 (1951): 484.

[10] S. Pommé *et al.*, “On decay constants and orbital distance to the Sun - Part II: Beta minus decay,” *Metrologia*, vol. 54, no. 1, pp. 19–35, Feb. 2017, doi: 10.1088/1681-7575/54/1/19.

[11] S. S. Alam *et al.*, “Lifetimes and transition probabilities for the low-lying states in i 131 and Xe 132,” *Phys Rev C*, vol. 99, no. 1, Jan. 2019, doi: 10.1103/PhysRevC.99.014306.

[12] JCY, “Manual on THERAPEUTIC USES OF IODINE-131 Incorporating: Applications Guide Procedures Guide Basics Guide.”

[13] J. S. Welsh, “Beta decay in science and medicine,” Aug. 2007. doi: 10.1097/01.coc.0000258753.09234.0c.

[14] S. Mahajan and C. R. Divgi, “The role of iodine-124 positron emission tomography in molecular imaging,” Aug. 01, 2016, *Springer-Verlag Italia s.r.l.* doi: 10.1007/s40336-016-0186-7.

[15] M. B. Chadwick *et al.*, “ENDF/B-VII.1 nuclear data for science and technology: Cross sections, covariances, fission product yields and decay data,” *Nuclear Data Sheets*, vol. 112, no. 12, pp. 2887–2996, 2011, doi: 10.1016/j.nds.2011.11.002.

[16] Y. Nagai *et al.*, “ Production of an Isomeric State of 90 Y by Fast Neutrons for Nuclear Diagnostics ,” *J Physical Soc Japan*, vol. 78, no. 11, p. 113201, Nov. 2009, doi: 10.1143/jpsj.78.113201.

[17] "Recommended Nuclear Decay Data Sr-90." [Online]. Available: www.nuclitec.de

[18] R. S. Lawson and R. Lawson, "Introduction to Radioactivity An Introduction to Radioactivity Chief Physicist Nuclear Medicine Department Manchester Royal Infirmary," 1999.

[19] O. of Radiation Protection, "Washington State Department of Health – Office of Radiation Protection - Molybdenum-99 (Mo-99) Fact Sheet," 2002. [Online]. Available: http://www.webelements.com/webelements/elements/text/Mo/key.html

[20] E. Browne and J. K. Tuli, "Nuclear Data Sheets for A = 99," *Nuclear Data Sheets*, vol. 112, no. 2, pp. 275–446, 2011, doi: 10.1016/j.nds.2011.01.001.

[21] T. Settlemyre, H. Zheng, and A. Bonasera, "Pair production as a probe for the dynamics of nuclear fission and α decay," *Phys Rev C*, vol. 107, no. 3, Mar. 2023, doi: 10.1103/PhysRevC.107.L031301.

[22] A. L. Nichols, "Decay data: review of measurements, evaluations and compilations," 2001.

[23] H. H. Erbil, "Half-life calculation in general radioactive decay," *Advances in Image and Video Processing*, vol. 9, no. 6, Dec. 2021, doi: 10.14738/aivp.96.11235.

[24] B. Collum, "Radiation," in *Nuclear Facilities*, Elsevier, 2017, pp. 45–60. doi: 10.1016/B978-0-08-101938-2.00002-7.

[25] J. Kónya and N. M. Nagy, "Interaction of Radiation with Matter," in *Nuclear and Radiochemistry*, Elsevier, 2012, pp. 83–127. doi: 10.1016/B978-0-12-391430-9.00005-6.

[26] "Chapter 2: Interaction of Radiation with Matter."

[27] D.E. Groom and S.R. Klein, " Passage of Particles Through Matter," 2022, ch. 34.

[28] S. M. Seltzer and S. M. Seltzer, "Editor's Note The original version of ICRU Report 85 published in the Downloaded from FUNDAMENTAL QUANTITIES AND UNITS FOR IONIZING RADIATION (Revised) Report Committee The International Commission on Radiation Units and Measurements," *JICRU*, vol. 11, no. 1, 2011, doi: 10.1093/jicru/nd.

[29] M. F. L'Annunziata, "Radiation Physics and Radionuclide Decay," in *Handbook of Radioactivity Analysis*, Elsevier Inc., 2012, pp. 1–162. doi: 10.1016/B978-0-12-384873-4.00001-3.

[30] B. I. Kharisov, O. V Kharissova, and U. Ortiz Méndez, "Radiation Synthesis of Materials and Compounds."

[31] "L'Annunziata, Michael F. "Introduction: radioactivity and our well-being." *Radioactivity* (2007): 1-45.

Chapter II:Principles of Radiation Protection and Shielding

II.1 Introduction

The main goal of radiation protection is to either prevent radiation exposure or reduce the risks of radiation exposure. External radiation, which comes from a source outside the body with energy that can enter the body, or internal radiation, which comes from radioactive materials that enter the body through the skin, respiratory tract, or digestive tract, can expose a person to ionizing radiation. Therefore, it is very important to take necessary precautions to reduce the amount of radiation exposure[1].

II.2 Principles of radiation protection

To hide the measurement of radiation exposure from radiation practices, three primary principles can be utilised to hide the value of exposure from an external radiation source. These principles are:

1- Augmenting the separation from the radiation source (distance).

2- Minimising the duration of interaction with radiation sources.

3- Utilising radiation shielding[1].

II.2.1 Distance

Distance is a critical factor in radiation protection. As the distance from a radiation source increases, radiation exposure diminishes. The influence of distance on radiation intensity parallels the impact of distance on the intensity of light emanating from a point source. The proximity to a light source correlates directly with its intensity, and conversely. This is also pertinent to the level of radiation exposure. The greater the distance from a radiation source, the diminished its intensity and hence the level of radiation exposure[2].

When there is a point source of electromagnetic radiation, the photons that come out of it will spread out in all directions evenly and with a certain amount of intensity. These photons show how intense the source is and how much radiation R is being emitted. If we pretend that there is a sphere around this source, the sphere's radius will be the made-up distance, and its surface area will be:

$$A = 4\pi r^2 \qquad \text{(II.1)}$$

At this distance, the amount of exposure R_0 will be distributed over the entire surface of the virtual sphere, and the amount of radiation exposure at this distance R_0 will be equal to the original amount of exposure distributed over the surface area of the sphere as follows:

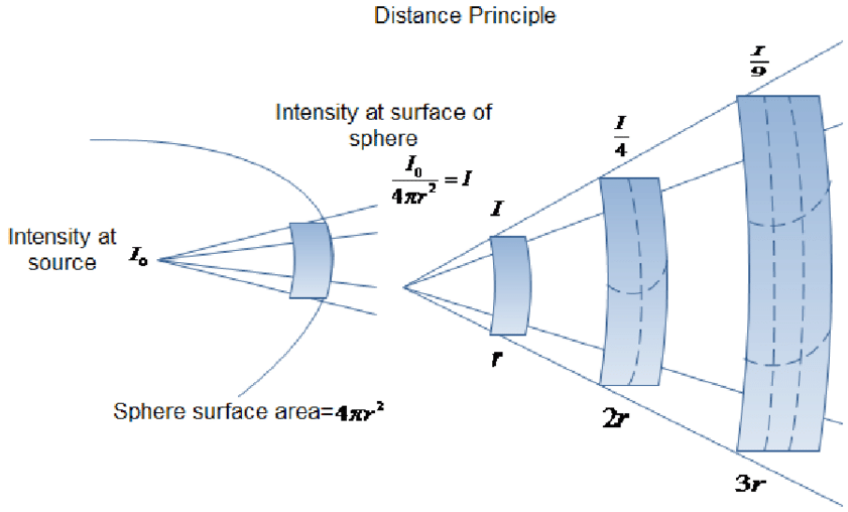

Figure 2. 1.How the inverse square law states that exposure diminishes with increasing distance. [3]

In the case of a non-point radiation source, the reduction in radiation dose is determined by its physical shape. As a result, each situation is studied individually. For example, if the radiation source is linear, as seen in Figure 2.2. the reduction in exposure is roughly inversely proportional to the distance[3].

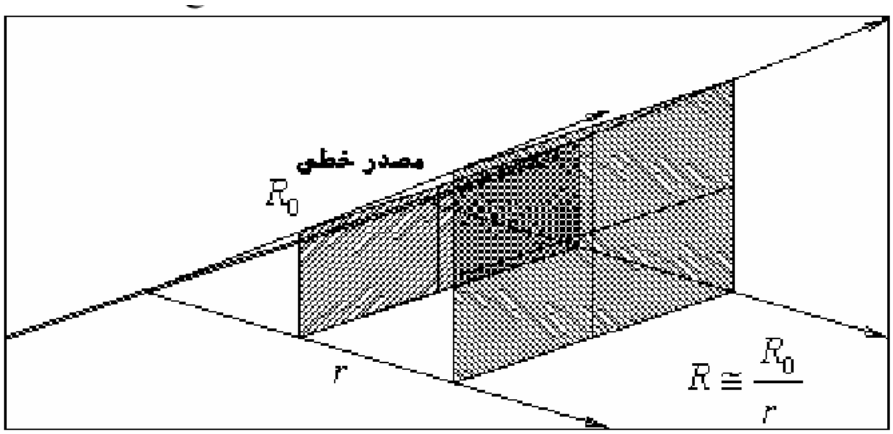

Figure 2. 2.The decrease in radiation exposure as distance from a linear radiation source rises[3].

Figure2.3. also graphically depicts the amount of decrease in radiation dose as distance from the point radiation source increases when compared to a linear radiation source such as radioactive material found in tubes or radioactive material spread throughout the patient's body during nuclear medicine examinations.

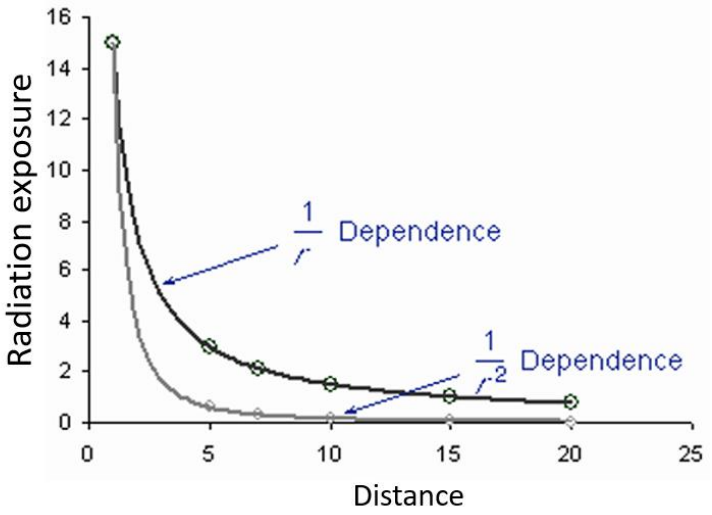

Figure 2. 3.Radiation exposure decrease curve as a function of distance from a point or line radiation source.[3]

II.2.2 Time

Based on the model rule used in radiation protection for the linear response of cells after the maximum radiation dose, and because the mechanism of cellular reconstruction is that total damage to cells is a type of accumulation, this question has a negative impact on the cell by increasing the duration of radiation exposure during the period of influence of the radiation source. Exposure time is an important consideration when exposed to an external radiation source or when radioactive components are absorbed during internal radiation exposure.

The adverse effects of prolonged interaction with the radiation source necessitate the formulation of suitable mechanisms to minimize the duration of exposure to the radioactive source, thereby decreasing radiation exposure through the application of this principle in radiation protection. This factor is utilized in various manners, primarily emphasizing high craftsmanship or professionalism in managing the radioactive source to accomplish tasks in the shortest timeframe. This is achieved through suitable qualifications and training, enhancing the professionalism of radiation workers by employing fictitious sources for training prior to engaging with actual radiation sources. This technique is referred to as dry runs or the formulation of protocols that guarantee the radiation worker is exposed to the radiation source for the minimal duration necessary[4].

To reduce and regulate radiation exposure, one can minimize exposure time, thereby enabling the calculation of radiation doses to ensure they remain within permissible limits. This can be achieved by determining the optimal duration for interacting with the radiation source, ensuring doses do not surpass acceptable thresholds[5].

$$Time\ Limit = \frac{Dose\ Limit}{Dose\ Rate} \qquad \text{(II.1)}$$

Considering the uniformity of the units while assessing the optimal duration that minimizes doses to the greatest extent.

II.2.3 Shielding

When radiation traverses matter, it imparts its energy by generating charged ions. Consequently, the substance either absorbs or attenuates the radiative energy. The material's absorption capacity is contingent upon various parameters, including the radiation type, its energy, and the material composition. Consequently, various materials have been utilized to fabricate shields that safeguard against radiation or mitigate its intensity. These substances are referred to as radiation shields[6].

Numerous materials can be employed to attenuate radiation and serve as radiation shields, owing to their capacity to absorb and diminish radiation. Radiation shields are employed to confine radioactive sources or establish radiation barriers. Consequently, radiation shields are regarded as fundamental principles in radiation protection, specifically the capacity to manage various types and sources of radiation by supplying suitable and technically sound shielding for radioactive sources, contingent upon the nature of radiation interaction with diverse materials[7].

The design and selection of suitable materials for radiation shields tailored to various radioactive sources and their engineering contexts can present challenges and complexities in identifying the most effective shield. This determination hinges on factors such as the type of radiation, its energy, the engineering circumstances of the source, and its physical configuration[8].

II.2.3.1 Alpha particle radiation shields

The limited penetration range of alpha particles in matter, attributable to their substantial mass and charge, is typically a few tens of micrometres in solid materials and several centimetres in air. Consequently, they are easily shielded and regarded as a relatively minor external threat to

living organisms, as their penetration does not surpass the dead layer of skin (7 mg/cm²) for the most energetic alpha particles. However, they pose a significant and effective hazard if ingested or inhaled, due to the high energy density they deposit upon absorption.[9].

A critical feature of managing alpha particle sources is their secure containment in containers that prevent contamination and subsequent entry into the body by touch, inhalation, ingestion, or consumption. This can be accomplished by putting a thin coating of cohesive paint or other effective stabilisers to isolate the source. Although contamination or alpha particle dispersion is feasible, this is adequate to confine and shield alpha sources. It is imperative to maintain ongoing and uniform security and isolation by performing regular inspections, conducting radiation surveys in areas where alpha particle sources are utilised, employing suitable radiation detectors for these particles, and ensuring the safe storage, disposal, and handling of alpha particle sources post-use.

II.2.3.2 Beta particle radiation shields

Beta particles have a limited range in matter, although this range exceeds that of alpha particles and can exhibit greater complexity. Depending on the particle's energy, it can travel several meters in air, and can reach 10 meters with an energy of 4 million electron volts[2].

Beta particles, being charged particles, dissipate their energy in matter through two mechanisms: direct ionization of atomic components, and the generation of bremsstrahlung radiation, which occurs as a result of the interaction and acceleration of electrons within the electrostatic field of the positive nucleus. Therefore, it is essential to take these considerations into account when constructing shields to absorb beta particles. This is achieved by considering the widest range of higher-energy particles, reflecting the diversity of the energy spectrum resulting from the energy distribution between them and their associated neutrinos. Neutrinos are assumed to be energy neutral. Furthermore, the extent of the resulting bremsstrahlung radiation must be evaluated and mitigated by using materials with low atomic numbers that generate this radiation.

The radiation protection required for beta particles can be determined by considering two main factors: direct ionization and the generation of bremsstrahlung radiation. The initial consideration determines the required thickness of the shield made up of the material or materials through which the particles will pass, while the subsequent consideration relates to the rate of production of braking rays within these materials, as well as the methods of

processing, attenuation and absorption, along with the range of beta particles at maximum energy[2], which can be indicated in Figure2.4.

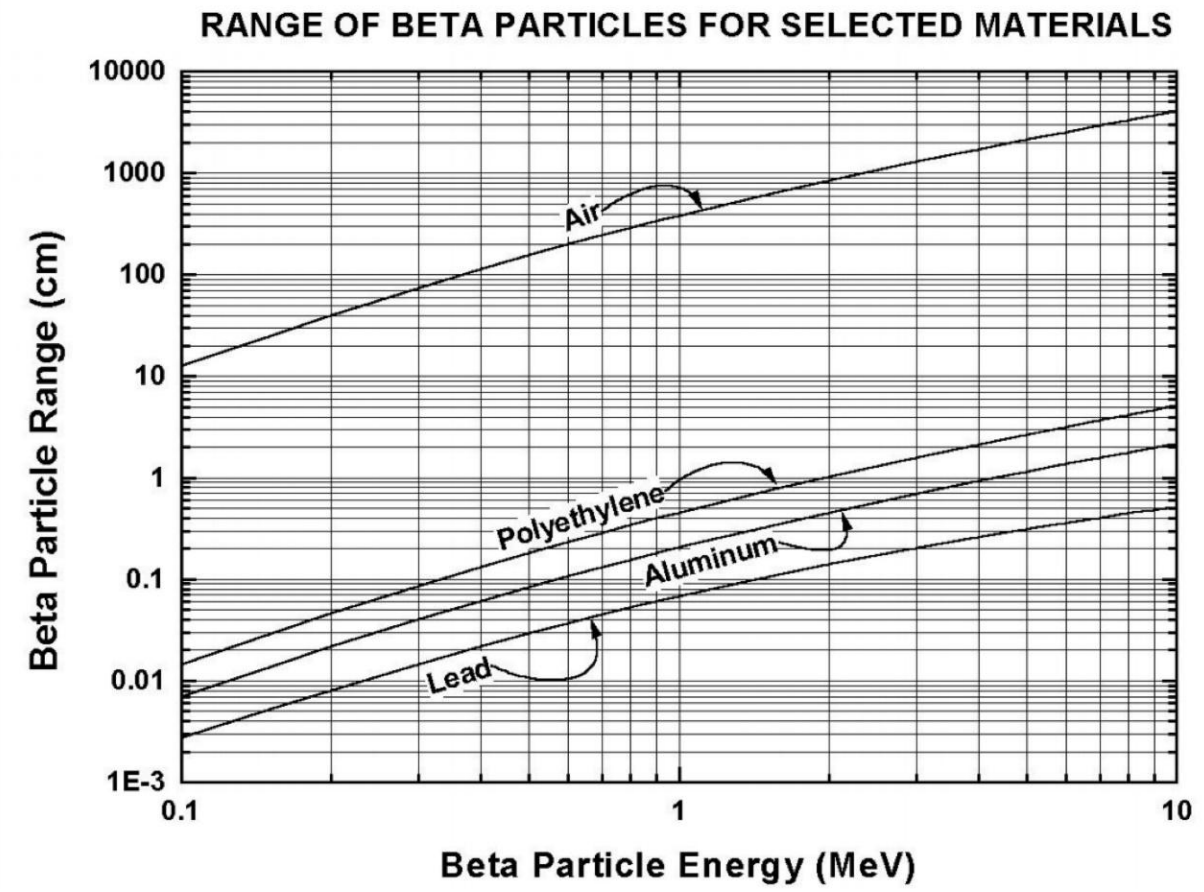

Figure 2. 4.the range of beta particles at maximum energy[8].

II.2.3.3 Gamma and X-rays radiation shields

The interaction of photons with matter is fundamentally distinct from that of charged particles. In the previous scenario, the photon may be entirely or partially absorbed, scattered, or may penetrate the substance without interaction. Consequently, the attenuation of photons in this instance is contingent upon the geometrical shape of the radiation beam, whether it is geometricallyuniform ornon-uniform, as illustrated in Figure 2.6[10].

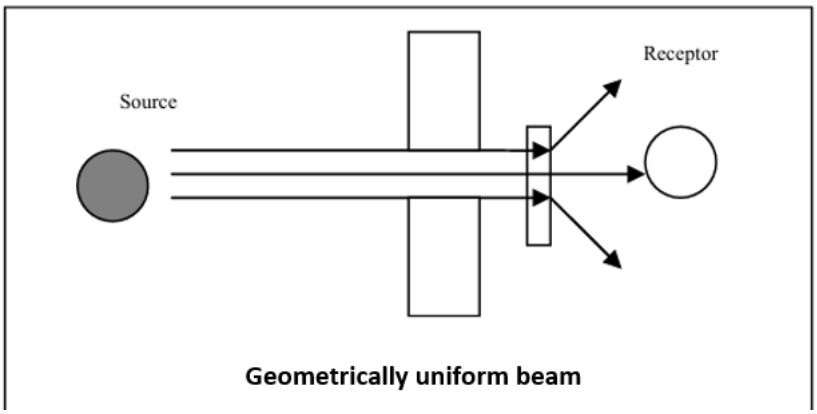

Figure 2. 5.the geometric shape of the radiation beam.[10]

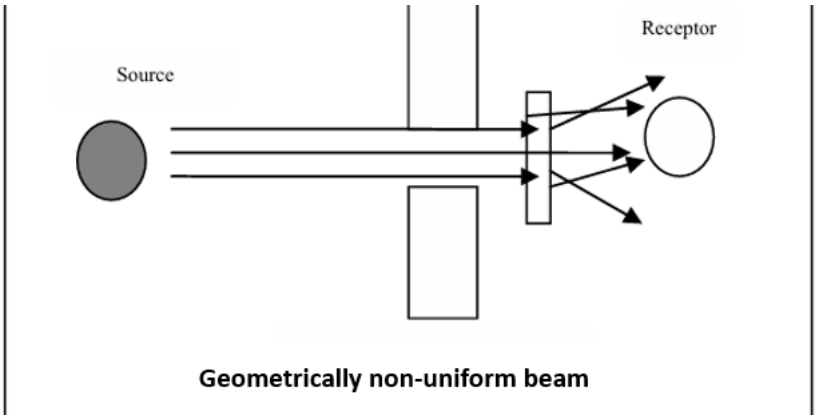

Figure 2. 6.the geometric shape of the radiation beam[10].

In a homogeneous beam, each interaction photon may either be absorbed or arrive at the receiving site with its initial energy intact. Although the majority of uniform sources are point sources, an irregular or weakly uniform source may result in a photon that, upon partial absorption and scattering, diminishes some of its initial energy. Consequently, a broad range of photon energies arrives at the detector. A segment of photons with varying energy is scattered. The computation and design of radiation shields significantly depend on this factor, so the methodology for determining the necessary shield thickness will invariably vary for each radiation beam type[3].

II.2.3.3.1 Shields against uniform beam radiation

The reduction of photons in a perfectly uniform beam as they traverse the shielding material is governed by the subsequent mathematical equation:

$$I = I_0 \exp(-\mu x) \qquad \text{(II.3)}$$

I_0The initial intensity of the radiation beam,Iis the intensity of the radiation beam post-attenuation as it traverses the shield, and x represents the thickness of the shield. The attenuation coefficient is contingent upon the atomic number of the shielding material and the photon energy, which dictate the characteristics of the photon-material interaction (photothermal interaction, Compton scattering, and diffraction). This coefficient can be determined by measuring various materials at different energy levels[11].

II.2.3.3.2 Non-uniform Beam Radiation Shields

When a barrier is interposed between a material and a radiation source, or in the presence of air, numerous scattered photons of varying energies (attributable to Compton scattering) arrive at the measurement location, leading to alterations in the beam flux and dimensions. The beam grows increasingly intricate and is designated as an irregular beam for radiation safety considerations. The computation of the attenuated beam, based on the attenuation coefficient of a uniform beam, yields inaccurate results when applied to an irregular beam, owing to the photon spectrum arising from the divergence of energies and directions within the beam. Consequently, the accurate approach for calculating radiation attenuation to ascertain the requisite shield thickness involves incorporating an additional variable known as the build-up factor, denoted by the symbol B. This factor consistently exceeds one. Consequently, the beam attenuation equation is reformulated as follows with the incorporation of the build-up factor.

$$I = \mathrm{B}\, I_0 \exp(-\mu x) \qquad \text{(II.4)}$$

II.3 Photon Attenuation and Absorption

Photon interactions, including charged particles, are distinct from those of other radiation types. As these photons traverse matter, some are entirely absorbed, others traverse without interaction, and the latter are deflected after dissipating a portion of their energy in a new direction. A photon beam of radiation with a specified intensity (I_0) and a uniform pattern traversing a barrier of thickness x will interact with the material's atoms, resulting in a modification of its intensity due to absorption and attenuation. Increased material thickness

results in heightened attenuation and absorption of the beam. In other words, an inverse relationship exists between the intensity of the radiation beam (dI) and the thickness of the material (dx). This can be articulated numerically as follows:

$$\frac{dI}{dx} = \boldsymbol{\mu I} \qquad \text{(II.5)}$$

μ is the linear attenuation coefficient of the material, equivalent to the slope of the linear graph illustrating the correlation between the material's thickness and the logarithm of the radiation beam intensity, as depicted in the picture.

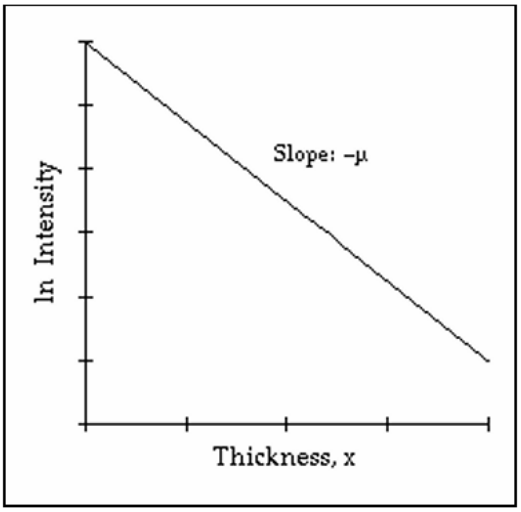

Figure 2. 7.The correlation between material thickness and radiation intensity[12].

By integrating this equation as seen below:

$$\int \frac{dI}{I} = \int_{-} \mu dx \qquad \text{(II.6)}$$

And from it

$$\ln I(x) - \ln I_0 = -\mu x \qquad \text{(II.7)}$$

$$\boldsymbol{I(x) = I_0 e^{-\mu x}}$$

The linear attenuation coefficient $\boldsymbol{\mu}$In this instance, it denotes the aggregate of the attenuation coefficients for the interactions experienced by the photon as it traverses the thickness of a specific material. The interactions include photoelectric interaction, Compton scattering, and dielectric generation. That is, it is equivalent to:

$$\mu = \tau + \sigma + k \qquad \text{(II.8)}$$

$\boldsymbol{\tau}$, $\boldsymbol{\sigma}$, and $\boldsymbol{k}$ represent the linear attenuation coefficients for the photoelectric effect, Compton scattering, and diffusion, respectively. Unexpectedly, this coefficient is linear, considering that the aggregate of these interactions is wholly contingent upon photon energy, atomic number, and material density. Although these connections are nonlinear, graphing the logarithm of beam intensity against thickness yields a linear relationship, applicable in contexts of absorption, attenuation, and scattering together. This coefficient is utilized for radiation protection in shielding calculations to quantify a photon's capacity to traverse the absorbing medium[12].

Given that the exponent in an exponential equation must be dimensionless, $\boldsymbol{\mu}$ and $\boldsymbol{x}$ must possess reciprocal dimensions; hence, if the absorber thickness is quantified in centimetres, the attenuation coefficient is referred to as the linear attenuation coefficient$\boldsymbol{\mu}$, which must have dimensions of "per cm."cm^{-1} If t is expressed in g/cm^2, the absorption coefficient is referred to as the mass attenuation coefficient$\boldsymbol{\mu_m}$, which must possess dimensions of per g/cm^2 or cm^2/g. The quantitative relationship between $\boldsymbol{\mu}$ and $\boldsymbol{\mu_m}$ for a substance with a density of ρ g/cm^3 is expressed by the equation:

$$\boldsymbol{\mu} cm^{-1} = \boldsymbol{\mu_m} \frac{\text{cm}^2}{g} \times \rho \frac{g}{\text{cm}^3} \qquad \text{(II.9)}$$

The attenuation coefficient is defined as the fractional reduction, or attenuation, of gamma-ray beam intensity per unit thickness of an absorber, as expressed by the equation below:

$$\lim_{\Delta x \to 0} \frac{\Delta I/I}{\Delta x} = -\mu \qquad \text{(II.10)}$$

where $\Delta I/I$ is the percentage of the gamma-ray beam diminished by an absorber of thickness x. The defined attenuation coefficient is occasionally referred to as the total attenuation coefficient. The attenuation coefficients for various materials are presented in the Table.

Table 2. 1.The correlation between material thickness and radiation intensity[12].

		QUANTUM ENERGY (MeV)												
	ρ,(g/cm³)	0.1	0.15	0.2	0.3	0.5	0.8	1.0	1.5	2	3	5	8	10
C	2.25	0.335	0.301	0.274	0.238	0.196	0.159	0.143	0.117	0.100	0.080	0.061	0.048	0.044
Al	2.7	0.435	0.362	0.324	0.278	0.227	0.185	0.166	0.135	0.117	0.096	0.076	0.065	0.062
Fe	7.9	2.72	1.445	1.090	0.838	0.655	0.525	0.470	0.383	0.335	0.285	0.247	0.233	0.232
Cu	8.9	3.80	1.830	1.309	0.960	0.730	0.581	0.520	0.424	0.372	0.318	0.281	0.270	0.271
Pb	11.3	59.7	20.8	10.15	4.02	1.64	0.945	0.771	0.579	0.516	0.476	0.482	0.518	0.552
Air	1.29×10^{-3}	1.95×10^{-4}	1.73×10^{-4}	1.59×10^{-4}	1.37×10^{-4}	1.12×10^{-4}	9.12×10^{-5}	8.45×10^{-5}	6.67×10^{-5}	5.75×10^{-5}	4.6×10^{-5}	3.54×10^{-5}	2.84×10^{-5}	2.61×10^{-5}
H_2O	1	0.167	0.149	0.136	0.118	0.097	0.079	0.071	0.056	0.049	0.040	0.030	0.024	0.022

For certain purposes, the atomic attenuation coefficient$\boldsymbol{\mu}_a$, is beneficial. The atomic attenuation coefficient represents the proportion of an incident gamma-ray beam that is diminished by a single atom. The atomic attenuation coefficient represents the likelihood that an absorber atom will engage with a photon from the beam. The atomic attenuation coefficient can be defined by the equation:

$$\boldsymbol{\mu}_a \text{cm}^2 = \frac{\boldsymbol{\mu}\frac{1}{\text{cm}}}{N\frac{atoms}{\text{cm}^3}} \qquad \text{(II.11)}$$

N represents the quantity of absorber atoms per cubic centimetre. Be aware that the dimensions of $\boldsymbol{\mu}_a$ are cm², the units of area. Consequently, the atomic attenuation coefficient is typically designated as the cross section of the absorber. The cross section is expressed in the unit known as the barn, abbreviated as b.

$$1\text{b} = 10^{-24}\text{cm}^2$$

The atomic attenuation coefficient, denoted as σ, is also referred to as the microscopic cross section, whereas the linear attenuation coefficientsymbolised by σ, is commonly known as the macroscopic cross section. This terminology is predominantly employed in discussions on neutrons. Consequently, Equation (5.30) can be expressed as:

$$\sum \text{cm}^{-1} = \sigma \frac{\text{cm}^2}{atoms} \times N \frac{atoms}{\text{cm}^3} \qquad \text{(II.12)}$$

By employing the relationship specified in Eq(II.3) ; Eq (II.12) can be reformulated as:

$$\frac{\boldsymbol{I}}{\boldsymbol{I_0}} = \boldsymbol{e}^{-\mu_a \boldsymbol{x}} = \boldsymbol{e}^{-\sigma N \boldsymbol{x}} \qquad \text{(II.13)}$$

The linear attenuation coefficient for a mixture of materials or an alloy is expressed as:

$$\boldsymbol{\mu} = \boldsymbol{\mu}_{a1} \times N_1 + \boldsymbol{\mu}_{a2} \times N_2 + \cdots = \sum_{n=1}^{n} \boldsymbol{\mu}_{an} \times N_n \qquad \text{(II.14)}$$

where $\boldsymbol{\mu}_{an}$ represents the atomic coefficient of the nth element

N_n is the number of atoms per cm³ of the nth element.

Numerical values for μa have been disseminated for numerous elements throughout a broad spectrum of quantum energies. Utilising atomic cross sections and Equation (5.33), we may calculate the attenuation coefficients of compounds or alloys comprising various elements.

The attenuation characteristics of matter systematically correlate with the atomic number of the absorber and the energy of the gamma radiatio. It is important to note that in the region where the Compton effect predominates, the mass attenuation coefficient is largely independent of the absorber's atomic number Figure 2.8.

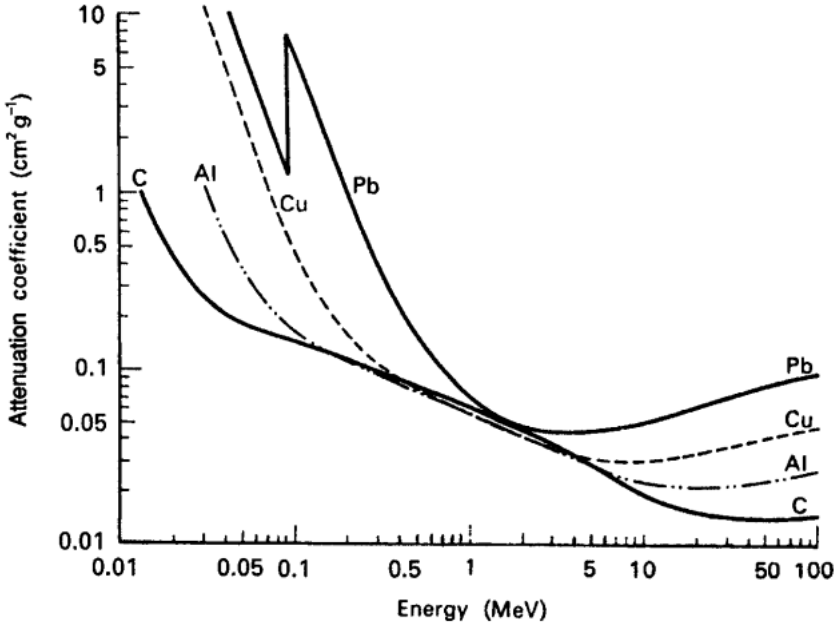

Figure 2. 8.Mass attenuation coefficients of different atomic numbers[10].

II.3.1 Half Value Layer and Tenth Value Layer

The half value layer (HVL) is the thickness of a shield or absorber that diminishes the radiation intensity by a factor of two, effectively halving the beginning level. The HVL is often referred to as half value thickness. The correlation between the half-value layer (HVL) of a shielding material and its attenuation coefficient is akin to the relationship between the half-life and the decay constant of a radioisotope. The requisite shield thickness to diminish the intensity of a beam, under optimal geometric conditions[11], to 1/2 is determined using Eq(II.3)as follows:

$$\frac{I}{I_\circ} = \frac{1}{2} = \boldsymbol{e}^{-\boldsymbol{\mu x}} \qquad \text{(II.15)}$$

$$\ln\frac{1}{2} = -0.693 = -\boldsymbol{\mu}_{x_{1/2}} \qquad \text{(II.16)}$$

$$x_{1/2} = \frac{0.693}{\boldsymbol{\mu}} = HVL \qquad \text{(II.17)}$$

In estimating shielding thickness, it may be advantageous to ascertain the number of half-value layers (HVLs) necessary to diminish the radiation to the desired level. For instance, to diminish the radiation level to one-tenth of its initial value, it would necessitate between 3 half-value layers (HVLs), resulting in a reduction to 1/23 or around 1/8, and 4 HVLs, which would decrease the level to 1/24 or about 1/16. The quantity of HVLs (n) necessary to diminish the beam intensity from $I_\circ$ to I is expressed as:

$$\frac{I}{I_\circ} = \frac{1}{2^n} \qquad \text{(II.18)}$$

To determine the quantity of HVLs required to diminish the gamma ray beam intensity to 10%, utilising Eq(II.1):

$$\frac{I}{I_\circ} = \frac{1}{10} = \frac{1}{2^n} \qquad \text{(II.19)}$$

$$n = 3.3 \text{ HVLs}$$

A shield that reduces a radiation beam to 10% of its original intensity, as depicted in the picture above, is referred to as a tenth value layer, denoted by the symbol TVL.

Mean Free Path

Mean free path. The mean free path is the average distance a single particle traverses through a medium before interacting with the material, computed using the following equation:

$$\textbf{MFP}=1/\mu \qquad \text{(II.20)}$$

The effective atomic number represents the ratio of the total number of electrons in the composite structure to the number involved in radiation-atom interactions. The Z-eff of materials can be derived using the mass attenuation coefficient values (μ/ρ) as outlined in the equation.:

$$Z_{eff} = \frac{\sigma_i f_i A_i \left(\frac{\mu}{\rho}\right)}{\sigma_i f_i \frac{A_i}{Z_i} \left(\frac{\mu}{\rho}\right)_i} \qquad \text{(II.21)}$$

Radiation Shielding for X-ray Devices:

X-ray machines are utilised for medical diagnosis and radiation therapy, in addition to certain non-medical uses like industrial imaging and laboratory analysis. The X-ray tube is often encased in a lead shield, with an exit aperture for the beam, along with an aluminium or copper filter to attenuate extraneous photons from the beam.

The X-ray tube shield typically adheres to designated design parameters to avoid or minimise leakage below allowed limits, in accordance with international standards and guidelines. The allowable radiation leakage rate must not surpass 0.1 retinogen per hour at a distance of one metre from the tube if the tube's maximum energy is below 500 kiloelectron volts, and 1 retinogen per hour at the same distance for tubes with a maximum energy exceeding 500 kiloelectron volts, such as therapeutic X-ray machines. This value may surpass these restrictions when the tube is utilised for non-medical applications, such as industrial imaging.

The X-ray tube shield is generally constructed according to shielding calculations for radioactive sources, determined by the maximum working voltage of the X-ray tube.

The radiation field in an x-ray room comprises multiple components: primary radiation, leakage radiation, diffuse radiation, and the orientation of effective radiation, as seen in Figure2.9. These factors are crucial when calculating and building the radiation shield for a machine that includes an x-ray apparatus. The primary shield must face the direction of the effective radiation. The effective radiation may likewise be directed in multiple directions. In this instance, all the walls adjacent to it serve as primary shields. Despite the emission of rays from the x-ray tube and scattered radiation from the patient's body as well as the walls, floor, and ceiling of the x-ray room, secondary shields must be established. These shields are not intended to mitigate effective radiation, leakage radiation, or radiation dispersed in all directions. Consequently, every shield apart from the primary shield is classified as a secondary shield.

In the design of radiation shields for x-ray rooms, the allowable dose in controlled areas (directly supervised by personnel) must not surpass 1 mSv per week, calculated on an 8-hour workday. In regions not directly monitored by personnel or radiation protection officers, the dose must not above 0.1 mSv per week, according to the estimated thresholds established by the International Commission on Radiological Protection (ICRP) in Publication No. 26. The Commission has set new limitations in Report No. 60. The International Atomic Energy Agency (IAEA) established these restrictions, which were disseminated in its Radiation Safety and Security Series No. 115, and are currently being embraced by numerous nations. The revised thresholds stipulate a permitted maximum of 0.4 mSv per week in regulated areas and 0.02 mSv per week in uncontrolled regions. In the context of calculations and the design of radiation shielding for X-ray equipment, these thresholds are referred to as the "weekly permissible limit." Interested parties may adhere to the limits set forth by national legislation, while also striving to minimise exposure to below these thresholds in accordance with the ALARA concept, which is endorsed in radiation protection.

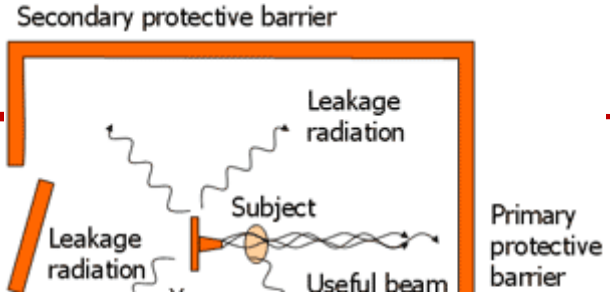

Primary radiation shielding computations

Several critical parameters are involved in determining the thickness of the primary shield to be designed. The aforementioned elements ascertain the value of the shield's transmission coefficient (K), measured in Ωm/min, at a distance of one meter. By utilizing this factor and experimental data for radiation attenuation across different materials and energy levels, the necessary thickness can be calculated to guarantee adherence to permitted limits. The factors are:

1. Permitted weekly exposure (P).
2. Weekly workload (W): Quantified in milliampere-minutes weekly. This is determined by the maximum workload. For instance, it can be determined by multiplying the weekly total of X-rays by the present value and the duration for each -ray.
3. The effective beam direction coefficient, denoted as U, signifies the operational effective beam direction. For instance, when the X-ray machine is oriented in a single direction, its directional coefficient is 1. If it operates in two directions, its directional coefficient is 1/2. If it can travel in all four directions, its directional coefficient is 1/4. This can be ascertained from the predetermined workflow corresponding to the anticipated task and the machine's operational characteristics.
4. The occupancy coefficient of the region requiring protection, denoted by T, is contingent upon the type and percentage of effective occupancy, whether complete or partial.
5. The distance d, measured in meters, between the X-ray tube and the shield (or the region requiring protection).

Secondary radiation shield

A secondary radiation shield is intended to safeguard against leakage and dispersed radiation, excluding the effective radiation field. The two components of the radiation field are qualitatively distinct from the primary radiation. Consequently, the secondary shield design is executed individually for each component, and the suitable combination is selected. The ideal calculating method is to consistently regard the beam direction of leakage and scattered radiation as equivalent to one. The uniform qualities of these two components inside the radiation field result in an equal likelihood of leakage and scattering in all directions. Leakage radiation is typically constrained by the manufacturing specifications of the X-ray tube, measuring 0.1 R/hr at a distance of one metre from the tube's centre in diagnostic radiology instruments utilised for radiological imaging. The dosage is 1 R/hr for therapeutic radiology devices employed in surface treatments, when the treatment area is on or near the body surface and does not necessitate high-energy penetrating radiation. For high-energy treatment devices, including gamma rays (cobalt and caesium) and X-rays generated by medical accelerators (exceeding 500 kV peak voltage), the allowable limit is either 0.1% of the effective radiation emitted, where this value is Yt in roentgen units per hour (Yt), or 1 R/hr.

The secondary shielding for leakage radiation is determined by calculating half the amount required to lower the exposure to tolerable levels. The tube functions for t minutes weekly, and since one hour comprises 60 minutes, the radiation leakage at a distance **d**from the tube each hour[1 R/hr] is:

$$Amount\ of\ exposure = \frac{\mathrm{Yt}}{60d^2} \qquad \text{(II.22)}$$

III. Conclusion

This chapter included a thorough examination of the principles and fundamentals of radiation shielding, highlighting the mechanisms of photon interaction with materials and the factors affecting attenuation. The linear and mass attenuation coefficients, half-value layer (HVL), and tenth-value layer (TVL) were examined as critical metrics for assessing shielding efficacy.

A theoretical comprehension of these principles is essential for the design and evaluation of protective materials against ionizing radiation. The knowledge provided in this chapter

constitutes the scientific basis for the computational and analytical methods discussed in the next chapters.

References

[1] L'Annunziata, Michael F. "Introduction: radioactivity and our well-being." *Radioactivity* (2007): 1-45.

[2] Cember, Herman, and Thomas E. Johnson. *Introduction to health physics*. McGraw-Hill Medical, 2009.

[3] M. C. ŞAHİN, K. MANİSA, and H. BİRCAN, "Validation of a Proposed Equation for Determining the Half-Thickness Value of Gamma and X-Ray Radiation," *Süleyman Demirel Üniversitesi Fen Edebiyat Fakültesi Fen Dergisi*, vol. 18, no. 1, pp. 10–17, May 2023, doi: 10.29233/sdufeffd.1244542.

[4] M. S. Al-Buriahi and B. T. Tonguc, "Mass attenuation coefficients, effective atomic numbers and electron densities of some contrast agents for computed tomography," *Radiation Physics and Chemistry*, vol. 166, Jan. 2020, doi: 10.1016/j.radphyschem.2019.108507.

[5] W. Mui *et al.*, "Development of ASTM International D8405—Standard Test Method for Evaluating PM2.5 Sensors or Sensor Systems Used in Indoor Applications," *J Occup Environ Hyg*, vol. 20, no. 9, pp. 373–389, 2023, doi: 10.1080/15459624.2023.2212739.

[6] C. W. Fabjan, "Particle Physics Reference Library Volume 2: Detectors for Particles and Radiation."

[7] Eisenbud, Merril. "Industrial uses of Ionizing radiation." *American Journal of Public Health and the Nations Health* 55.5 (1965): 748-759.

[8] E. Sakher, B. Smili, M. Bououdina, and S. Bellucci, "Structural Study of Nano-Clay and Its Effectiveness in Radiation Protection against X-rays," *Nanomaterials*, vol. 12, no. 14, Jul. 2022, doi: 10.3390/nano12142332.

[9] Shultis, J. Kenneth, and Richard E. Faw. "Radiation shielding and radiological protection." *Handbook of nuclear engineering*. Springer, Boston, MA, 2010. 1313-1448.

[10] D. R. Mcalister, "Gamma Ray Attenuation Properties of Common Shielding Materials," 2018.

[11] P. S. DAHINDE, G. P. DAPKE, S. D. RAUT, R. R. BHOSALE, and P. P. PAWAR, "ANALYSIS OF HALF VALUE LAYER (HVL), TENTH VALUE LAYER (TVL) AND MEAN FREE PATH (MFP) OF SOME OXIDES IN THE ENERGY RANGE OF 122KeV to 1330KeV," *Indian J Sci Res*, vol. 9, no. 2, pp. 79–84, 2019, doi: 10.32606/ijsr.v9.i2.00014.

[12] "مصطفى محمد عبدالمهدي اجملالي ا لدكتور المهندس أعداد وتأ ليف المبادئ وا لتطبيقات ا لوقا ية الإشعاعية."

Chapiter III:Methodology

(Sample Analysis and Computational Methods)

III.1 Introduction

This chapter delineates the experimental methodologies and computational instruments employed to assess the elemental composition and radiation interaction characteristics of diverse soil samples obtained from the Adrar region in southern Algeria. A mixture of laboratory study and numerical modelling was utilised to ascertain the mass attenuation coefficients of these materials, frequently applied in conventional building. The methodology encompasses sample preparation, elemental analysis, and the utilisation of two simulation programs: WinXCom and Geant4.

III.2 Preparation and Analysis of Samples

III.2.1 Description of locations

The term Adrar is regarded as one of the most commonly utilised words in the Amazigh lexicon among the region's original inhabitants, since numerous sources indicate it is a translation of the word Adagagh, which is synonymous with stone or stones in Arabic[1]. Adrar is situated in the southwestern region of Algeria (27°59’ N, 0°17’ W), as illustrated in Figure 3. 1. The area encompasses 427,968 km² and has a population of 43,903 residents. Presidential Decree 15-140 established administrative districts within the mandated states and delineated their regulations. This decree encompassed the state of Adrar, which was partitioned into three districts: Timimoune, Bordj Badji Mokhtar, and Adrar[2].

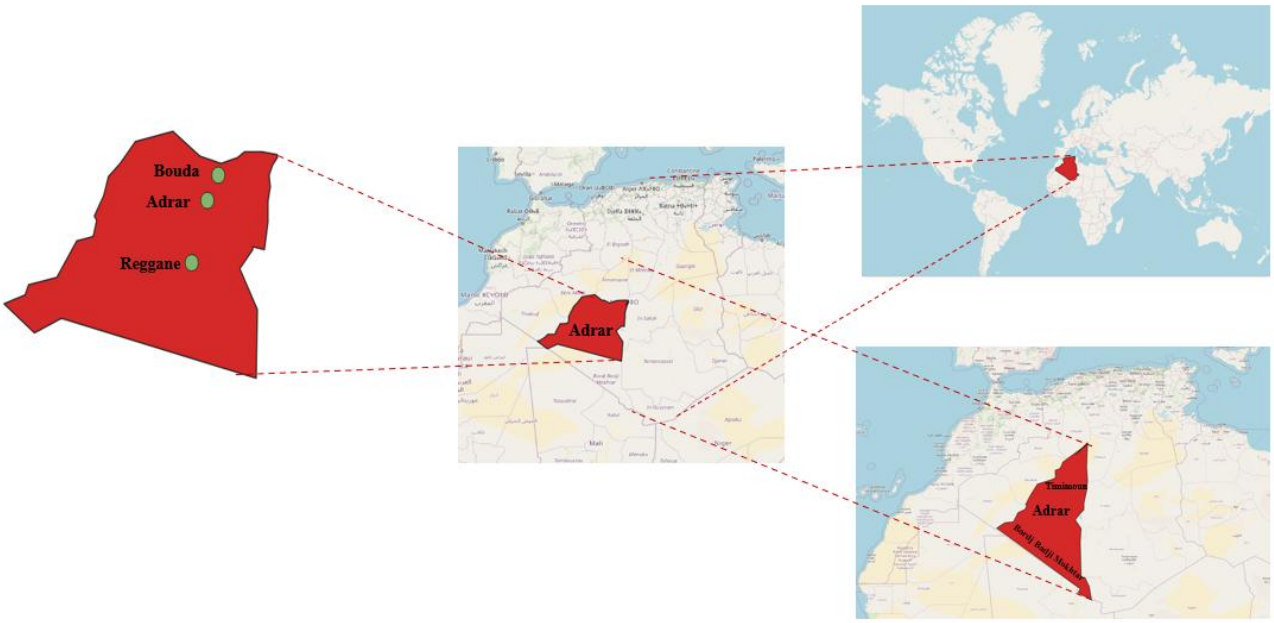

Figure3. 1.The geographical position of the Adrar region.

This study involved the collection and analysis of samples from three unique regions in southwestern Algeria: Adrar, Bouda, and Reggane Figure 3. 1.These areas are situated within the Saharan platform and are distinguished by varied geomorphological and climatic conditions. Adrar is characterised by its rugged plateaus and gravel plains, Bouda is a historically significant oasis region, and Reggane is situated at the periphery of the expansive sandy Erg Chich desert. The selection of these geographically and environmentally varied sites aims to acquire representative samples that reflect the natural attributes and mineral variety of the broader Sahara region[3].

III.2.2 Geographical formations

The state's land surface comprises Hamada, Al-Raqq, Erg, Sabkha, other minor mountain ranges, and the Tadmait plateau[1], [2].

Hamada: is a rocky plateau characterised by stacked layers of extensive calcareous rocks.
Raqq: is a flat expanse scattered with arid stones from which sand, referred to as arak, is produced.
Al-Arak: It is a prominent sand dune formed by the winds. It proliferates extensively in the northern region of the state, extending from east to west, beside Arak Shash to the south.
Sabkha: a lake whose water evaporates over the summer, resulting in the formation of Sabkha.
Mountain ranges: these are modest mountains prevalent in Qawrarah and south of Tediclet.

The Tadmaite plateau: standing at 600 meters, is the most prominent plateau.

In this specific geological environment, the Adrar region possesses substantial reserves of clayey sedimentary deposits beside a significantly thick layer of dune sand.

III.2.3 General Definitions and Properties of Clay and Sand

III.2.3.1 Clay and Clay Minerals: Definition, Properties, and Formation

Clay and clay minerals are natural materials classified as **hydrated phyllosilicates**, characterized by a crystalline structure composed of two-dimensional sheets. The term "clay" originates from the Greek word "argilos," meaning white, and refers to fine-grained materials with particle sizes less than 2 microns. These materials exhibit **plasticity when wet** and **harden upon drying or firing**[4].

The physical, chemical, and mineralogical properties of clay are strongly influenced by the **formation conditions** and the **nature of the parent rock**. Clayey rocks are widespread on the Earth's surface and consist of both clay and non-clay minerals. Physical, chemical, and biological weathering processes produce natural clays with heterogeneous compositions. Clay minerals may form from the decomposition of minerals such as feldspar or from chemical alteration of volcanic ash[4].

Temperature and pressure are crucial in determining the type of clay minerals formed. In cold regions, weak alteration leads to minerals closely resembling the parent rock, such as **illite and chlorite**. In contrast, hot and humid climates promote strong hydrolysis, resulting in minerals like **kaolinite and smectite**. Temperate climates favor the formation of **illite, chlorite, or vermiculite**.

Generally, three main processes contribute to the formation of clays and clay minerals:

1. **Direct decomposition of the parent rock** due to erosion factors like rain, wind, freezing, and thawing.
2. **Transformation of minerals by substances transported through soil water**, converting them into clayey materials.
3. **Deposition or accumulation of mineral ions** caused by soil degradation or sediment build-up in watercourses.

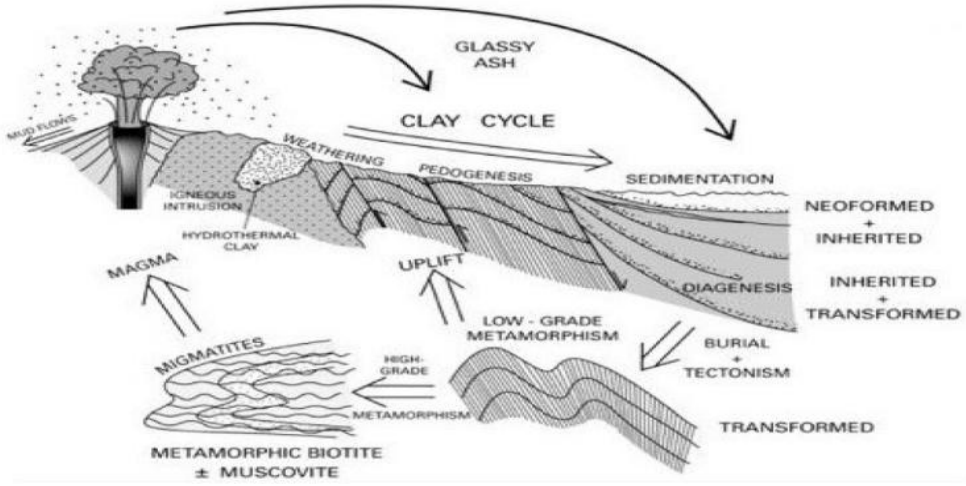

Figure3. 2.The process of clay formation.[4]

III.2.3.2 Classification of Clay Minerals

Classification based on Structure

The clay minerals are categorised into four classes based on their structure. The initial category comprises the 1:1 family of minerals, characterised by a structure formed by the combination of a tetrahedral sheet and an octahedral sheet (Figure3. 3.The hydrogen bond formed between the oxygen atoms[5].

The interaction between the tetrahedral sheet and the hydroxyl groups of the octahedral sheet imparts significant stability to this structure. This stability inhibits the incorporation of chemical components and water molecules into the interlayer region, hence averting the swelling of these minerals. This results in a minimal basal distance of approximately 7 Å. Examples of clay minerals in this category include kaolinite, halloysite, and dickite. Conversely, when the fundamental layer consists of two tetrahedral sheets encasing an octahedral sheet, it is classified as 2:1 Figure3. 3.The layer thickness is approximately 10 Å, although the basal distance ranges from 9 to 15 Å, contingent upon the elements in the interlayer space. The isomorphic substitutions in the tetrahedral and/or octahedral sheets impart a negative charge to the fundamental layer. The principal minerals of this group include micas, illites, smectites, and vermiculites. For a four-layer stack, the classification is designated as 2:1:1 Figure3. 3.This structure represents a specific instance of the 2:1 structure, wherein the interlayer space is filled by an octahedral layer, yielding a basal spacing of around 14 Å. The final category is inter-stratified minerals, characterised by a relatively regular arrangement of sheets of varying compositions. The thickness of the sheet in this category is vary[6]. Among

the interstratified minerals, the regular interstratified types include corrensite (chlorite-smectite), allevardite, and rectorite (illite-vermiculite)

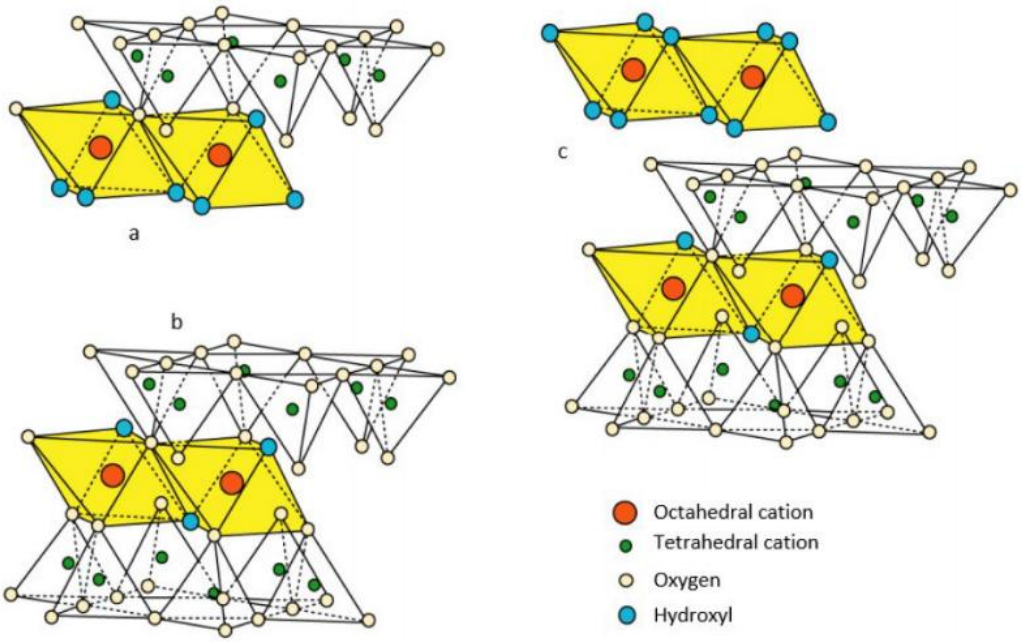

Figure3. 3.Type of clay minerals. (a):1/1.(b):2/1.(c):2/1/1.[5]

whereas kaolinite-smectite, chlorite-chlorite, and vermiculite-smectite are classified as irregular interstratified groups.

Classification by Color

The presence of specific ions (Fe, Mg), even in minimal amounts, affects the coloration of clay minerals.

Clays come in red, yellow, blue, pink, green, white, and various other colors. Each color enhances the properties of a clay mineral for more specialized applications. The most common varieties are white, green, and red clays.[6]

Green Clays

This category encompasses clay minerals characterised by low iron oxide concentrations. These are primarily illites and smectites, specifically montmorillonite. The oxidative characteristics of these minerals promote their application in eradicating viruses and bacteria, while highlighting their ability to attract diverse contaminants.

Figure3. 4.Green Clay .[5]

White Clays

Clays and clay minerals are white when they form in very uniform conditions and are not moved. This means that the material doesn't have any colouring.

This trait of not having any colouring elements makes these minerals very useful in medicine, cosmetics, and ceramics. Kaolinite and smectites are in this group.[5]

Figure3. 5.White Clay.[5]

Red Clays

The red clays abundant in iron oxides are typically illites.

Figure3. 6.Red Clay[5].

III.2.3.2Definition of sand

Sand is a natural substance consisting of a collection of grains, predominantly quartz. Their size, shape, and geological parameters fluctuate, typically spanning from 0.063 mm to 2 m.

Sand formation results from erosion, the interaction of rocks, notably those in desert environments, with severe temperatures and persistent winds, causing the disintegration and fragmentation of rocks into sand grains of diverse sizes and forms.

Sand is created when particles deposited by water in rivers, lakes, or streams, or by air in deserts and dunes, become buried under successive layers of sediment. This burial process leads to the dispersion and bonding of the particles through the precipitation of calcium carbonate, iron oxide, or silicates from groundwater that permeates the spaces between the grains.

Sand grains exhibit a spectrum of colours, influenced by the quantity and hue of the binders, as well as the predominant colour of the mineral grains that constitute them. The predominant sand colours are brown, red, and pink, attributable to the presence of limestone and iron oxide. Brighter hues arise from the lack of binders.

Figure3. 7.sand.[6]

III.3 Sample Collection and Preparation

Four samples were collected from different locations within the Adrar region (southern Algeria). Figure3.1. indicates the geographical locations where each sample was collected.

The regions and types of samples collected are as follows:

S1 = Red Clay: Collected from Reggane, a site historically known for French nuclear tests.

S2 = Green Clay: Taken from the central area of Adrar.

S3 = White Clay: Obtained from the Buda region.

S4 = Sand: Also collected from within the Adrar region.

III.4 Sample Preparation Procedure

After collecting clay samples from the designated site and documenting their initial condition, we then conducted a series of laboratory tests according to the American Society for Testing and Materials ASTM standards[7]:

Impurity Removal: Visible impurities were manually removed from each sample.

Grinding: Samples were finely ground to achieve a uniform particle size.

Drying: The ground samples were left to dry naturally in the sunlight.

Thermal Treatment: Finally, samples were baked at 100°C to remove any remaining moisture and stabilize them for further analysis.

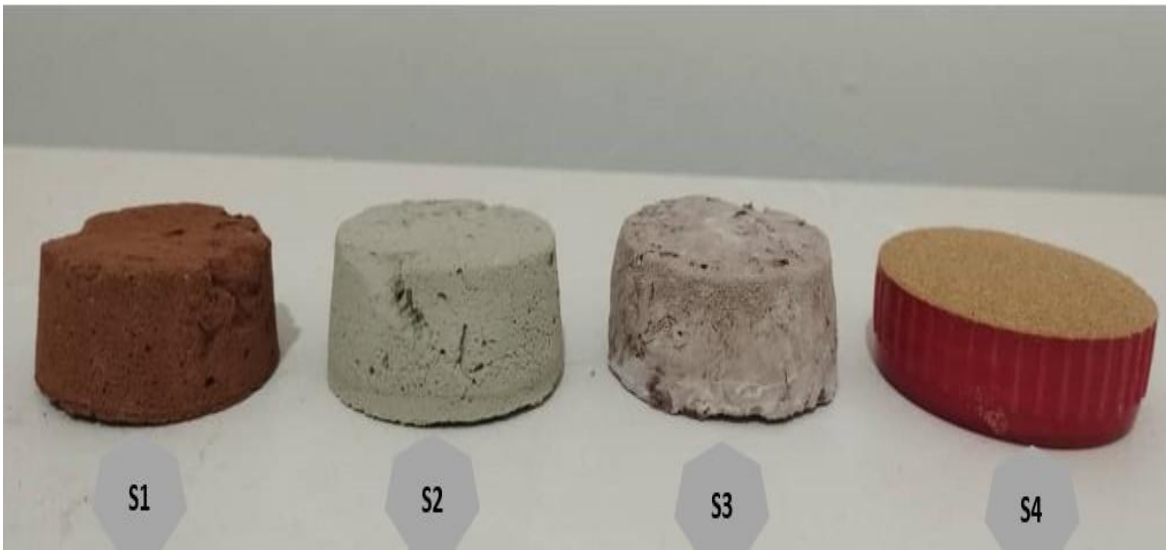

Figure3. 8.Photo of the studied samples.

III.5 Microstructural and Chemical Characterization of Clay by SEM/EDX Technique

In scanning electron microscopy (SEM), a concentrated primary electron beam is systematically rastered across the sample. At every pixel, the reflected electrons are recorded, producing a minuscule greyscale image of the specimen. Two imaging modalities exist:

Backscattered electrons (BE) yield material contrast.

Secondary electrons (SE) yield topographical contrast.[8]

Furthermore, the primary electron beam induces the sample to release distinctive X-rays. The elements in the sample and their corresponding modal weights can be accurately ascertained by examining the colour spectrum in an EDX detector.

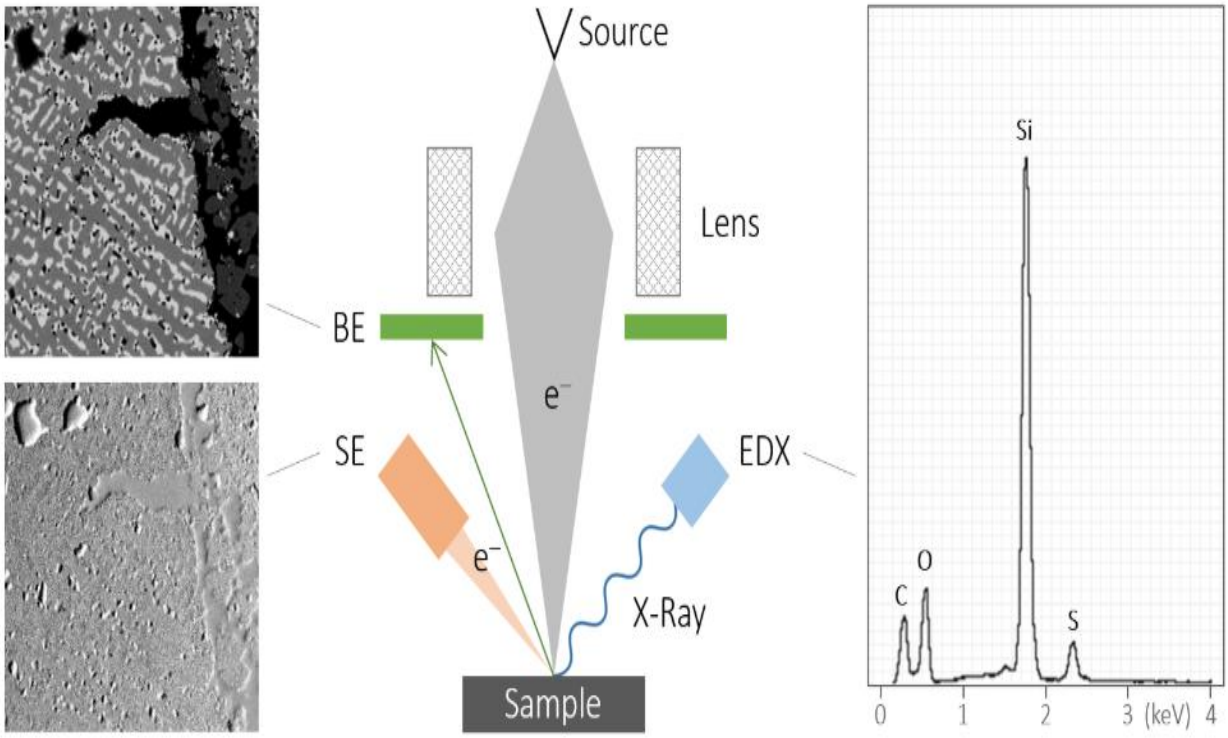

Figure3. 9.Principle of Functioning of the Scanning Electron Microscope (SEM).[9]

Applications

- Analysis of damage and wear at a microscopic scale.
- Examination of ageing, corrosion, and oxidation of components.
- Identification of the source of the particles, chips, and debris that result in failure.
- Analysis of errors in the delamination of coatings and paints.
- Examination of electrical contact issues.
- Examination of surfaces and coatings.
- Material characterization and microstructural examination.

III.5.1 Description of the Scanning Electron Microscope (SEM-FEG: Quattro S) Utilised in the Study

The FEG SEMshown in the image and used in this study, from the National Polytechnic School of Constantine, is a microscope that can produce and gather comprehensive data from any sample material. It can be effortlessly and readily transitioned among three vacuum modes,

facilitating the examination of incompatible conductive, non-conductive, and high-vacuum materials:

- High vacuum mode (<6 x 10^-4 Pa) for imaging and microanalysis of conductive and/or conventionally prepared specimens; - Low vacuum mode (10 to 130 Pa) for imaging and microanalysis of non-conductive specimens without preparation; - ESEM™ mode (10 to 4000 Pa) for incompatible specimens under high vacuum that cannot be examined using traditional electron microscopy methods.

The microscope is additionally outfitted with an EDS system and an EBSD system.

Figure3. 10.SEM-FEG: Quattro S.[9]

III.6Computational Tools and Simulation Software: WinXCom and Geant4

III.6.1Computational Tools and Simulation Software: WinXCom

XCOM calculates total and partial cross sections for phenomena including incoherent and coherent scattering, photoelectric absorption, and pair creation. It considers absorption edge effects and permits output in both tabular and graphical formats. The program computes mass interaction coefficients for compounds based on their chemical formulas, whereas for mixtures, the user inputs weight fractions.

Data on photon scattering and absorption are crucial for scientific, technical, and medicinal applications. Printed cross-section tables are frequently inadequate and constrained in scope due to the diverse array of materials and energy levels involved. The XCOM tool provides a pragmatic answer by calculating photon cross sections and attenuation coefficients for any element, compound, or mixture over an extensive energy range (1 keV to 100 GeV).

XCOM is tremendously beneficial, although it has limitations: it presumes neutral isolated atoms and excludes solid-state effects or less prevalent interactions such as nuclear photo effects or energy absorption by secondary particles.

III.6.1.1 Element Database

A complete database of photon cross-sections was created by integrating data on incoherent and coherent scattering, photoelectric absorption, and pair creation. Incoherent scattering was computed utilising the Klein-Nishina formula in conjunction with Hartree-Fock functions, incorporating requisite adjustments. Coherent scattering employed the Thomson formula and relativistic atomic form factors. Photoelectric absorption data were obtained utilising a central potential and the Hartree-Slater model, which was extended to higher energies by a semi-empirical method. Cross sections for pair creation were aggregated utilising diverse theoretical models to guarantee precise outcomes throughout energy spectra.

Despite the existence of correction parameters for renormalizing photoelectric cross sections to align with more sophisticated atomic models, these were not utilised in the XCOM database. This choice was predicated on evidence indicating superior concordance with experimental results without renormalisation.

Instructions for Executing the XCOM Program

The XCOM database can be utilised in two ways. The text-based version produces a fundamental text table of data. The alternative version provides the user with additional options and functionalities, such as file uploading, graphing, and graphical tables. The remaining information in this page is suitable for both output channels. Two forms must be completed to obtain data. The initial form generates the corresponding second form. The initial form pertains to generic information regarding the sort of material: element, compound, or mixture ($Z \leq 100$). The latter is more precise, encompassing energy values and graphing possibilities. The following delineates the specific input fields.[10]

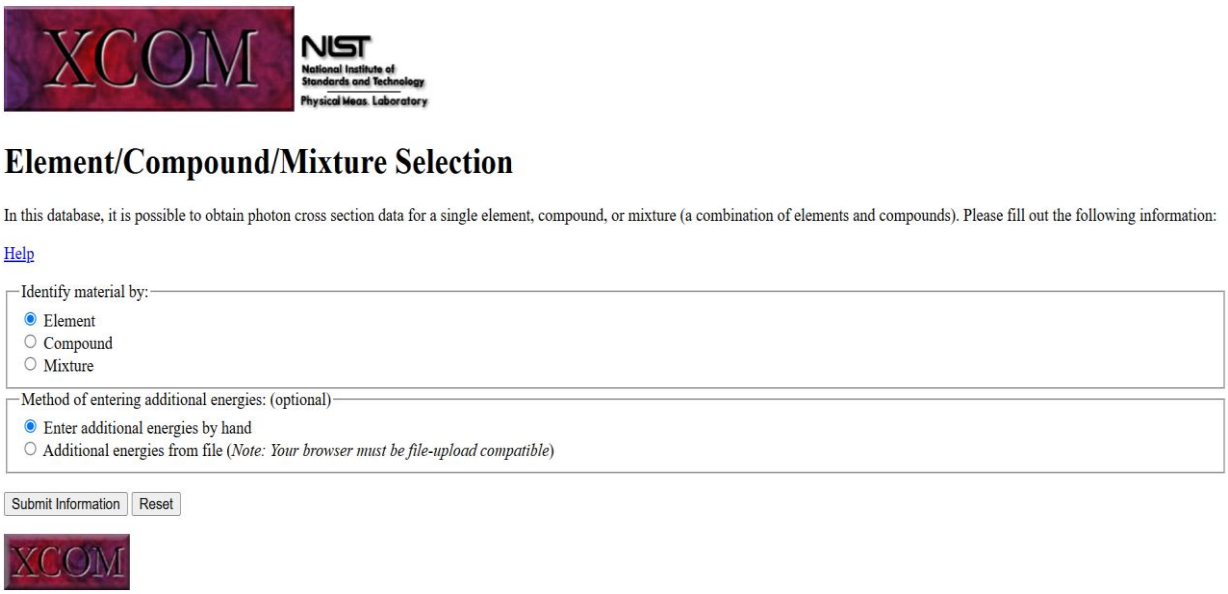

Figure3. 11.XCOM program interface.

The First Form

The substance for which cross sections are to be calculated may be classified as an element, compound, or mixture. The application will calculate values for standard energies, while allowing the user to input supplementary energies as well. This can be accomplished by manually entering the values or by utilising file upload (note: your browser must support file uploads). This information is utilised to prepare a particular form using the alternatives defined below.

Elements

Elements can be identified by their atomic number or their chemical symbol. Only elements one to one hundred are accessible.

Select by: (only elements 1 - 100)

Atomic Number:

or

Symbol:

Compounds

Chemical formulas for compounds must be presented in conventional chemical notation, utilising correct upper and lower case letters. Nonetheless, due to hardware constraints, subscripts must be inscribed inline. The formula for calcium tungstate is shown as CaWO4. Parentheses, spaces, and periods are prohibited. The formula for calcium phosphate should be written as Ca3P2O8, rather than Ca3(PO4)2.

Substances composed solely of molecules containing a single type of atom can be classified as either elements or compounds. Molecular nitrogen may be regarded as a "element" denoted by the symbol N, or as a "compound" represented by the formula N2.

Formula for compound (e.g. H2O for water):

Mixtures

Mixtures may comprise "elemental" constituents and/or "compound" constituents. This is an issue of expedience as it does not alter the outcomes.

The user must indicate the chemical symbol or formula, along with the weight fraction for each component. The program subsequently use the input data to calculate the weight fractions of the individual atomic parts and their cumulative sum. If the sum of the weight fractions in the input data does not equal one, the input data is accepted, and the software renormalises the weight fractions to ensure they sum to one.

Enter the formulae and relative weights separated by a space for each compound. One compound per line. For example:

```
H2O 0.9
NaCl 0.1
```

Note: Weights not summing to 1 will be normalized.

The Discretionary Output Title

The title, which may contain embedded spaces, will be shown at the top of the output page.

Optional output title:

The Energy Catalogue

Users may 1) restrict output to the conventional energy grid, 2) incorporate preferred energies into the standard grid, or 3) confine output to their chosen set of energies. In scenario 2), the supplementary energies are integrated into the conventional energy system based on their magnitude. They are represented by a distinct colour in the output table to differentiate them from the regular grid values. In scenario 3), the energies will be arranged in numerical order, and duplicates will be eliminated.

Users can input extra energy either via the keyboard or from a pre-prepared input file. This file, located in any preferred location on a floppy or hard disc, must include a list of energies, with entries delineated by Return or Enter. Alert: A maximum of 75 energies may be allocated to a single element. A lesser amount may be deemed inappropriate if many elements are present. The typical grid may encompass excessive energies if numerous elements are present.

Additional energies in MeV: (optional) (up to 100 allowed)

Note: Energies must be between 0.001 - 100000 MeV (1 keV - 100 GeV) (only **4** significant figures will be used). One energy per line. Blank lines will be ignored.

Include the standard grid

Energy Range:

Minimum: 0.001 MeV

Maximum: 100000 MeV

Output Units

The user is presented with three options for elements: 1) All measurements are in cm^2/g; 2) All measurements are in barns/atom, where 1 barn = 10^{-24} cm^2; 3) Partial interaction coefficients are expressed in barns/atom, and total attenuation coefficients are expressed in cm^2/g. All quantities for compounds and mixtures are expressed in cm^2/g.

Options for output units:

- (●) All quantities in cm^2/g
- ( ) All quantities in *barns/atom*
- ( ) Partial interaction coefficients in *barns/atom* and total attenuation coefficients in cm^2/g

The Graph

Any quantity of the seven coefficients may be represented graphically at the same time. If the "none" option is selected, it will supersede all other choices, and no graph will be presented. Note: Data can be displayed more rapidly without graphing, and a greater number of curves requires more time to graph than fewer curves. Zooming in can be achieved by redefining the energy spectrum. Nevertheless, the minimum energy range (maximum zoom) is an order of magnitude (e.g., 0.01 to 0.1). The buttons on the right facilitate the alteration of the image size, which may be advantageous for printing purposes. The provided values represent the image width in pixels.

Graph options:

- [ ] Total Attenuation with Coherent Scattering
- [ ] Total Attenuation without Coherent Scattering
- [ ] Coherent Scattering
- [ ] Incoherent Scattering
- [ ] Photoelectric Absorption
- [ ] Pair Production in Nuclear Field
- [ ] Pair Production in Electron Field

- [ ] None

The Output Table

The atomic numbers and weight fractions of the atomic constituents are provided above the table. The table's main body is equipped with sufficient headings to be self-explanatory. The leftmost column presents the designations of the absorption edges (K, L1, L2, L3, M1, M2, ...) along with the atomic number of the relevant atomic ingredient. Data for energies immediately below and beyond each threshold are presented on two lines. The conventional energy grid inherently incorporates a minimum of one additional energy level between any two consecutive absorption edges. For materials with an atomic number $Z < 10$, no absorption edges exist above the minimum energy of 1 keV.

III.6.2 Computational Tools and Simulation Software: Geant4

GEANT4 Scope Of Application

Geant4 is a complimentary software suite of tools designed for the precise simulation of particle interactions with materials. The toolkit encompasses all facets of the simulation process, including:

- system geometry.
- involved materials.
- pertinent fundamental particles.
- primary event generation.
- particle tracking through materials and electromagnetic fields, physics processes dictating particle interactions.
- responses of sensitive detector components.
- event data generation.
- event and track storage.
- visualization of the detector and particle trajectories.
- capture and analysis of simulation data at varying levels of detail and refinement.

Users can create independent apps or applications based on another object-oriented framework. The tools will assist them from the original problem formulation to the generation of results and graphics for dissemination. The toolkit comprises:

- user interfaces.

- integrated steering procedures.
- command interpreters that function at all levels of the simulation.

Geant4 encompasses a comprehensive array of physics models designed to manage particle interactions with matter over an extensive energy spectrum. Data and expertise have been sourced globally, and in this context, Geant4 serves as a repository that encompasses a significant portion of the existing knowledge on particle interactions. Geant4 is developed in C++ and utilises sophisticated software engineering methodologies and object-oriented principles to get transparency. The method of inputting or calculating cross sections is distinct from their utilisation or retrieval. The user can exceed the capacity of both functions. The calculation of the final state can be categorised into alternative or complementary models based on the energy range, particle type, and material. To develop a particular application, the user-physicist choose from these options and executes code within user action classes provided by the toolkit. A significant issue with prior simulation systems was the challenge of incorporating new or alternative physics models; development was hindered by the augmented size, complexity, and interdependence of the procedure-based code. Conversely, object-oriented methodologies facilitate complexity management and reduce dependencies by establishing a standardised interface and shared organisational principles for all physics models.

Within this framework, the functionality of models can be readily identified and comprehended, and the development and integration of new models is a clearly defined process that requires minimal or no alterations to the existing code.

GEANT4 Functionality Overview

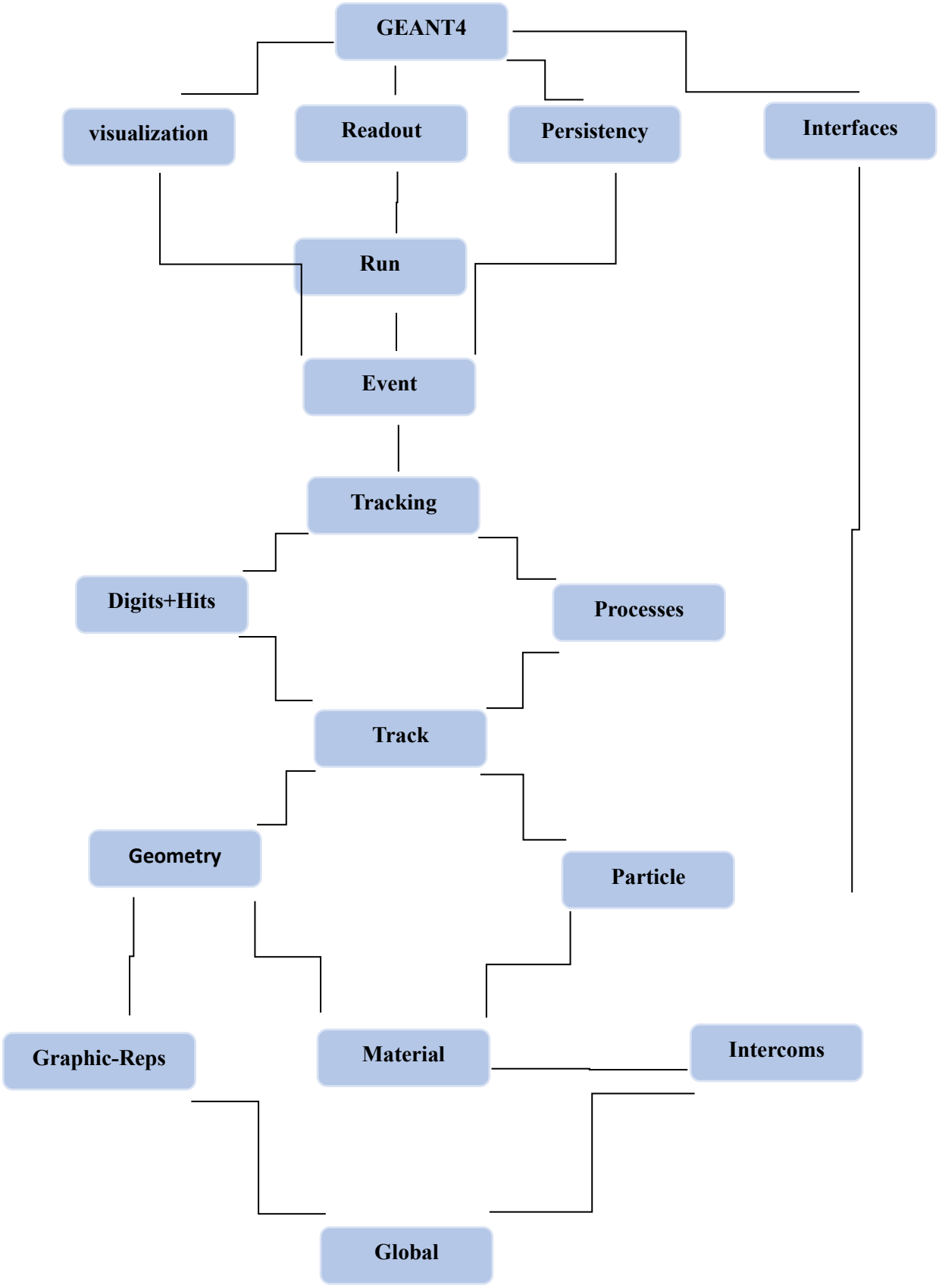

Figure3. 12.Geant4 class categories.

The categories at the base of the figure are utilised by nearly all higher categories and provide the foundation of the toolkit.

The global

category encompasses the system of units, constants, numerics, and random number management.

The two classifications:

• materials

• Particles

Implement mechanisms essential for delineating the physical characteristics of particles and materials pertinent to the simulation of particle-matter interactions. • **Geometry**

The module provides the capability to articulate a geometrical framework and facilitate the effective propagation of particles within it.

Above these exist categories necessary for delineating the tracking of particles and the physical processes they experience.

The track

category has classes for tracks and steps, utilised by

the processes

category which comprises implementations of models for physical interactions, including electromagnetic interactions of leptons, photons, hadrons, and ions, as well as hadronic interactions. All operations are initiated by

the tracking

category which oversees their impact on the progression of a track's state and supplies data in critical quantities for hits and digitisation.

The event

category oversees events based on their tracks, whereas

the run

category organises groupings of events that utilise a shared beam and detector configuration.

readout

category facilitates the management of pile-up.

Procedure for Utilizing GEANT4 to Compute the Attenuation Coefficient of Photons

1. Definition of Sample and Medium

Specify the materials for each sample: include their elemental makeup, weight/molar fractions, and density (g/cm³

2. Selection of Physics List

. Select an appropriate electromagnetic physics list for photons:

G4EmLivermorePhysics or G4EmPenelopePhysics for enhanced precision in the keV–MeV spectrum, orG4EmStandardPhysics ensures an equilibrium between velocity and accuracy.

. Activate mechanisms: photoelectric effect, Compton scattering, pair creation, and Rayleigh scattering.

3. Definition of Primary Generator

. Particle type: photons.

.Energy: the specified photon energies (e.g., 662 keV, 1.25 MeV).

.Beamorientation: perpendicular to the specimen (along the -axis).

.Beam dimensions: point source or diminutive disk encompassing the sample surface.

.Quantity of events: adequately substantial (e.g.,) to diminish statistical uncertainty.

4. Management of Runs/Events/Tracking

. Conduct an individual run for each energy level and each sample thickness.

. Preserve outputs: $\boldsymbol{N_{trans}}$,$\boldsymbol{N_{inc}}$and the quantity of simulated events.

5. Transmission Computation

$$\boldsymbol{T} = \frac{\boldsymbol{N_{trans}}}{\boldsymbol{N_{inc}}}$$

6. Linear and Mass Attenuation Coefficients

Linear attenuation coefficient:

$$\mu = \frac{1}{x} Ln(T) \qquad [cm^{-1}]$$

Mass attenuation coefficient :

$$\mu_m = \frac{\mu}{\rho} \qquad [\frac{cm^2}{g}]$$

IV.Conclusion

This chapter meticulously delineated the experimental methodologies and computational processes employed during the study. The preparation and analysis of the examined samples were executed using systematic and reproducible processes to guarantee data correctness and consistency.

The computational methodology, utilizing Geant4 simulations and XCOM theoretical calculations, established the requisite foundation for modeling photon interactions and assessing the shielding efficacy of the samples.

The approach outlined above provides a robust framework for the ensuing analysis and discussion of outcomes, which are elaborated in the succeeding chapter.

References

[1] B. Bouhania, “A propos de quelques Toponymes du Touat-Tidikelt-Gourara dans la Wilaya d’Adrar About some Toponyms of Touat-Tidikelt-Gourara in the Wilaya of Adrar”.

[2] M. Benmedjahed, A. Dahbi, A. Hadidi, A. Khelfaoui, S. Mouhadjer, and O. Djaafri, “Adrar Initial State Investigation for the Use of Renewable Energies in Irrigation Systems,” International Journal of Sustainable Development and Planning, vol. 18, no. 6, pp. 1671–1680, Jun. 2023, doi: 10.18280/ijsdp.180603.

[3] M. A. B. A. Kadri Yasser, “Étude ethnobotanique de quelques plantes médicinales dans une région hyper aride du Sud-ouest Algérien «Cas du Touat dans la wilaya d’Adrar».,” J Anim Plant Sci, vol. Vol.36, no. 2: 5844-5857, 2018.

[4] A. Mohammed, M. O. Hassan, S. Abdélaziz, and K.-A. Fatiha, “Characterization of clay deposits in the Adrar region, with a view to their valorization in the building materials industry,” MATEC Web of Conferences, vol. 149, p. 01079, 2018, doi: 10.1051/matecconf/201814901079.

[5] Ochieng Ombaka, “Characterization and classification of clay minerals for potential applications in Rugi Ward,” 2016.

[6] Prof Ahmed-Umran-Dogan, “Clay minerals (classification, identification, structure and application),” 2017BC.

[7] J. M. Keller and G. W. Gee, “Comparison of American Society of Testing Materials and Soil Science Society of America Hydrometer Methods for Particle-Size Analysis,” Soil Science Society of America Journal, vol. 70, no. 4, pp. 1094–1100, Jul. 2006, doi: 10.2136/sssaj2005.0303n.

[8] Analytical Techniques in Forensic Science. (2021). United Kingdom: Wiley. Rosalind Wolstenholme, Sue Jickells, Shari Forbes.

[9] ptemf.enp-constantine. Equipment of the Analysis, Evaluation and Maintenance Section.

[10] W. Mui et al., “Development of ASTM International D8405—Standard Test Method for Evaluating PM2.5 Sensors or Sensor Systems Used in Indoor Applications,” J Occup Environ Hyg, vol. 20, no. 9, pp. 373–389, 2023, doi: 10.1080/15459624.2023.2212739.

Chapter IV: Results and discussion

IV.1 Introduction

This chapter delineates the findings derived from the elemental analysis and the assessment of the photon shielding characteristics of the examined clay samples. Several characteristics were computed, including the μ_s , μ , HVL , TVL , MFP. The shielding indicators were evaluated for four distinct clay kinds and compared with values obtained from the XCOM database and the Geant4 Monte Carlo simulation toolbox. The congruence between the two methodologies was assessed to confirm the reliability of the findings.

Additionally, the computed shielding characteristics were juxtaposed with previously published data to assess the efficacy of the examined clays in radiation protection applications. This comparative analysis underscores the impact of elemental composition on attenuation efficiency and enhances the comprehension of the prospective application of natural materials in shielding design. The discourse additionally examines any identified disparities, and the practical ramifications of the results.

IV.2 Analysis of elements

Table 4. 1.The proportions of the sample's elemental composition (%)

Element	*Sample S1 Density = 1.97 g/cm3*	*Sample S2 Density = 1.99 g/cm3*	*Sample S3 Density = 1.98g/cm3*	*Sample S4 Density = 1.99 g/cm3*
O	**58.35**	**45.69**	**42.77**	**53.40**
Fe	**0.21**	**1.91**	**0.71**	**3.55**
Co	**0.03**	**1.10**	**0.58**	**0.62**
Al	**6.70**	**9.38**	**18.53**	**6.48**
Si	**27.78**	**28.44**	**26.44**	**28.53**
K	**4.65**	**7.64**	**4.85**	**4.09**
Ca	**2.29**	**2.47**	**0.43**	**3.33**
Mg	------	**3.36**	------	-----
Na	------	------	**5.69**	-----

Table 1 delineates the elemental makeup of the analyzed clay samples as ascertained using SEM/EDX analysis. The statistics reveal that oxygen (O) is the predominant element in all samples, consistent with its established prevalence in the Earth's crust. Silicon (Si) regularly ranks as the second most abundant element, with concentrations varying from 26.44% in white clay to 28.44% in green clay.

Additional identified elements comprise several alkali and alkaline earth metals, including Fe, Co, Al, K, and Ca.Green clay notably possesses a substantial magnesium (Mg) concentration

of 3.36%, a characteristic not found in the other samples. Conversely, white clay possesses a notably elevated sodium (Na) percentage of 5.69%, setting it apart from others.

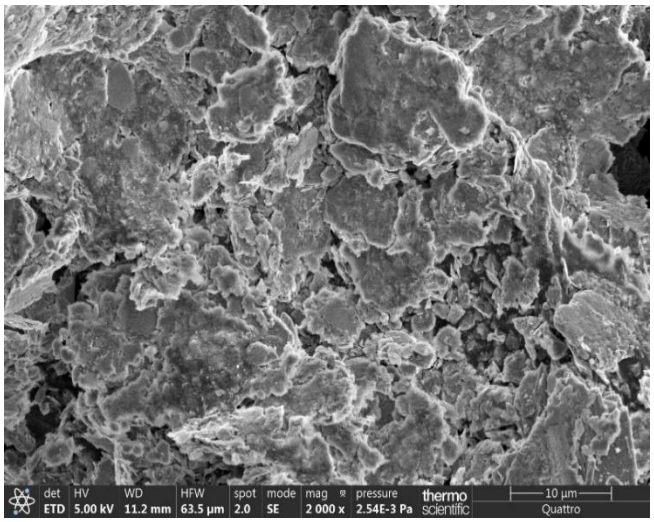

S1= Red clay

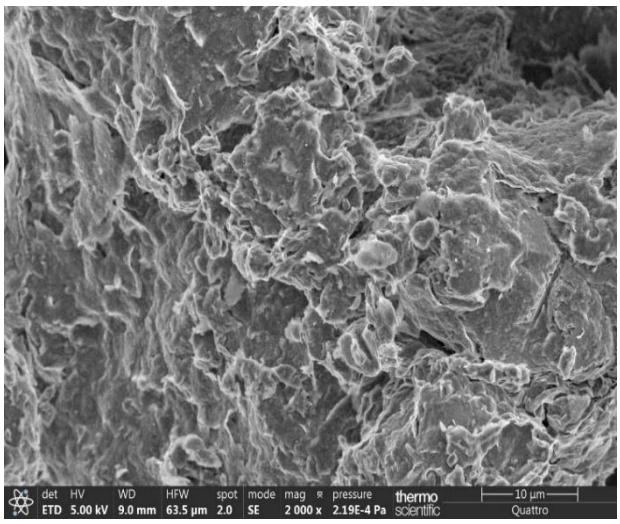

S2= Green clay

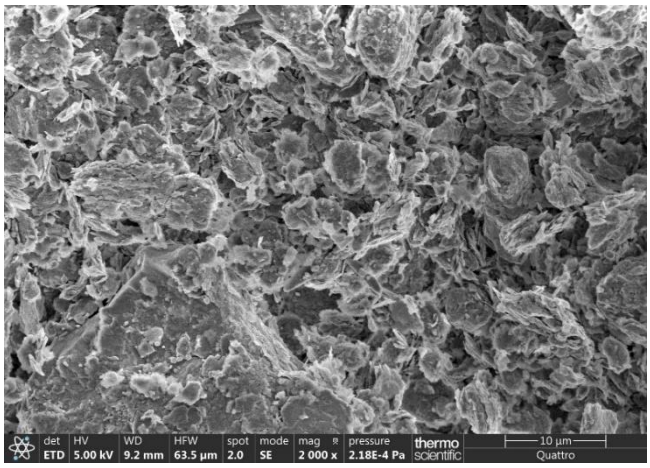

S3= White clay

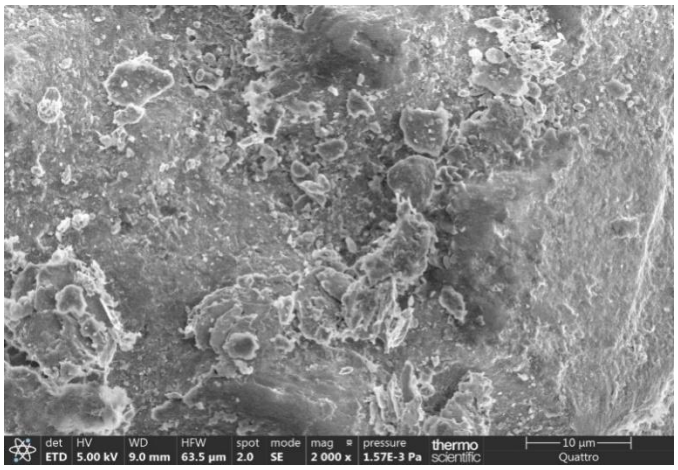

S4= Sand

Photos of the studied samples obtained using a Scanning Electron Microscope (SEM)

The SEM micrographs presented in Figure X illustrate the surface morphology of four different materials: red clay (S1), green clay (S2), white clay (S3), and sand (S4). The red clay exhibits a dense and compact structure with irregular surfaces and fine microcracks, indicating a tightly packed grain arrangement. In contrast, the green clay shows a more fibrous and intertwined texture, with a less compact morphology and higher porosity. This structure may contribute to the unique elemental composition of green clay, such as the presence of magnesium. The white clay sample presents a more homogeneous distribution of granular particles, with relatively uniform porosity and smoother surface features compared to the red and green clays. Finally, the sand sample displays a coarse, loosely bound structure characterized by large voids and

weak interparticle cohesion, suggesting high permeability and low shielding capability. Overall, the microstructural differences among the samples are likely to influence their physical properties, including their potential performance as radiation shielding materials.

IV.3 Results of the S1& S2 comparison with the lead

Table 4. 2.Linear attenuation coefficient (μ) of the samples.

Samples	Pb	S1	S2
Density (g/cm3)	11.3	2.02	2.44
81(Kev)	2.346	0.191	0.244
662(Kev)	0.110	0.072	0.076
1173 (Kev)	0.062	0.059	0.058
1332 (Kev)	0.0562	0.052	0.054

Table 4. 3.Linear attenuation coefficient (μ) of the samples.

Samples	Pb	S1	S2
81(Kev)	26.509	0.385	0.595
662(Kev)	1.243	0.145	0.185
1173 (Kev)	0.701	0.119	0.142
1332 (Kev)	0.633	0.105	0.132

Table 4. 4. 4Half value layer (HVL) of the samples.

Samples	Pb	S1	S2
81(Kev)	0.026	1.800	1.164
662(Kev)	0.557	4.779	3.746
1173 (Kev)	0.988	5.823	4.880
1332 (Kev)	1.094	6.600	5.250

Figure 4. 1.Energy Dependence of The Mass Attenuation Coefficient for Pb.S1.S2

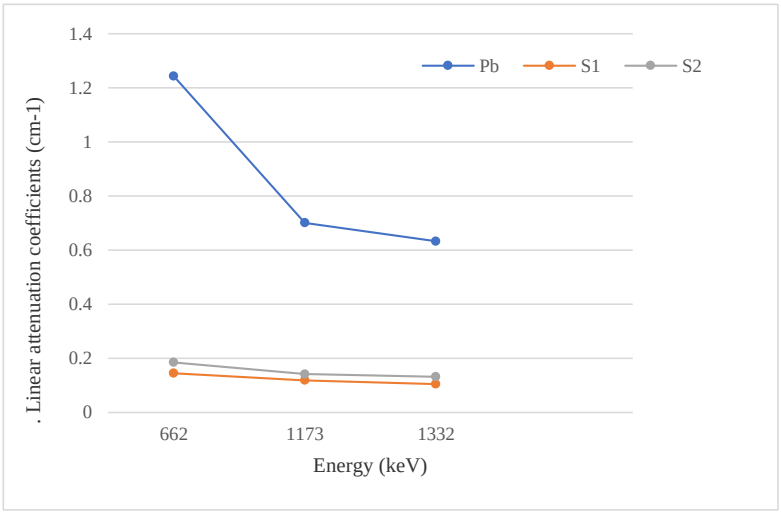

Figure 4. 2.Energy Dependence of The Linear Attenuation Coefficient for Pb.S1.S2

The basic composition of the building material samples is provided in Table 4.1. The most prevalent elements in the samples are Si, O, and Al, listed in order of abundance from greatest to least. Sample S1 has a high concentration of iron.

•Upon inputting the sample components and photon energies ranging from 81 KeV to 1332 KeV into the WinXcom application, we received the results presented in Table 4.2. and Figure 4.1 indicate that at various energy levels, the mass attenuation coefficient of Pb surpasses that of the other samples with a notable difference. This occurs at low energies, with the disparity diminishing as energy increases. Subsequent to the Pb material, the samples are arranged in the following sequence: S2, S1.

• Table 4.2 and Figure 4.2 indicate that the linear attenuation coefficient for Pb surpasses that of the other samples. Furthermore, the linear attenuation correlates with sample density; as density increases, so does the attenuation coefficient, thereby enhancing gamma radiation

shielding efficacy. Additionally, linear attenuation is relatively effective at low energies but diminishes at higher energies.

IV.4Calculation of μ_s , μ , HVL , TVL , MFP

Tables 4.5 through 4.6 display the theoretical outcomes for essential photon interaction parameters, encompassing the μ_s, μ, HVL, TVL, and MFP. The parameters were calculated utilising two reputable simulation programs, XCOM and Geant4, at four designated photon energies associated with frequently employed gamma-ray sources: Am-241 (0.060 MeV), Cs-137 (0.662 MeV), and Co-60 (1.173 MeV and 1.333 MeV). The study was performed on four independent samples: red clay (S1), green clay (S2), white clay (S3), and sand (S4).

A significant observation is the robust consistency between the XCOM and Geant4 results across all energy levels and materials. The percentage difference (Δ) between the two datasets varied from 0.040% to 2.04%, demonstrating significant reliability and compatibility between the simulation tools. This close agreement substantiates the accuracy of the calculated shielding settings.

Table 4.5 demonstrates that the mass attenuation coefficient (μ/ρ) diminishes with increasing photon energy, a phenomenon attributed to the energy dependence of interaction cross sections. Sample S1 has a μ/ρ value of 0.241 cm^2/g at 0.060 MeV, which markedly decreases to 0.055 cm^2/g at 1.333 MeV. This pattern is uniform across all samples and indicates the diminishing prevalence of photoelectric absorption at elevated energy.

Table 4.6 illustrates the linear attenuation coefficients (μ), which exhibit a declining trend as energy increases. Nonetheless, discrepancies among samples with identical energy levels are comparatively minimal. This is mainly attributable to the analogous bulk densities and comparable chemical compositions of the samples. Samples S2 and S4exhibited marginally elevated linear attenuation values attributable to their greater concentrations of heavy components, including Si, Ca, Fe, and Co, which enhance photon interaction probability.

Tables 4.7 and 4.8 present the HVL and TVL values, respectively, both of which escalate with photon energy. This indicates that higher-energy photons necessitate larger shielding layers to attain equivalent attenuation effects. The HVL for sample S2 escalates from 2.875 cm at 0.060 MeV to 6.333 cm at 1.333 MeV, highlighting the necessity for energy-specific shielding design. Likewise, the TVL readings exhibited a steady rise, consistent with the exponential attenuation law.

Table 4.9 ultimately displays the mean free path (MFP) values, which similarly rise with photon energy. This metric measures the mean distance a photon traverses within the material prior to interaction. Among the four samples, S2 consistently demonstrated the shortest MFPs, indicating enhanced attenuation capacity. Subsequently, S4, S1, and S3 were observed, indicating that mineral composition and density significantly influence shielding efficacy.

The theoretical research demonstrates that green clay (S2) and sand (S4) are the most efficient materials for gamma-ray shielding throughout the examined energy range, attributable to their superior densities and advantageous elemental compositions.

Table 4. 5.Mass attenuation coefficients (μ_s) of the samples.

Samples	Energy (Mev)	$\mu_s(cm^2g^{-1})$		Δ (%)
		XCOM	Geant 4	
S1	0.060	0.241	0.240	0.290
	0.662	0.077	0.077	0.129
	1.172	0.059	0.058	2.041
	1.333	0.055	0.055	1.578
S2	0.060	0.261	0.261	0.038
	0.662	0.077	0.078	0.898
	1.172	0.059	0.059	0.337
	1.333	0.055	0.055	0.543
S3	0.060	0.247	0.247	0.040
	0.662	0.077	0.077	0.389
	1.172	0.058	0.058	0.172
	1.333	0.054	0.055	1.276
S4	0.060	0.249	0.251	0.603
	0.662	0.077	0.077	0.388
	1.172	0.058	0.059	1.529
	1.333	0.055	0.056	1.253

Table 4. 6.Linear attenuation coefficient (μ) of the samples.

Samples	Energy (Mev)	μ (cm^{-1})	
		XCOM	Geant 4
S1	0.060	0.475	0.473
	0.662	0.152	0.155
	1.172	0.115	0.117
	1.333	0.108	0.111
S2	0.060	0.519	0.519
	0.662	0.153	0.155
	1.172	0.117	0.117
	1.333	0.109	0.109
S3	0.060	0.489	0.489

	0.662	0.152	0.154
	1.172	0.114	0.116
	1.333	0.106	0.110
S4	0.060	0.496	0.499
	0.662	0.153	0.153
	1.172	0.115	0.117
	1.333	0.109	0.111

Table 4. 7.Half value layer) HVL (of the samples.

Samples	Energy (Mev)	HVL(cm)	
		XCOM	Geant 4
S1	0.060	1.459	1.465
	0.662	4.560	4.471
	1.172	5.975	5.924
	1.333	6.418	6.245
S2	0.060	1.34	1.33
	0.662	4.523	4.472
	1.172	5.903	5.924
	1.333	6.333	6.359
S3	0.060	1.417	1.417
	0.662	4.560	4.501
	1.172	6.080	5.975
	1.333	6.539	6.301
S4	0.060	1.397	1.398
	0.662	4.523	4.530
	1.172	6.005	5.924
	1.333	6.333	6.245

Table 4. 8.Tenth Value Layer (TVL)of the samples.

Samples	Energy (Mev)	TVL(cm)	
		XCOM	Geant 4
S1	0.060	4.847	4.868
	0.662	15.146	14.855
	1.172	19.849	19.680
	1.333	21.320	20.744
S2	0.060	4.437	4.437
	0.662	15.026	14.855
	1.172	19.611	19.680
	1.333	21.037	21.125
S3	0.060	4.708	4.709
	0.662	15.149	14.951
	1.172	20.198	19.845
	1.333	21.723	20.933
S4	0.060	4.642	4.614
	0.662	15.026	15.049
	1.172	19.949	19.680

	1.333	21.037	20.744

Table 4. 9.Mean free path (MFP) of the samples.

Samples	Energy (Mev)	MFP (cm)	
		XCOM	Geant 4
S1	0.060	2.105	2.11
	0.662	6.579	6.452
	1.172	8.621	8.547
	1.333	9.259	9.009
S2	0.060	1.962	1.927
	0.662	6.526	6.452
	1.172	8.517	8.547
	1.333	9.136	9.174
S3	0.060	2.045	2.044
	0.662	6.579	6.493
	1.172	8.772	8.621
	1.333	9.434	9.091
S4	0.060	2.016	2.132
	0.662	6.536	6.461
	1.172	8.664	8.589
	1.333	9.136	9.174

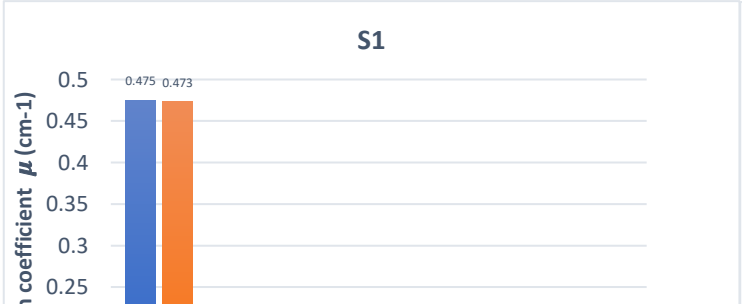

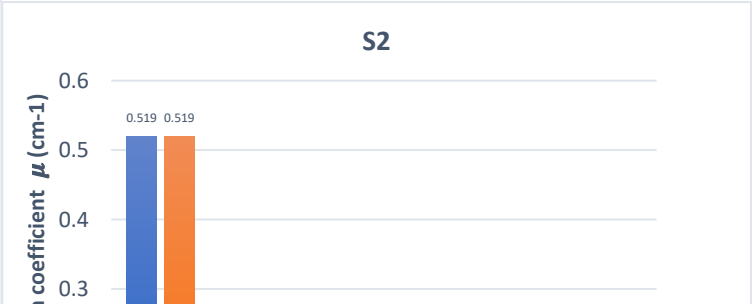

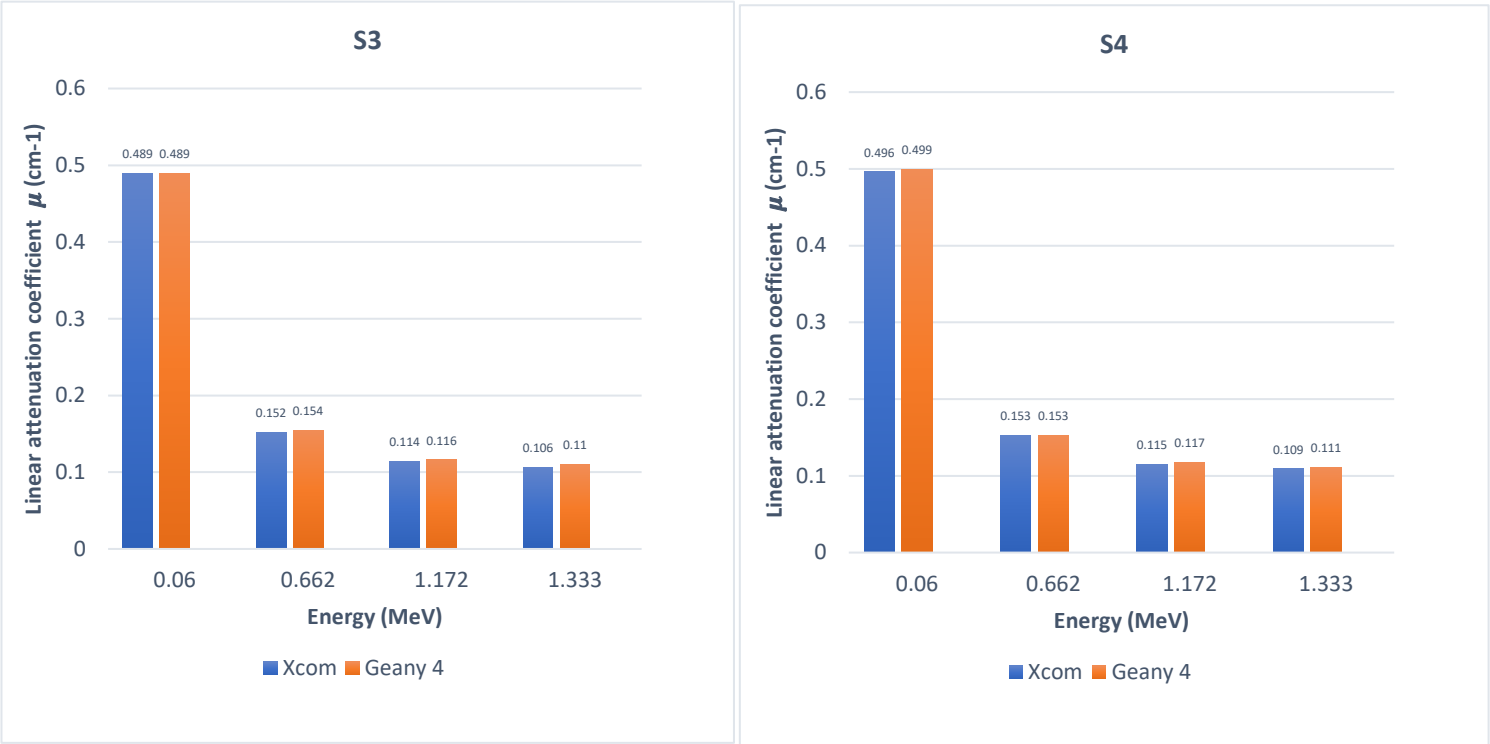

Figure 4. 3.Comparison of LAC values calculated by Geant 4.

The bar charts depict the change of the linear attenuation coefficient (μ) as a function of photon energy for the four examined samples (S1),(S2),(S3), and (S4)—as estimated using the XCOM and Geant4 simulation tools. Across all samples, a definite inverse relationship is detected between the energy and the linear attenuation coefficient: as the photon energy increases, the value of μ drops. This tendency is compatible with the physics of gamma-ray interactions, where lower-energy photons are more likely to be reduced by photoelectric absorption, which is strongly dependent on atomic number and decreases rapidly with increasing energy.

Sample S2 displayed the highest linear attenuation coefficients at all energy levels, significantly surpassing the other samples. This reflects its considerably higher density and richer elemental composition, particularly in high-Z elements such as Fe, Ca, and Co. In contrast, sample S1 showed lower μ values at higher energies, indicating less shielding efficiency under high-energy gamma radiation. Samples S3 and S4 demonstrated relatively comparable attenuation characteristics, with S4 showing somewhat superior attenuation overall.

It is also worth mentioning that the results acquired from both XCOM and Geant4 are surprisingly consistent, with just small changes (visually and mathematically). This consistency verifies the dependability and compatibility of both methodologies for radiation shielding tests. The agreement also supports the credibility of employing simulation methods for predictive modeling of attenuation qualities in natural materials.

IV.5High-Energy Gamma Shielding Evaluation of S1–S4 Compared to Previous Studies

Table 4. 10.the shielding parameters of four different clay types were compared to previously published data.

shielding parameters	Energy (Mev)	ThisWork				[16]		[17]	
		S1	S2	S3	S4	Ball clay	Kaolin Clay	Bentonite Clay	Red Clay
LAC	1.172	0.116	0.117	0.114	0.115	0.115	0.115	0.224	0.117
	1.333	0.108	0.109	0.106	0.109	0.108	0.108	0.114	0.110
HVL	1.172	5.975	5.903	6.080	6.005	6.025	6.015	5.664	5.899
	1.333	6.418	6.333	6.539	6.333	6.425	6.413	6.047	6.297
MFP	1.172	8.621	8.517	8.772	8.664	8.694	8.679	8.172	8.510
	1.333	9.259	9.136	9.434	9.136	9.271	9.254	8.725	9.085

The table 4.10. presents a comprehensive comparison of shielding parameters (LAC), (HVL), (MFP)for the four analyzed clay samples (S1 to S4) at elevated photon energies (1.172 MeV and 1.333 MeV), in relation to values from prior studies [16] and [17]. At 1.172 MeV, the LAC values for S1 to S4 vary from 0.114 cm^{-1} (S3) to 0.117 cm^{-1} (S2), closely resembling the values for ball clay and kaolin clay from [16], both at 0.115 cm^{-1}. Conversely, bentonite clay from [17] exhibits a significantly elevated LAC of 0.224 cm^{-1}, suggesting enhanced attenuation, either attributable to increased density or varying elements makeup. At 1.333 MeV, the LAC values for S1 to S4 range from 0.106 cm^{-1} to 0.109 cm^{-1}, closely aligning with the stated value of 0.108 cm^{-1} for both ball and kaolin clays, however bentonite clay decreases to 0.114 cm^{-1}.

Concerning HVL, indicative of the thickness required to diminish intensity by fifty percent, S2 exhibited the lowest value at 1.172 MeV (5.903 cm), whilst S3 presented the greatest at 6.080

cm. These measurements are analogous to ball clay (6.025 cm) and kaolin clay (6.015 cm), and marginally exceed those of bentonite (5.664 cm) and red clay (5.899 cm). At 1.333 MeV, all samples exhibited a rise in half-value layer (HVL) owing to decreased attenuation at elevated energy levels. S1 exhibited a half-value layer (HVL) of 6.418 cm, closely approximating that of red clay at 6.297 cm and kaolin at 6.413 cm.

Correspondingly, the MFP values escalated with energy. At 1.172 MeV, sample S2 exhibited the lowest mean free path (MFP) of 8.517 cm, whereas S3 had the highest MFP of 8.772 cm, which corresponds closely with the results for ball clay (8.694 cm) and kaolin clays (8.679 cm). At 1.333 MeV, the mean free path (MFP) for all samples was uniform, varying from 9.136 cm (S2 and S4) to 9.434 cm (S3), closely aligning with the range recorded for prior clays—ball (9.271 cm), kaolin (9.254 cm), and red clay (9.085 cm).

The comparisons indicate that the examined natural clays, particularly S2 and S4, exhibit shielding efficacy at elevated energies that closely parallels that of commercial clays, suggesting their applicability in radiation protection contexts.

Table 4. 11.the shielding parameters of four different clay types were compared to previously published data[17].

Clay type	Energy (Mev)	MAC (cm^2g^{-1})			Δ_1 (%) [17]	Δ_2 (%)
		XCOM [17]	Experimental [17]	Geant 4 [This work]		
Red clay	0.06	0.352	0.346	0.351	1.55	1.49
	0.662	0.076	0.077	0.076	-2.01	-0.78
	1.172	0.058	0.056	0.057	1.95	2.29
	1.333	0.054	0.053	0.054	0.98	1.86
Ball clay	0.06	0.287	0.282	0.286	1.54	1.40
	0.662	0.077	0.076	0.076	1.22	-0.26
	1.172	0.058	0.058	0.058	- 0.88	-0.51
	1.333	0.276	0.270	0.271	1.11	0.48
Kalion clay	0.06	0.276	0.270	0.274	2.05	1.47
	0.662	0.077	0.075	0.076	1.95	2.50
	1.172	0.058	0.059	0.058	-2.85	- 1.88
	1.333	0.055	0.054	0.054	1.66	0.61
Bentonite clay	0.06	0.372	0.383	0.379	-3.02	-1.04
	0.662	0.077	0.078	0.077	-1.55	- 0.51
	1.172	0.058	0.057	0.058	0.88	2.08
	1.333	0.055	0.054	0.054	0.78	0.73

The table provides a comprehensive comparison of the mass attenuation coefficients (MAC, in cm^2/g) for four clay varieties—Red clay, Ball clay, Kaolin clay, and Bentonite clay—at four gamma photon energies: 0.06, 0.662, 1.172, and 1.333 MeV. The values are derived from three sources: theoretical data from XCOM, experimental measurements, and simulation findings from Geant4 (designated as "This work").

At the minimal energy level (0.06 MeV), all samples demonstrate the maximum mass attenuation coefficients, aligning with the anticipated pattern where attenuation is more pronounced at lower photon energies due to the predominance of photoelectric interactions. Red clay exhibits a MAC of 0.357 (XCOM), 0.341 (Experimental), and 0.355 (Geant4), demonstrating substantial concordance across the three sources. Bentonite clay exhibits the greatest attenuation at this energy, with a MAC of 0.379 (Geant4), rendering it the most efficient shielding material at low energy.

As energy rises to 0.662 MeV, the MAC values markedly diminish. Red clay exhibits values of 0.076 (XCOM and Geant4) and 0.077 (Experimental). Comparable tendencies are observed for other clay varieties. This decline indicates the prevalence of Compton scattering, which is less energy-absorptive than the photoelectric effect.

At elevated energies (1.172 and 1.333 MeV), the MAC values persist in a gradual decline. The MAC for Red clay is 0.058 (XCOM) and 0.057 (Geant4) at 1.172 MeV, and 0.054 (XCOM and Geant4) at 1.333 MeV. The figures are almost equal among all three sources, demonstrating remarkable consistency. Ball clay and Kaolin clay exhibit values that closely approximate those of Red clay. Bentonite clay exhibits somewhat elevated MAC values at high energies—0.058 (1.172 MeV) and 0.054 (1.333 MeV).

The statistics indicate that all four clay kinds are more effective in attenuating gamma radiation at lower energy levels. Bentonite clay exhibits a distinct value of 0.06 MeV, although the disparities among various clays diminish with increasing energy levels. The strong correlation between Geant4 results and both XCOM and experimental data validates the precision of the simulation model employed in this study.

VI. Conclusion

This chapter has given and analyzed the results obtained from Geant4 simulations and XCOM theoretical calculations, which collectively provide a thorough evaluation of photon interaction mechanisms and the radiation shielding efficacy of the examined materials. The amalgamation of these two methodologies guaranteed the precision and reliability of the acquired outcomes.

The investigation revealed that the photoelectric effect prevails at low photon energies, Compton scattering dominates the intermediate range, and pair creation is predominant at elevated energies. Materials possessing elevated atomic and effective atomic numbers demonstrated enhanced attenuation properties, especially in the low-energy spectrum.

The examined material demonstrated significant promise for low-energy gamma radiation shielding, bolstered by its accessibility, structural integrity, and chemical resilience, rendering it appropriate for integration into fortified and protective constructions. The robust concordance between the Geant4 and XCOM results further substantiates the dependability of the simulation findings.

The comparative assessment indicates that the samples can be rated in declining order of shielding efficiency as follows: S2, S4, S1, and S3. The results detailed in this chapter establish a robust basis for the overarching conclusions and recommendations articulated in the subsequent section.

References

[1]"IAEA SAFETY STANDARDS for protecting people and the environment Radiation Protection and Safety in Medical Uses of Ionizing Radiation," 2016.

[2]R. O. Abdel Rahman and Y. T. Hung, "Application of ionizing radiation in wastewater treatment: An overview," Water (Switzerland), vol. 12, no. 1. MDPI AG, Jan. 01, 2020. doi: 10.3390/w12010019.

[3]M. Abdillah, H. Qonit, and R. Indiarto, "A Review Of Irradiation Technologies On Food And Agricultural Products," Article in International Journal of Scientific & Technology Research, vol. 9, p. 1, 2020, [Online]. Available: www.ijstr.org

[4]O. Bawazeer et al., “A review on using nanocomposites as shielding materials against ionizing radiation,” Journal of Umm Al-Qura University for Applied Sciences, vol. 9, no. 3. Springer, pp. 325–340, Sep. 01, 2023. doi: 10.1007/s43994-023-00042-9.

[5]Z. Alsayed, M. S. Badawi, R. Awad, A. M. El-Khatib, and A. A. Thabet, “Investigation of γ-gamma attenuation coefficients, effective atomic number and electron density for ZnO/HDPE composite,” Phys Scr, vol. 95, no. 8, Aug. 2020, doi: 10.1088/1402-4896/ab9a6e.

[6]C. V. More, Z. Alsayed, M. S. Badawi, A. A. Thabet, and P. P. Pawar, “Polymeric composite materials for radiation shielding: a review,” Environmental Chemistry Letters, vol. 19, no. 3. Springer Science and Business Media Deutschland GmbH, pp. 2057–2090, Jun. 01, 2021. doi: 10.1007/s10311-021-01189-9.

[7]M. Sarihan, “Simulation of gamma-ray shielding properties for materials of medical interest,” Open Chem, vol. 20, no. 1, pp. 81–87, Jan. 2022, doi: 10.1515/chem-2021-0118.

[8]D. R. Mcalister, “Gamma Ray Attenuation Properties of Common Shielding Materials,” 2018.

[9]S. S. Obaid, M. I. Sayyed, D. K. Gaikwad, and P. P. Pawar, “Attenuation coefficients and exposure buildup factor of some rocks for gamma ray shielding applications,” Radiation Physics and Chemistry, vol. 148, pp. 86–94, Jul. 2018, doi: 10.1016/j.radphyschem.2018.02.026.

[10] N. J. AbuAlRoos, N. A. Baharul Amin, and R. Zainon, “Conventional and new lead-free radiation shielding materials for radiation protection in nuclear medicine: A review,” Radiation Physics and Chemistry, vol. 165. Elsevier Ltd, Dec. 01, 2019. doi: 10.1016/j.radphyschem.2019.108439.

[11] G. Lakshminarayana et al., “Correction to: Li2O–B2O3–Bi2O3 glasses: gamma-rays and neutrons attenuation study using ParShield/WinXCOM program and Geant4 and Penelope codes (Applied Physics A, (2020), 126, 4, (249), 10.1007/s00339-020-3418-7),” Applied Physics A: Materials Science and Processing, vol. 126, no. 5. Springer, May 01, 2020. doi: 10.1007/s00339-020-3447-2.

[12] M. S. Al-Buriahi and B. T. Tonguc, “Mass attenuation coefficients, effective atomic numbers and electron densities of some contrast agents for computed tomography,” Radiation Physics and Chemistry, vol. 166, Jan. 2020, doi: 10.1016/j.radphyschem.2019.108507.

[13] R. A. R. Bantan, M. I. Sayyed, K. A. Mahmoud, and Y. Al-Hadeethi, “Application of experimental measurements, Monte Carlo simulation and theoretical calculation to estimate the gamma ray shielding capacity of various natural rocks,” Progress in Nuclear Energy, vol. 126, Aug. 2020, doi: 10.1016/j.pnucene.2020.103405.

[14] A. L. Wani, A. Ara, and J. A. Usmani, “Lead toxicity: A review,” Interdisciplinary Toxicology, vol. 8, no. 2. Slovak Toxicology Society, pp. 55–64, Jun. 01, 2015. doi: 10.1515/intox-2015-0009.

[15] A. H. Taqi and H. J. Khalil, “Experimental and Theoretical Investigation of Gamma Attenuation of Building Materials,” Journal of Nuclear and Particle Physics, vol. 2017, no. 1, pp. 6–13, 2017, doi: 10.5923/j.jnpp.20170701.02.

[16] S. F. Olukotun et al., “Investigation of gamma radiation shielding capability of two clay materials,” Nuclear Engineering and Technology, vol. 50, no. 6, pp. 957–962, Aug. 2018, doi: 10.1016/j.net.2018.05.003.

[17] M. Elsafi, Y. Koraim, M. Almurayshid, F. I. Almasoud, M. I. Sayyed, and I. H. Saleh, “Investigation of photon radiation attenuation capability of different clay materials,” Materials, vol. 14, no. 21, Nov. 2021, doi: 10.3390/ma14216702.

[18] L. Gerward, N. Guilbert, K. B. Jensen, and H. Levring, “WinXCom - A program for calculating X-ray attenuation coefficients,” in Radiation Physics and Chemistry, Oct. 2004, pp. 653–654. doi: 10.1016/j.radphyschem.2004.04.040.

[19] M. E. Medhat and V. P. Singh, “Mass attenuation coefficients of composite materials by Geant4, XCOM and experimental data: Comparative study,” Radiation Effects and Defects in Solids, vol. 169, no. 9, pp. 800–807, Sep. 2014, doi: 10.1080/10420150.2014.950264.

[20] N. Damla, H. Baltas, A. Celik, E. Kiris, and U. Cevik, “Calculation of radiation attenuation coefficients, effective atomic numbers and electron densities for some building materials,” Radiat Prot Dosimetry, vol. 150, no. 4, pp. 541–549, Jul. 2012, doi: 10.1093/rpd/ncr432.

[21] C. W. Fabjan, “Particle Physics Reference Library Volume 2: Detectors for Particles and Radiation.”

[22] P. S. DAHINDE, G. P. DAPKE, S. D. RAUT, R. R. BHOSALE, and P. P. PAWAR, "ANALYSIS OF HALF VALUE LAYER (HVL), TENTH VALUE LAYER (TVL) AND MEAN FREE PATH (MFP) OF SOME OXIDES IN THE ENERGY RANGE OF 122KeV to 1330KeV," Indian J Sci Res, vol. 9, no. 2, pp. 79–84, 2019, doi: 10.32606/ijsr.v9.i2.00014.

[23] M. Abdeldjalil, "Determining the characteristics of dune sand used in the building of different sites for the desert environment," 2023, doi: 10.21203/rs.3.rs-3016446/v1.

[24] M. , B. A. & A. M. Abdeldjalil, "Identification of dune sands used in building by their characteristics and a granular model for an arid environment," Asian Journal of Civil Engineering, vol. 25, no. 3, pp. 2883–2901, Apr. 2024.

[25] P. R. Danesi, J. Moreno, M. Makarewicz, and D. Louvat, "Residual radionuclide concentrations and estimated radiation doses at the former French nuclear weapons test sites in Algeria," Applied Radiation and Isotopes, vol. 66, no. 11, pp. 1671–1674, Nov. 2008, doi: 10.1016/j.apradiso.2007.08.022.

[26] W. Mui et al., "Development of ASTM International D8405—Standard Test Method for Evaluating PM2.5 Sensors or Sensor Systems Used in Indoor Applications," J Occup Environ Hyg, vol. 20, no. 9, pp. 373–389, 2023, doi: 10.1080/15459624.2023.2212739.

[27] G. Zadora and Z. Brozek-Mucha, "SEM-EDX - A useful tool for forensic examinations," in Materials Chemistry and Physics, Aug. 2003, pp. 345–348. doi: 10.1016/S0254-0584(03)00018-X.

[28] M. O. Mohamed, A. S. A. Dib, and A. H. Belbachir, "Energy distribution of cosmic rays in the Earth's atmosphere and avionic area using Monte Carlo codes," Pramana - Journal of Physics, vol. 87, no. 1, Jul. 2016, doi: 10.1007/s12043-016-1210-1.

[29] G. Ali Al-zaidi, H. A. Saudi, I. A. Nassar, and K. Sedeek, "Investigation of the radiation Shielding Behavior of Monocrystalline and Polycrystalline solar cell Using experimental, Geant4 Simulation Code and WinXCOM Database," 2023, doi: 10.21203/rs.3.rs-3368703/v1.

[30] L. de la Fuente Rosales, S. Incerti, Z. Francis, and M. A. Bernal, "Accounting for radiation-induced indirect damage on DNA with the Geant 4-DNA code," Physica Medica, vol. 51, pp. 108–116, Jul. 2018, doi: 10.1016/j.ejmp.2018.06.006.

[31] C. Belamri, A. S. A. Dib, and A. H. Belbachir, “Monte Carlo simulation of proton therapy using bio-nanomaterials,” J Radiother Pract, vol. 15, no. 3, pp. 290–295, Sep. 2016, doi: 10.1017/S1460396916000145.

[32] C. C. Ban et al., “Modern heavyweight concrete shielding: Principles, industrial applications and future challenges; review,” Journal of Building Engineering, vol. 39. Elsevier Ltd, Jul. 01, 2021. doi: 10.1016/j.jobe.2021.102290.

General Conclusion
and
Perspectives

General Conclusion and Perspective

The Geant4 simulation has demonstrated efficacy and reliability as a substitute to experimental work, especially in scenarios where access to physical experimental components is restricted or unfeasible. This computational method not only emulates physical interactions with remarkable accuracy but also provides substantial benefits for cost-effectiveness, time optimisation, and safety. Furthermore, conducting simulations before actual experimentation affords researchers a crucial opportunity to meticulously build the experimental framework, foresee probable variables, and perform a comprehensive investigation of the interaction mechanisms involved.

The interaction of photons with materials in gamma radiation shielding is significantly influenced by energy levels. At low gamma energies, the photoelectric effect predominates as the interaction mechanism, resulting in significant attenuation in high atomic number materials. As the energy level ascends to the intermediate range, Compton scattering becomes more pronounced, with photons experiencing inelastic collisions that lead to energy dissipation and angular deviation. At elevated energy levels, the pair creation process (cogeneration) becomes prominent, especially in the proximity of intense electromagnetic fields, such as those around heavy atomic nuclei.

The choice of shielding materials must be customised to the prevailing interaction processes at each energy level. Materials with elevated atomic numbers (Z) and high effective atomic numbers (Z_eff) are very effective at absorbing gamma radiation across various energy spectra. This investigation revealed that the materials analysed exhibited significant efficacy in attenuating low-energy gamma rays, indicating their appropriateness for protective use in radiation-prone areas.

Moreover, the practical attributes of the examined material — such as its local availability, chemical and thermal stability, and structural integrity — augment its suitability for radiation shielding applications. These attributes render it particularly suitable for reinforced infrastructures, like nuclear facilities, research laboratories, and medical imaging rooms, where enduring and reliable protection is needed.

Ultimately, based on the simulation outcomes and comparative analysis of attenuation characteristics, the samples examined can be classified by their shielding effectiveness in descending order as follows: S2, S4, S1, and S3. This classification establishes a definitive

framework for material selection in future applications and enhances the overall comprehension of economical and effective radiation shielding systems.

Viewpoints:

The present work establishes a robust basis for additional investigation in multiple avenues. One such approach entails expanding the study to encompass wider energy ranges, including ultra-high gamma energies, to evaluate material behaviour under extreme radiation circumstances. Furthermore, empirical validation of the Geant4 simulation outcomes would yield a more thorough understanding and assist in enhancing the computational models employed.

Future study may investigate the improvement of shielding efficacy via composite material design, such as the incorporation of nanoparticles, metal oxides, or polymer matrices to enhance attenuation while maintaining mechanical and thermal stability. Environmental sustainability may be prioritised by assessing the ecological impact of materials and incorporating recycled or naturally plentiful components.

From a pragmatic perspective, integrating these materials into tangible structures—such as protective panels, mobile shielding units, or personal protective equipment—necessitates engineering analyses that assess mechanical resistance, manufacturability, and long-term durability. Interdisciplinary collaboration among materials science, medical physics, and civil engineering may yield innovative, customisable shielding solutions for civilian and industrial applications.

The incorporation of simulation tools like Geant4 in the initial phases of material development provides a strategic benefit, enabling researchers to refine designs prior to engaging in expensive experimental stages — a viewpoint increasingly pertinent in contemporary research and development paradigms.